NUCLEAR PHYSICS LABORATORY

UNIVERSITY OF
WASHINGTON

ANNUAL REPORT

JUNE 1966

U.S. ATOMIC ENERGY COMMISSION
CONTRACT A.T. (45-1)-1388

ANNUAL REPORT

Nuclear Physics Laboratory
University of Washington
June, 1966

Program "A" --
Experimental Nuclear Physics
Program (Cyclotron)
under
U. S. Atomic Energy Commission
Contract A. T. (45-1) - 1388

PREFACE

This report reviews the research and technical development conducted at the Nuclear Physics Laboratory at the University of Washington during the year ending June 15, 1966. Two accelerators are presently in use, a 60-inch cyclotron and a two-stage FN tandem Van de Graaff. The latter was placed in operation about one year ago. A second, injector stage, FN tandem will be installed this summer.

Research at this Laboratory is performed by the faculty and graduate students of the Departments of Physics and Chemistry of the University of Washington. Support for these projects is provided by the State of Washington, the U.S. Atomic Energy Commission, and the National Science Foundation.*

The arrangement of this report follows the pattern of previous years. The sections are numbered consecutively through the report; each table and figure is assigned the number of the section to which it pertains. As has been our practice, the names of investigators listed at the end of each section are in alphabetical order.

The investigations described in the report for the most part continue and extend experimental work described in earlier reports, to which reference is generally made. Continued emphasis is placed on elastic and inelastic scattering, pickup and stripping reactions, photons emitted in nuclear reactions, angular correlations in nuclear reactions, compound nuclear reactions, and nuclear fission. Two sections describing new instrumentation for research and accelerator research and development complete the report. A list of laboratory personnel, advanced degrees granted during the past year, and a list of laboratory publications since the last report are given in an Appendix.

---

* The National Science Foundation provided the funds to purchase the three-stage tandem Van de Graaff accelerator and some of its associated equipment, and a portion of the funds to construct the laboratory building to house them.

TABLE OF CONTENTS

I. ELASTIC AND INELASTIC SCATTERING

1. Proton Scattering From Isobaric Analog States in the Lead Region

A number of different experiments have shown that isobaric analog states exist at high excitation energies in medium and heavy nuclei. For example, if the nucleus (Z,A) contains low lying states with isospin quantum numbers $(T,T_Z = T)$, where $T_Z = (N - Z)/2$, the neighboring isobar (Z + 1,A) contains analogs of these states which have the quantum numbers (T,T - 1) and differ in energy by the Coulomb displacement. Analogs of ground states of heavy nuclei were first identified in residual nuclei following direct (p,n) reactions.[1] In this case the target ground state is converted to its isobaric analog by simple exchange of a neutron for a proton.

More recently isobaric analogs of excited states as well as ground states have been observed in compound reactions involving the addition of a proton to a target nucleus.[2-5] In proton elastic scattering,[2,3] analog states are excited in the proton plus target system which correspond to states observed in the target plus neutron system by the (d,p) reaction. The proton widths, Γ_p, for formation of the analogs are closely related to the spectroscopic factors obtained from the stripping reaction to the corresponding states. Inelastic proton scattering from analog states[4,6] is of particular interest since the widths for decay may yield information about the matrix elements connecting excited states of the target with excited states of the target plus neutron system. This information is related to that which would be obtained if neutron stripping and pick-up experiments could be performed starting with excited states of a target.

An experiment is under way to investigate analog states in the lead region using the (p,p) and (p,p') reactions. Since the derivation of nuclear structure information in the manner mentioned above has not yet been quantitatively formulated, the well known states in the lead nuclei which possess simple configurations are particularly suitable for exploring the usefulness of analog states for nuclear spectroscopy. In addition, if well separated analog states at high excitation energies (15 - 20 MeV) in the heaviest stable nuclei can be excited, further information about the nature of analog states and the reaction mechanisms may be obtained.

The experimental procedure involves the measurement of (p,p) and (p,p') differential cross sections as a function of energy using the tandem accelerator. The measurements were begun at 11.5 MeV incident energy and continued up to the energy limit of the machine (at present 16.5 MeV). Targets, about 15 keV thick, of Pb^{206}, Pb^{207} and Pb^{208} were used and the scattered protons were measured with 2 mm lithium-drifted silicon detectors. The scattering at two angles was measured simultaneously with pulses from the detectors routed into two halves of a 512 channel pulse height analyzer. The energy resolution was between 60 and 80 keV, and a calibration of about 20 keV per channel was achieved using biased amplifiers to spread the top 5 MeV of each proton spectrum into 256 channels.

Figure 1-1 contains the results for Pb^{206} (p,p') between 11.5 and 14.0 MeV. At 12.3 MeV, resonances are observed in the elastic scattering and in the

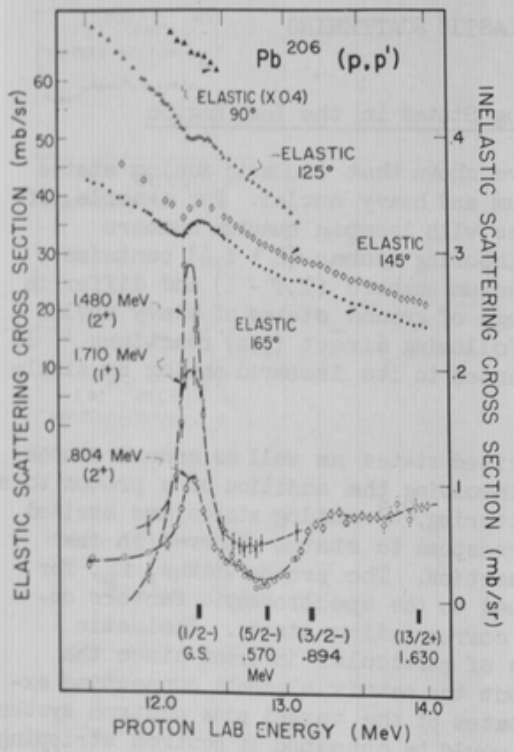

Fig. 1-1 Pb^{206} (p,p) and (p,p') excitation functions from 11.5 to 14 MeV. The inelastic scattering data were taken at 165° (lab). The energies and spins indicated by the arrows refer to states in Pb^{206} to which the inelastic scattering was observed. Solid bars at the bottom of the figure show the expected positions of the analogs of the indicated states in Pb^{207}.

inelastic scattering to three states in Pb^{206} at 0.804 MeV (2^+), 1.48 MeV (2^+) and 1.71 MeV (1^+). Using the Coulomb displacement energy of 18.9 MeV between Pb^{207} and Bi^{207}, these resonances are found to occur at the expected energy of the analog of the $p_{1/2}^{-1}$ ground state of Pb^{207}. At 13.1 MeV there is an indication of the analog of the 0.894 MeV $p_{3/2}^{-1}$ state of Pb^{207} in the elastic scattering and an anomaly in the inelastic scattering to the 0.804 MeV 2^+ state of Pb^{206} which also may be related to the analog state. With the exception of the 3^- state mentioned below, inelastic scattering could not be measured to states other than the first 2^+ state of Pb^{206} for incident energies greater than 13 MeV due to the elastic scattering from light contaminants in the target that was used.

In Figure 1-2 the 165° elastic and inelastic scattering cross sections between incident proton energies of 14.0 and 16.5 MeV for Pb^{206}, Pb^{207} and Pb^{208} are displayed. The isobaric analogs of the $g_{9/2}$ neutron single particle state[7] of Pb^{207} (2.74 MeV) and of Pb^{209} (g.s.) are both observed near 15.0 MeV in the elastic scattering and in the inelastic scattering to the 3^- states at 2.6 MeV in Pb^{206} and Pb^{208}. At this incident energy inelastic scattering to the 0.804 MeV 2^+ state of Pb^{206} also produces a resonance. In Pb^{207} (p,p) the isobaric analogs of the 5^- and 4^- states of Pb^{208} (3.197 and 3.475 MeV, respectively) appear as a doublet in the elastic scattering between 14.7 and 15.0 MeV. This doublet is probably also related to the $g_{9/2}$ neutron state since the two states are thought to contain predominantly the $(g_{9/2}, p_{1/2}^{-1})$ neutron configuration. It is interesting that (p,p') to the $p_{3/2}^{-1}$ state at 0.894 MeV in Pb^{207} also produces a resonance at this energy, while the structure (if any) is much less pronounced for the $f_{5/2}^{-1}$ state at 0.57 MeV.

The Pb^{208} (p,p') results obtained between 14.0 and 16.5 MeV at 145° are given in Fig. 1-3. In addition to the 3^- state, scattering was measured to the 5^- and 4^- states mentioned above, neither of which could be observed clearly at 165° due to target impurities. The most prominent feature in the 145° data for

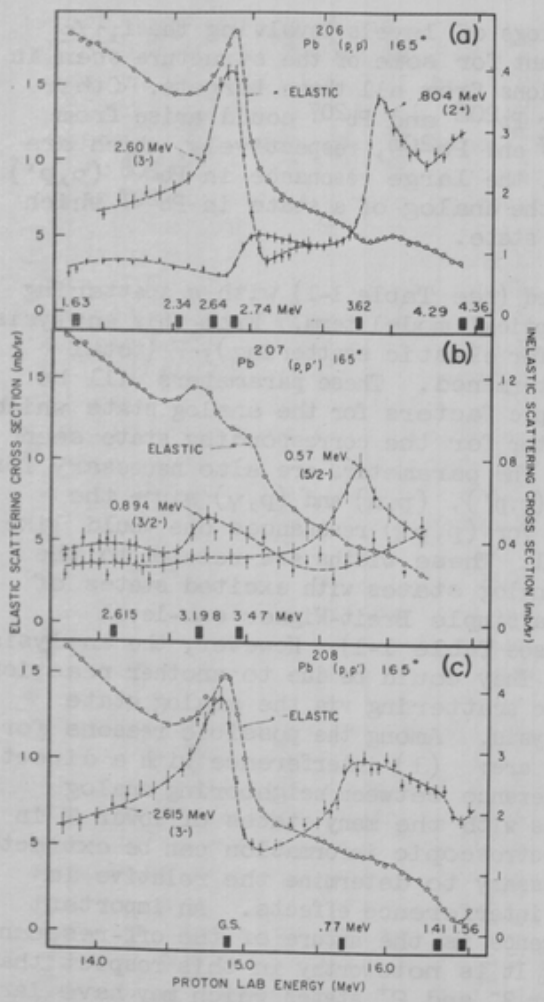

Fig. 1-2 (p,p) and (p,p') excitation functions at 165° (lab) for (a) Pb^{206}, (b) Pb^{207}, and (c) Pb^{208} between 13.8 and 16.5 MeV. Energies and spins indicated by the arrows refer to states in the target nucleus to which inelastic scattering was observed. Solid bars at the bottom of each figure show the expected positions of the analogs of the indicated states in target + neutron system.

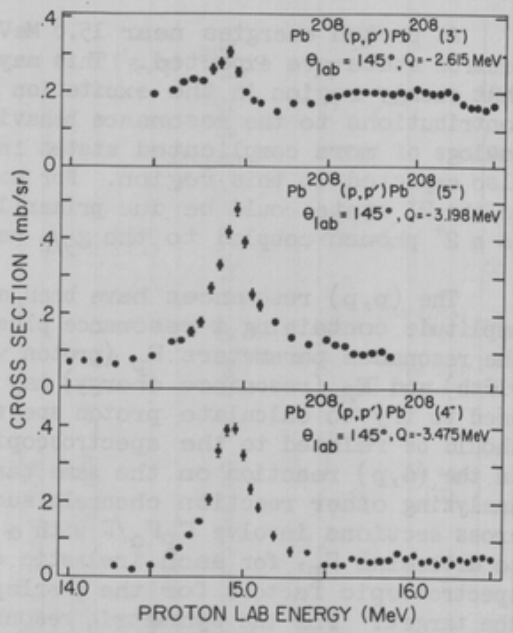

Fig. 1-3 $Pb^{208}(p,p')$ excitation functions at 145° for the 3^-(2.615 MeV), 5^-(3.197 MeV) and 4^-(3.475 MeV) states of Pb^{208}.

state of Pb^{206}. The interpretation of the all three excitation functions is the sharp resonance near 15.0 MeV corresponding to the analog of the ground state of Pb^{209}. The results for the 5^- and 4^- states are particularly interesting since they may be compared with the data described above in which the analogs of these states occur as resonances in the $Pb^{207}(p,p)$ excitation function. Both sets of data imply a large $g_{9/2}$ neutron contribution to the wave functions of these states.

A distinction should be made between: (a) the largely symmetric resonances such as those for the 5^- and 4^- states of Pb^{208} near 15 MeV, and: (b) the anomalies in the excitation functions leading to the 3^- states of Pb^{206} and Pb^{208} and the 2^+ latter may not be so straightforward because of the strong asymmetries in the resonance shapes.

At proton energies near 15.8 MeV, analogs of levels involving the $i_{11/2}$ neutron state are expected. This may account for some of the structure seen in that energy region in the excitation functions from all three targets. Other contributions to the resonance behavior for Pb^{206} and Pb^{207} could arise from analogs of more complicated states in Pb^{207} and Pb^{208}, respectively, which are also expected in this region. For example, the large resonance in Pb^{206} (p,p') to the 2^+ state could be due primarily to the analog of a state in Pb^{207} which is a 2^+ phonon coupled to the $g_{9/2}$ neutron state.

The (p,p) resonances have been analyzed (see Table 1-1) with a scattering amplitude containing a resonance plus an optical model term. From this analysis the resonance parameters Γ_p (proton width for elastic scattering), Γ (total width) and E_R (resonance energy) may be determined. These parameters will be used to try to calculate proton spectroscopic factors for the analog state which should be related to the spectroscopic factor for the corresponding state seen in the (d,p) reaction on the same target. The parameters are also necessary for analyzing other reaction channels such as (p,p'), (p,n) and (p,γ) since the cross sections involve $\Gamma_p\Gamma_\alpha/\Gamma$ with $\alpha \neq p$. For (p,p') resonances one would like to determine $\Gamma_{p'}$ for each inelastic channel. These widths are related to the spectroscopic factors for the overlap of analog states with excited states of the target. For the symmetric resonances a simple Breit-Wigner one-level resonance formula was used to obtain $\Gamma_{p'}$ (see Table 1-1). However, the analysis of asymmetric shapes is more complicated. They could be due to another reaction mechanism in addition to compound inelastic scattering via the analog state which was assumed in the Breit-Wigner analysis. Among the possible reasons for the observed asymmetric resonance patterns are: (1) interference with a direct reaction amplitude, (2) level-level interference between neighboring analog states, and (3) mixing of the analog states with the many states of lower T in the same energy region. Before useful spectroscopic information can be extracted from the (p,p') resonances it will be necessary to determine the relative importance of the various possibilities for interference effects. An important question for the mechanism of the interference is the nature of the off-resonance contribution to the inelastic scattering. It is noteworthy in this respect that the strongest interference shapes occur for 3^- and 2^+ states which may have large direct reaction contributions to their cross sections at 165°.

It is hoped that a better understanding of the experimental data will result from further excitation functions to additional final states in the lead nuclei and from angular distributions. To accomplish this we are attempting to improve the targets in order to reduce the light element contamination. This has obscured the inelastic scattering to many final states at backward angles where the resonance effects are expected to be largest. Good energy resolution for the detected protons is also crucial for separating the inelastic groups. Finally, since (p,p') cross sections are small in the back hemisphere, it would be advantageous to increase the number of detectors which can be used to acquire data simultaneously. (C. D. Kavaloski, J. S. Lilley, Patrick Richard and Nelson Stein)

Table 1-1. Resonance Analysis for Elastic[a] and Inelastic[b] Scattering[c]

Target Nucleus	E_R^{Lab}[d] (MeV)	ℓ	Γ_p[e] (keV)	$\Gamma_{p'}^{2^+}(.804)$[f] (keV)	$\Gamma_{p'}^{2^+}(1.48)$ (keV)	$\Gamma_{p'}^{1^+}(1.71)$ (keV)	Γ[g] (keV)	J^π
Pb^{206}	12.28	1	12	12.5	38.5	21	170	$1/2^-$
	14.97	4	23				230	$9/2^+$
Pb^{208}	14.97	4	17	--	--	--	215	$9/2^+$

a. C. F. Moore and P. Richard, Florida State University, 1965 Technical Report, No. 8 (unpublished). Equations in this reference were modified (private communication - D. Robson) to include optical model phases.

b. A single-level Breit-Wigner resonance equation was used to analyze the inelastic resonances.

c. Errors in resonance parameters are estimated to be less than 20%.

d. E_R^{Lab} is the resonance energy obtained from elastic scattering analysis.

e. Γ_p is the proton partial width for elastic scattering.

f. $\Gamma_{p'}^{2^+}(0.804)$ is the proton partial width for inelastic scattering to the 2^+ state at 0.804 MeV.

g. Γ is the total width for the resonance.

1 J. D. Anderson, C. Wong, and J. W. McClure, Phys. Rev. 126, 2170 (1962).
2 J. D. Fox, C. F. Moore, and D. Robson, Phys. Rev. Letters 12, 198 (1964).
3 C. F. Moore, P. Richard, C. E. Watson, D. Robson, and J. D. Fox, Phys. Rev. 141, 1166 (1966).
4 D. L. Allan, Phys. Letters 14, 311 (1965).
5 J. L. Black and N. W. Tanner, Phys. Letters 11, 135 (1964).
6 S. A. A. Zaidi, P. Von Brentano, D. Rieck, and J. P. Wurm, Phys. Letters 19, 45 (1965).
7 P. Mukherjee and B. L. Cohen, Phys. Rev. 127, 1284 (1962).

2. Spectra of Inelastic Alpha Particles Scattered from Sn, Au and U

Previous studies[1] of the spectra of 42 MeV α-particles scattered by Ta, Bi and Au revealed the following features.

(1) A forward peaking of the cross section, implying direct reaction processes.

(2) A minimum in the energy spectrum approximately 7 MeV below the elastic peak in all three elements at all angles.

(3) A decrease in the cross section at energies corresponding to the emission of the α-particle below the Coulomb barrier.

(4) An increase of the differential cross section with nuclear size at a given scattering angle.

(5) A lack of gross structure in the energy spectra at energies corresponding to excitations in the residual nucleus above 10 MeV.

This earlier work was extended by doing (α,α') on Sn, Au and U, the purpose being threefold: (1) to determine if the features seen in Bi, Au, and Ta would remain when the mass of the target nucleus was varied by a large amount, (2) to investigate the decrease in cross section in the neighborhood of the Coulomb barrier more carefully, and (3) to confirm the early conclusion that subtraction of the contaminants would leave a structureless spectrum in the region of high residual excitations.

42 MeV He ions were used to bombard the three targets. A conventional dE/dx-E multiplier system was used to identify doubly-charged particles. Although He^3 particles were also accepted by the analyzing system, they were few in number and Q values limited their appearance to a relatively small part of the spectrum (see for example the peak in the Sn spectrum at 26 MeV in Figure 2-1). Except for uranium, the targets were prepared as free as possible from carbon and oxygen in order to reduce the correction for these contaminants.

A difficulty in earlier runs had been caused by a low-energy background due to the elastic scattering of incident ions degraded in energy by slit scattering in the collimator at the entrance to the scattering chamber. This background was so intense in previous studies that it limited observation of the fall-off of

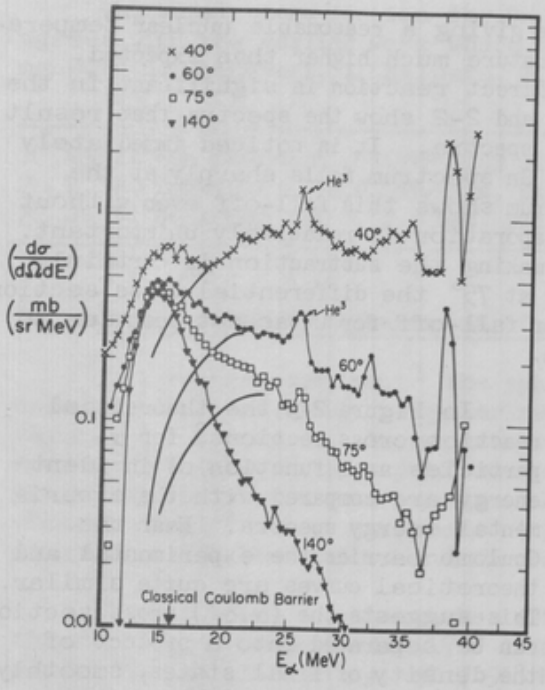

Fig. 2-1 Sn energy spectrum at 40°, 60°, 75° and 140° for 42 MeV incident α-particles. The lines indicate the low energy positions of the spectra when the 140° data points are subtracted from the data at the other angles.

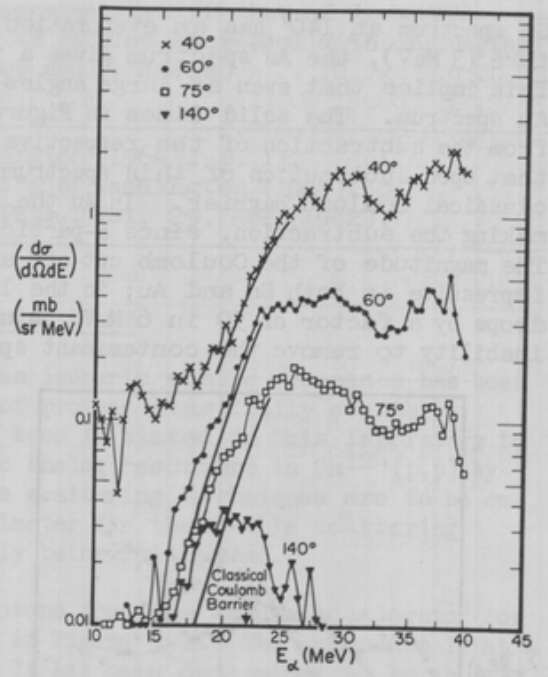

Fig. 2-2 Au energy spectrum at 40°, 60°, 75° and 140° for 42 MeV incident α-particles. The lines indicate the low energy positions of the spectra when the 140° data points are subtracted from the data at the other angles.

yield at the Coulomb barrier in gold to a factor of only two or three. The degraded beam component was greatly reduced by removing the scattering chamber collimator completely and relying on the slits in the cyclotron duct before the analyzing magnet to define the beam spot on the target. Only a minute fraction of beam scattered by these slits was able to pass through the magnet and reach the scattering chamber, and a large clean-up aperture prevented this from hitting the thick target frame. With this system the background was reduced to the point where it was comparable with that due to counting statistics and the yield from light element target impurities.

Figures 2-1 and 2-2 show the results of Sn(α,α') and Au(α,α') respectively at 40°, 60°, 75°, and 140°. The (α,α') spectra from oxygen and carbon were measured separately and then subtracted from the raw tin and gold spectra with the aid of a computer code.[2] The uranium data are not shown because the target thickness was not known and the oxygen in the target was too great for its effects to be subtracted out. Spectra for Sn and Au taken at 159° were almost identical in magnitude and shape to the respective spectra at 140°, implying that with certain reservations these spectra are mainly the result of compound nuclear processes. The main reservations concern the Au spectra. Although the

Sn spectrum at 140° has an evaporation shape giving a reasonable nuclear temperature (3 MeV), the Au spectrum gives a temperature much higher than expected. This implies that even at large angles the direct reaction is significant in the Au spectrum. The solid lines in Figure 2-1 and 2-2 show the spectra that result from the subtraction of the respective 140° spectra. It is noticed immediately that upon subtraction of this spectrum, the Sn spectrum falls sharply at the classical Coulomb barrier. In Au the spectrum shows this fall-off even without making the subtraction, since α-particle evaporation is relatively unimportant. The magnitude of the Coulomb cut-off after making the subtraction is certainly impressive in both Sn and Au; in the latter at 75° the differential cross section drops by a factor of 50 in 6 MeV. A similar fall-off for U was not seen due to inability to remove the contaminant spectra.

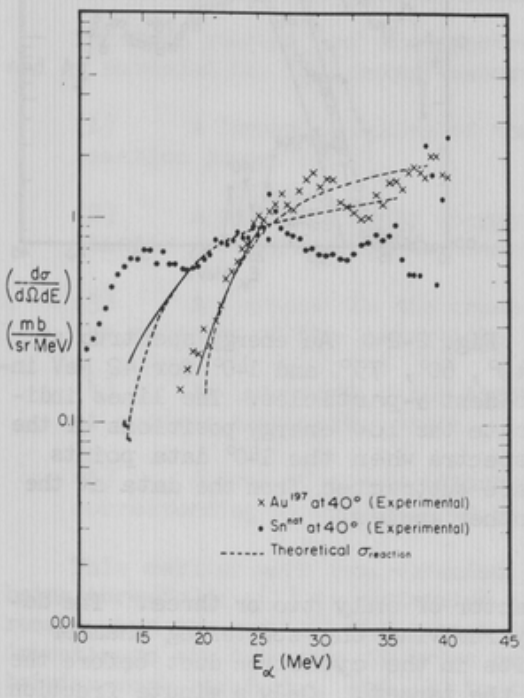

Fig. 2-3 Comparison of the theoretical and experimental reaction cross section for Sn and Au at 40°.

In Figure 2-3 the theoretical reaction cross sections[3] for α-particles as a function of incident energy are compared with the experimental energy spectra. Near the Coulomb barrier the experimental and theoretical curves are quite similar. This suggests the (α,α') cross section can be separated into a product of the density of final states, smoothly increasing with nuclear excitation, and an inverse reaction cross section. Therefore had the nucleus been bombarded with a higher energy the (α,α') cross section would have continued to rise with increasing nuclear excitation. The above conclusion depends on two questionable assumptions: (1) application of a theoretical compound nuclear calculation of cross section to a direct reaction, and (2) the separating of the cross section into a product. However some justification for this procedure rests in the close agreement of the curve so calculated with the experimental observations.

In general the angular distribution is less forward-peaked for lower energies of the outgoing α-particle. This would be expected simply from the greater influence of the Coulomb field for the slower ions, but the angular momentum transferred to the nucleus must also be considered. In particular for E_α = 20 MeV, the outgoing particle has the energy it would receive just from falling out of the Coulomb field from the nuclear surface. Under these circumstances the nucleus would have had to accept almost all the incident α-particle's angular momentum, approximately 20 units, as well as the excitation energy. It therefore appears necessary to develop a theory that not only explains the absorption of a large amount of energy but one that predicts a large angular momentum transfer.

The total cross section for Sn is approximately 1/2 that of Au which agrees with the earlier work where the cross section increased with increasing mass. (G. Chenevert, I. Halpern, J. Lilley and N. Stein)

---

1 Cyclotron Research, University of Washington (1964), p. 13.
2 E. R. Parkinson, Ph.D. Thesis, University of Washington (1965).
3 J. R. Huizenga and G. J. Igo, Nuclear Phys., Vol. 29, 462 (1962).

---

3. Spin and Parity Measurement of an Analog State

In a recent experiment[1] the spin of an isobaric analog resonance has been determined by measuring the polarization of protons elastically scattered through the resonance. An experiment has been initiated in this laboratory to measure the spin and parity of an isobaric analog resonance in $Sn^{124}(p,p)$ by measuring the proton polarization. Double scattering techniques are to be employed using C^{12} as an analyzer. A polarimeter for the double scattering experiment has been built, and is presently being calibrated.

An excitation function taken with protons from the tandem accelerator for the $Sn^{124}(p,p)$ resonance at 170° is shown in Figure 3-1. The resonance is at a proton energy (laboratory) of 7.918 MeV. It has been determined to be an $\ell_p = 2$ resonance,[2] which gives a $J^\pi = 5/2^+$ or $3/2^+$. Figure 3-2 shows the expected shapes of the polarization for the two possible spins using the resonance parameters given in Ref. 2. An $\ell_p = 0$ resonance occurs at 8.134 MeV but it does not interfere with the polarization measurement of the d-wave resonance.

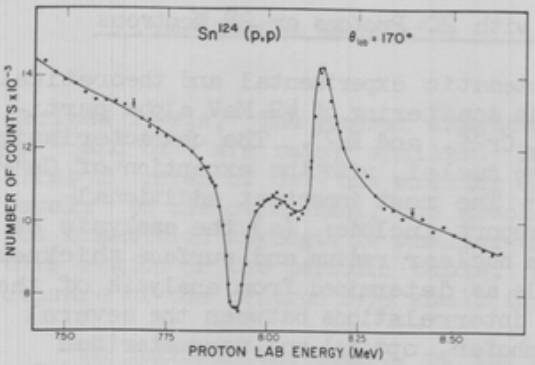

Fig. 3-1 Sn^{124} proton elastic scattering excitation function at 170°. A d-wave resonance occurs at $E_p^{lab} = 7.918$ MeV and an S-wave resonance at 8.134 MeV.

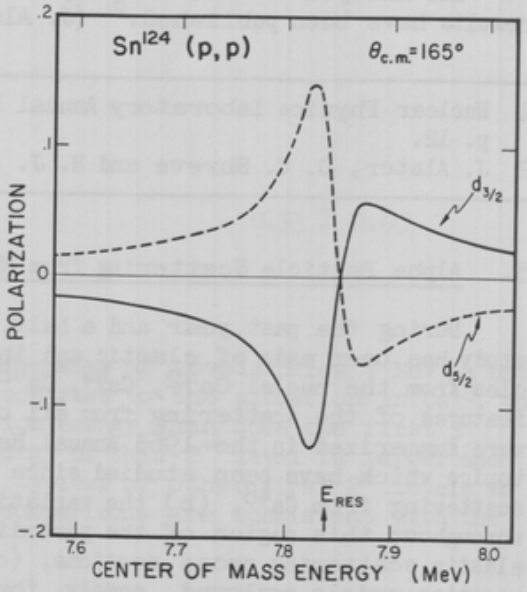

Fig. 3-2 Predicted polarization for $J^\pi = 3/2^+$ and $5/2^+$ using the elastic scattering resonance parameters $\Gamma_p = 8.5$ keV, $\Gamma = 56$ keV and $E_{Res}^{c.m.} = 7.84$ MeV.

The isobaric analog of the d-wave resonance is the first excited state of Sn^{125} which has been studied by $Sn^{124}(d,p)$.[3] Since members of the same isobaric multiplet should have the same spin and parity, the polarization measurements are capable of measuring or confirming spin assignments of low-lying nuclear levels. In the case of the lowest d-wave state in Sn^{125}, as seen in $Sn^{124}(d,p)$, the assignment[3] of $d_{3/2}$ was made based on shell model systematics inferred from other isotopes of Sn. A $d_{3/2}$ determination of similar states in Sn^{115}, Sn^{117}, Sn^{119}, Sn^{121}, and Sn^{123} was based on the ratio of the (d,p) and (d,t) cross sections leading to the above-mentioned states. This technique is not directly applicable to Sn^{125} states since $Sn^{126}(d,t)$ measurements would be necessary and Sn^{126} is not a stable nucleus. (P. Richard and W. G. Weitkamp)

---

1 C. F. Moore and G. E. Terrell, Isotopic Spin Conference, paper C5, Tallahassee, Florida (1966).
2 P. Richard, C. F. Moore, J. A. Becker, and J. D. Fox, submitted for publication in Phys. Rev.
3 B. L. Cohen and R. F. Price, Phys. Rev. 121, 144 (1961); E. J. Schneid, A. Prakash, and B. L. Cohen, submitted for publication.

---

4. Elastic and Inelastic Scattering of 42 MeV Alpha Particles from Sr^{88} and Y^{89}

The analysis of the work reported last year[1] has been completed and the results have been published.[2] (J. Alster, R. J. Peterson and D. C. Shreve)

---

1 Nuclear Physics Laboratory Annual Report, University of Washington (1965), p. 12.
2 J. Alster, D. C. Shreve and R. J. Peterson, Phys. Rev. 144, 999 (1966).

---

5. Alpha Particle Scattering from Nuclei with 20 Protons or 28 Neutrons

During the past year and a half, a systematic experimental and theoretical study has been made of elastic and inelastic scattering of 42 MeV alpha particles from the nuclei Ca^{42}, Ca^{44}, Ca^{48}, V^{51}, Cr^{52}, and Fe^{54}. The characteristic features of the scattering from all of these nuclei, with the exception of Ca^{48}, were summarized in the 1965 Annual Report.[1] The most important additional topics which have been studied since that report include: (a) the analysis of scattering from Ca^{48}, (b) the variations in nuclear radius and surface thickness throughout this region of the periodic table as determined from analysis of the elastic scattering cross sections, (c) the interrelations between the several reaction models employed, namely, the Fraunhofer, optical and parameterized phase shift models, and (d) calculations of inelastic cross sections in which the nuclear states are described by several versions of the shell model. A detailed report on this project is contained in the Ph.D. thesis of R. J. Peterson.[2]

(a) According to the nuclear shell model, the nucleus Ca^{48} is doubly magic since the neutrons have filled the $f_{7/2}$ shell while the protons have a closed s-d shell. Prior to this investigation, little spectroscopic information was available on the levels of this nucleus. The spin-parity assignments of these levels and the corresponding transition strengths, δ_I ($\equiv \beta_I R$), as deduced in this experiment, are given in Table 5-1. The assignments for the more strongly excited levels are consistent with those found in other recently performed experiments[3,4] but there are some disagreements concerning the weakly

Table 5-1. Energies, Spin-parity and Transition Strengths for Levels in Ca^{48}

-Q(MeV)	I^π	δ_I(fm)
3.83	2^+	0.53 ± 0.03
4.29		
4.51	3^-	0.56 ± 0.05
5.15	$(3^-)^*$	0.17 ± 0.05
5.37	3^-	0.23 ± 0.05
5.73		
6.11		
6.34		
6.75		
7.05		
7.75	3^-	0.33 ± 0.05

*Assignment uncertain.

excited levels. The general character and density of levels below 7 MeV in both Ca^{40} and Ca^{48} are rather similar. But in contrast to the situation in Ca^{40}, the first 2^+ level of Ca^{48} has smaller excitation energy than does the first 3^- level. On the other hand, the absolute energy of this 2^+ level is larger and its transition strength is smaller than is typical of other first 2^+ levels in this region of the periodic table. These comparisons are consistent with the closure of the neutron $f_{7/2}$ shell in Ca^{48}.

To indicate the quality of the theoretical fits to the observed angular distributions, Figure 5-1 shows the observed elastic scattering differential cross section and those computed for the Fraunhofer, parameterized phase shift, and optical models. Similarly, Figure 5-2 shows the differential cross sections for excitation of the 3.83 MeV state in Ca^{48} and the comparison to the 2^+ prediction of the Austern-Blair parameterized phase shift model.[5] A detailed discussion of the scattering from Ca^{48} has been published.[6]

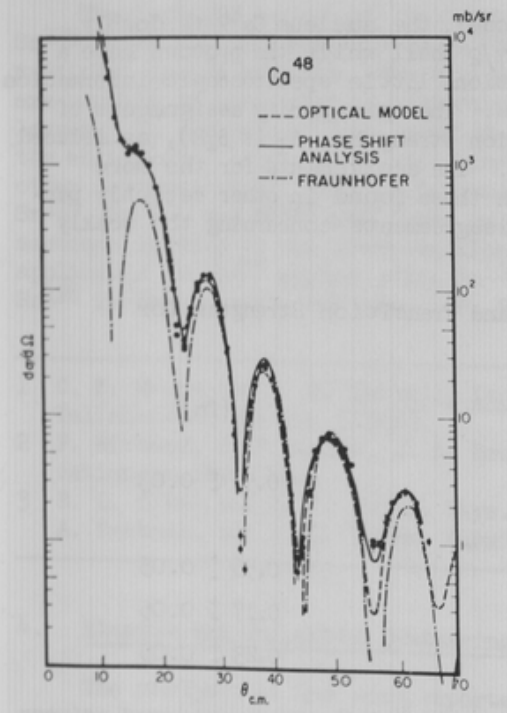

Fig. 5-1 The differential cross sections for the elastic scattering of 42 MeV alpha particles from Ca^{48}. Also shown are the predictions of the Fraunhofer, parameterized phase shift and optical models.

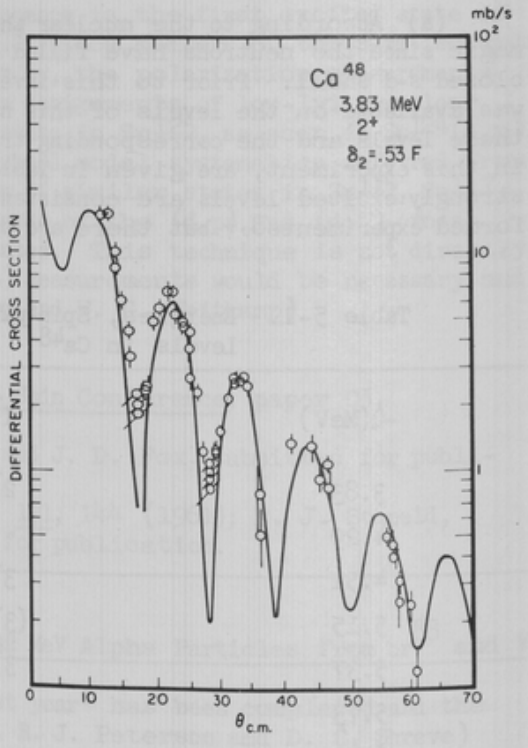

Fig. 5-2 The differential cross sections for excitation of the 3.83 MeV state in Ca^{48} and the comparison to the 2^+ prediction of the Austern-Blair parameterized phase shift model.

(b) Recent measurements of electron elastic scattering cross sections[7] and the energies of mu-mesic X-rays[8] have indicated that the electromagnetic radius of Ca^{44} is only slightly larger than that of Ca^{40}. The observed increase is not in accord with the expected $A^{1/3}$ dependence. It is therefore worthwhile to determine radii appropriate to alpha particle scattering for these and other closely related nuclei. Unlike the situation that exists in electromagnetic experiments, the radii deduced in nuclear scattering experiments depend sensitively on the manner of analysis; further, even for a given theoretical model, one is frequently confronted with several possible definitions of an appropriate radius parameter. In the present analysis, we have chosen as relevant radius parameters those which are most closely related to the scattering amplitudes. Specifically, we here consider the strong absorption radius corrected for Coulomb distortion of the Fraunhofer model, and the radii corresponding to the angular momentum at which the real parts of the scattering amplitudes in the parameterized phase shift model have the value 1/2. These radii are listed in Table 5-2 for the nuclei mentioned previously as well as for Ca^{40} and K^{39}. The values obtained from corresponding optical model analyses are still preliminary and are not listed in the table.

Table 5-2. Radii (in units of fermis) Determined from Analyses of the Elastic Scattering of 42 MeV Alpha Particles

A	39	40	42	44	48	51	52	54
R_c(Fr)	7.22	7.42	7.35	7.46	7.49	7.64	7.68	7.74
R_c(par)	7.22	7.37	7.32	7.40	7.33	7.51	7.64	7.62

Inspection of the table indicates

(i) that both the Fraunhofer and parameterized phase shift models lead to essentially the same values for strong absorption radii.

(ii) that these radii do not increase with A as rapidly as might be expected; the strong absorption radii determined in previous analyses of scattering from a wide range of targets[9] conform well to the formula, $R = 1.446(A^{1/3} + 4^{1/3})$, and thus the predicted increase in radius in going from Ca^{40} to Ca^{48} is twice as much as here observed. This anomaly may prove to be illusionary, however; incomplete analysis based on the optical model leads to values for analogously-defined strong absorption radii which are similar to those of Table 5-2 but the increase of radii with A may not be much less than that predicted from the simple formula above.

(c) The similarity in elastic scattering cross sections computed from the Fraunhofer, parameterized phase shift, and optical models has already been demonstrated by Figure 5-1. Analogous studies have also been made of the inelastic scattering cross sections computed with these three models. It is found, not surprisingly, that the cross sections predicted for all three models are nearly equivalent as long as the angular momentum transfer, I, and the excitation energy, Q, are small. For an angular momentum transfer as large as 5 units, however, the extended optical model requires a value of deformation parameter, δ_5, which is 65 per cent larger than that required for the adiabatic parameterized phase shift calculation. Also it was found that the decrease with increasing Q of the inelastic cross sections computed from the extended optical model is more marked at small rather than large values of I. These and other comparisons provide a measure of the reliability of deformation parameters derived from the more approximate parameterized phase shift models.

(d) All three of the scattering models discussed above picture the nucleus as a deformable or deformed liquid drop. It is well known, however, that such a description is oversimplified and it therefore seemed worthwhile to relate the inelastic cross sections to a description of individual nucleon motions. Such a connection is achieved by a version of the extended optical model in which the effective transition potentials are generated from matrix elements of the two body interactions of the projectile and target nucleons taken between shell model wave functions.[10]

A systematic comparison of the spectra and transition strengths of Z = 20 and Z = 28 sequences provides some support to a simple version of the shell model in which only $f_{7/2}$ orbitals are considered, especially if some collective quadrupole enhancements are incorporated into that model. A more sophisticated shell model, which introduces a pairing-plus-multipole force between the nucleons may also be applied to inelastic scattering.[11,12] We find that this model can reproduce the observed energies of the low-lying positive parity states and the collective enhancement of the differential cross sections to the first 2^+ states; however, the predicted cross sections to the higher positive parity states are much smaller than observed. (J. S. Blair and R. J. Peterson)

---

1 Nuclear Physics Laboratory Annual Report, University of Washington (1965), p. 8.
2 R. J. Peterson, Ph.D. Thesis, University of Washington (1966).
3 A. Bernstein and E. P. Lippincott, private communication.
4 O. Hansen, private communication.
5 N. Austern and J. S. Blair, Ann. Phys. (N.Y.) 33, 15 (1965).
6 R. J. Peterson, Phys. Rev. 140, B1479 (1965).
7 R. Hofstadter, G. K. Nödelke, K. J. Van Oostrom, L. R. Suelze, M. R. Yearian, B. C. Clark, R. Herman and D. G. Ravenhall, Phys. Rev. Letters 15, 758 (1965).
8 J. A. Bjorkland, S. Raboy, C. C. Trail, R. D. Ehrlich and R. J. Powers, Phys. Rev. 136, B341 (1964).
9 R. H. Venter and W. E. Frahn, Ann. Phys. (N.Y.) 27, 401 (1964).
10 See, for example, H. O. Funsten, N. R. Roberson and E. Rost, Phys. Rev. 134, B117 (1964).
11 V. A. Madsen and W. Tobocman, Phys. Rev. 139, B864 (1965).
12 N. K. Glendenning and M. Veneroni, Phys. Letters 14, 228 (1965).

---

6. Phase Correlations in $Mg^{24}(\alpha,\alpha')$

In attempting to characterize a nuclear reaction process such as inelastic scattering, one can make the simplifying assumption that the lifetime of the intermediate nuclear state in the reaction is either very long ($\sim 10^{-18}$ sec) or very short ($\sim 10^{-22}$ sec), with no significant contribution to the reaction from states of intermediate lifetimes. This picture permits one to characterize the reaction process in terms of a single parameter, the ratio of short-lived to long-lived processes contributing to the reaction; in other words the ratio of direct reaction to compound nucleus formation.

Experimentally it has proved extremely difficult to measure or even to obtain a crude estimate of this parameter. The best estimates obtained thus far have come from analysis of cross section fluctuations.[1] This analysis assumes (and indeed defines) direct reaction amplitudes (DR) to be slowly varying functions of energy while compound nucleus amplitudes (CN) change rapidly with bombarding energy. Since the DR mechanism asserts its presence only in an essentially negative way (by failing to change with energy) all estimates of the DR to CN ratio obtained in this way have been highly ambiguous and subject to large probable errors arising from finite sample size effects.

In the inelastic scattering of strongly absorbed particles, however, there is a positive characteristic of the DR mechanism which can be employed to obtain information relevant to the DR:CN ratio. This characteristic is the well known phase relation between the differential cross sections for elastic and inelastic scattering, i.e., the Blair phase rule.[2] This rule states that the even parity states will have angular distributions which are out of phase with the elastic angular distribution, while the odd parity states are in phase. This rule, although the result of a simple diffraction picture of the reaction, is also valid (at least at forward angles) in the more accurate DWBA and coupled channel descriptions of the DR process. One would thus expect that in a reaction which is pure DR this characteristic phase relation would be observed at all energies.

However, to make an effective comparison between DR and CN we must also inquire into the expected phase relationship in a pure CN inelastic process. An average CN angular distribution can be obtained from a Hauser-Feshbach statistical model calculation.[3] Such a distribution does not represent the expected angular distribution at any particular energy, but rather an average distribution about which observed angular distributions will fluctuate. Calculation of such angular distributions have been made and prove to be fairly structureless, and in fact, only about 10 per cent anisotropic in the energy region of interest here. Thus qualitatively, a CN inelastic scattering angular distribution would not be expected to have any particular fixed phase relationship with the elastic distribution, assuming (fairly accurately) that the latter was pure DR.

To use the phase relationships between angular distributions in a more quantitative way, it is necessary to find some basis for characterizing the phase between two rather dissimilar angular distributions. To do this we borrow the correlation coefficient from statistics:

$$R_{xy} = \frac{\sum_i (x(i)-\bar{x}) \cdot (y(i)-\bar{y})}{\sqrt{\sum_i (x(i)-\bar{x})^2 \sum_{i'} (y(i')-\bar{y})^2}} \quad ,$$

where $x(i)$ and $y(i)$ are the elastic and inelastic differential cross sections measured at angle $\theta(i)$, and $\bar{x}$ and $\bar{y}$ are the average values of these cross sections in the angular range of interest. This function varies between ± 1 and has the property that $R_{xy} = +1$ for $x(i) = y(i)$ over all i, and $R_{xy} = -1$ for $x(i) = 2\bar{y} - y(i)$ over all i. Thus a positive coefficient indicates that the distributions are in phase and a negative coefficient indicates that the coefficients are out of phase. Unfortunately, the correlation coefficient given above is also strongly influenced by the slow angular dependence of the cross sections, and this effect often masks the effect of phasing. To overcome this difficulty, we define a new function P_{xy}, the phase correlation coefficient, of x and y which differs from the function given above in that the deviations from the average are replaced by their logarithmic derivatives. Thus:

$$P_{xy} = \frac{\Sigma_i D_x(i) \cdot D_y(i)}{\sqrt{\sum_i D_x(i)^2 \cdot \sum_i D_y(i)^2}} \quad , \qquad (-1 < P_{xy} < 1)$$

where

$$D_x(i) = \frac{x(i+1) - x(i)}{\theta(i+1) - \theta(i)} \Big/ \frac{x(i+1) + x(i)}{2} \cong \frac{d}{d\theta} \ln(x(i)) .$$

A DWBA calculation was made using optical model parameters obtained from fitting experimental Mg^{24} + α elastic scattering data at E_α = 22 MeV. The calculation was made in 1 MeV steps between 18 and 25 MeV and the phase correlation coefficient between the Mg^{24} elastic and 2^+ first excited state angular distributions were calculated at each energy, thus giving an estimate of how the phase correlation coefficient might be expected to vary with energy for a pure DR. The transmission coefficients generated by the DWBA calculation were used in a Hauser-Feshbach CN calculation to obtain an estimate of the expected 2^+ angular distribution for a pure CN process. The phase correlation between this distribution and the DWBA elastic distribution was calculated. The value of this coefficient should represent an average about which the CN values should fluctuate with energy. Figure 6-1 shows these two predictions, representing estimates of the expected behavior of the phase correlation coefficient for an extreme DR model and an extreme CN model. Naively, one would expect a mixture of the two processes to produce a coefficient lying somewhere between these two limits.

The reaction $Mg^{24}(\alpha,\alpha')$ is being studied in the energy range 15 to 24.5 MeV at laboratory angles between 20° and 70°, in order to measure the actual behavior of the phase correlation coefficient between the elastic and the strongly excited 2^+(1.368 MeV) state. A simple multiple detector array was used in the experiment in conjunction with a beam of helium ions from the tandem accelerator. Figure 6-2 shows one such typical cross section of the elastic and 2^+ states for 21.000 MeV. The two distributions show strong diffraction patterns and are almost out of phase, as would be predicted by the Blair phase rule. This phasing is not quite as anti-correlated for 17.500 MeV (Figure 6-3) and the diffraction patterns are weaker.

Figure 6-4 shows the excitation function of the phase correlation coefficient P_{xy} at energies between 15 and 41 MeV. (The data for 28, 34, and 41 MeV were taken from a previous work.[4]) We see that the coefficient has an essentially constant negative value at the higher energies and begins to fluctuate and tend towards zero as we go down in incident alpha energy. This seems to indicate the expected transition from DR to CN with decreasing energy. Fluctuations in P_{xy} are expected to be much larger for lower energies and finer-grain energy variations are planned to study this behavior. An attempt will also be made to put the interpretation of these data on a more quantitative basis by trying to duplicate its general form in a calculation which adds a DWBA amplitude to a CN amplitude generated by a Monte Carlo calculation. (W. J. Braithwaite, J. G. Cramer and R. A. Hinrichs)

---

1 T. Ericson, Phys. Rev. Letters 5, 430 (1960); D. M. Brink and R. O. Stephen, Phys. Letters 5, 77 (1963).
2 J. S. Blair, Phys. Rev. 115, 982 (1959).
3 W. Hauser and H. Feshbach, Phys. Rev. 87, 366 (1952).
4 D. McDaniels, Ph.D. Thesis, University of Washington (1960).

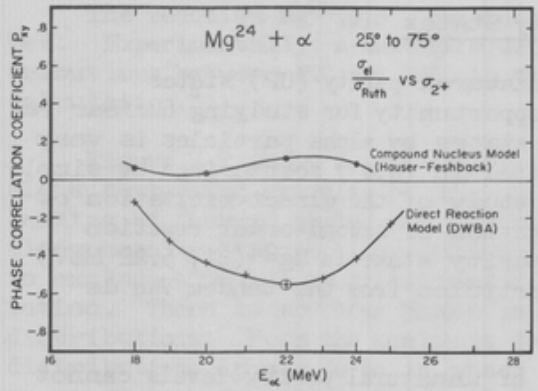

Fig. 6-1 Phase correlation coefficient between Mg^{24} elastic and 2^+ first excited states, obtained from Hauser-Feshback CN and DWBA calculations, using optical model parameters at 22 MeV.

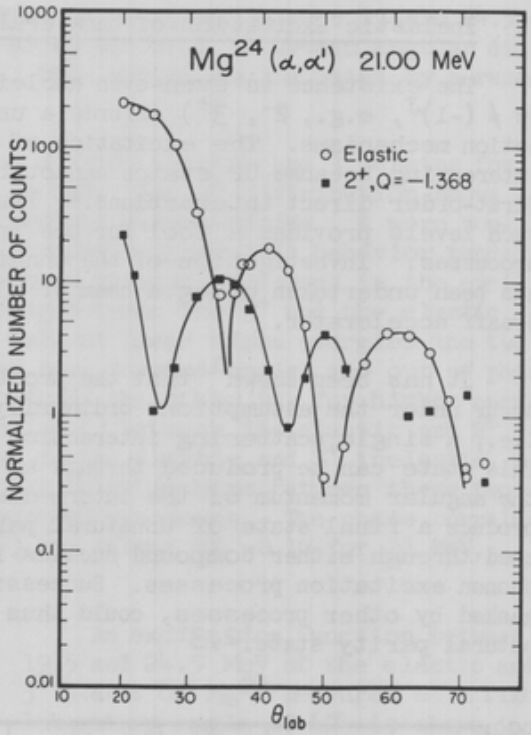

Fig. 6-2 $Mg^{24}(\alpha,\alpha')$ angular distributions at 21.000 MeV for elastic and 2^+ first excited states.

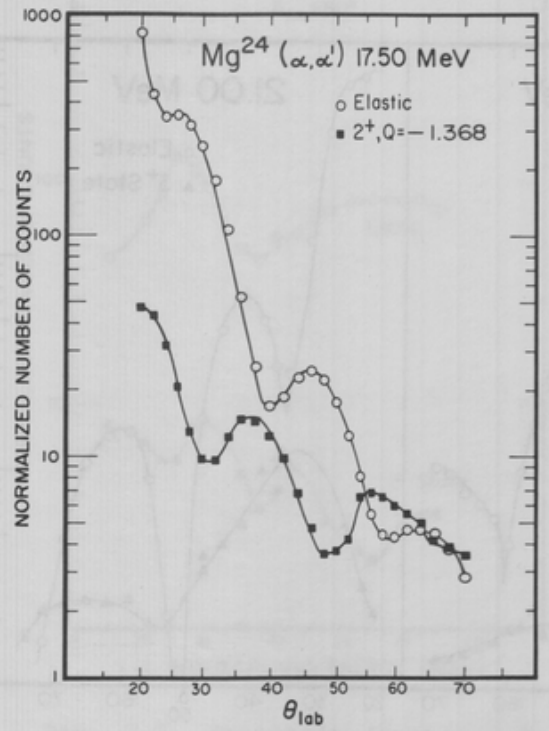

Fig. 6-3 $Mg^{24}(\alpha,\alpha')$ angular distribution at 17.500 MeV for elastic and 2^+ first excited states.

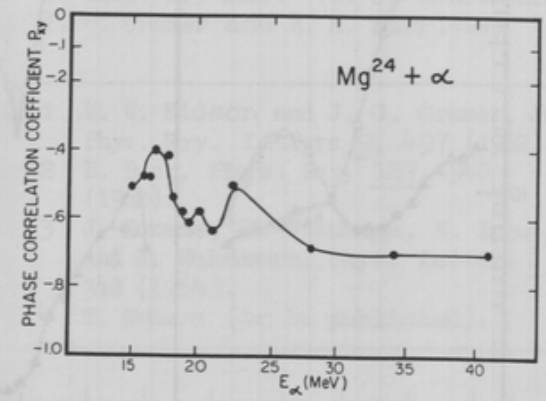

Fig. 6-4 Experimental excitation function of phase correlation coefficient between elastic and 2^+ states for alpha energies between 15 and 41 MeV.

7. Inelastic Excitation of Unnatural Parity States

The existence in even-even nuclei of unnatural parity (UP) states ($\pi \neq (-1)^J$, e.g., 2^-, 3^+) affords a unique opportunity for studying nuclear reaction mechanisms. The excitation of these states by alpha particles is very interesting because UP states cannot be excited in (α,α') scatterings by simple first-order direct interactions.[1] Thus the study of the direct excitation of such levels provides a tool for the investigation of second-order reaction processes. Investigation of the unnatural parity state in $Mg^{24}(3^+, 5.22\ MeV)$ has been undertaken using a beam of alpha particles from the tandem Van de Graaff accelerator.

It has been shown[1] that the production of unnatural parity levels cannot occur under the assumptions ordinarily made in direct interaction calculations, i.e., a single scattering interaction with a single transfer of angular momentum. This state can be produced through an intermediate state, since a coupling of the angular momentum of the intermediate state with that of the final system can produce a final state of unnatural parity. Therefore this excitation can proceed through either compound nucleus formation or non-simultaneous, multiple phonon excitation processes. Successive phonon production, which is normally masked by other processes, could thus be the primary excitation mode of the unnatural parity state.[2,3]

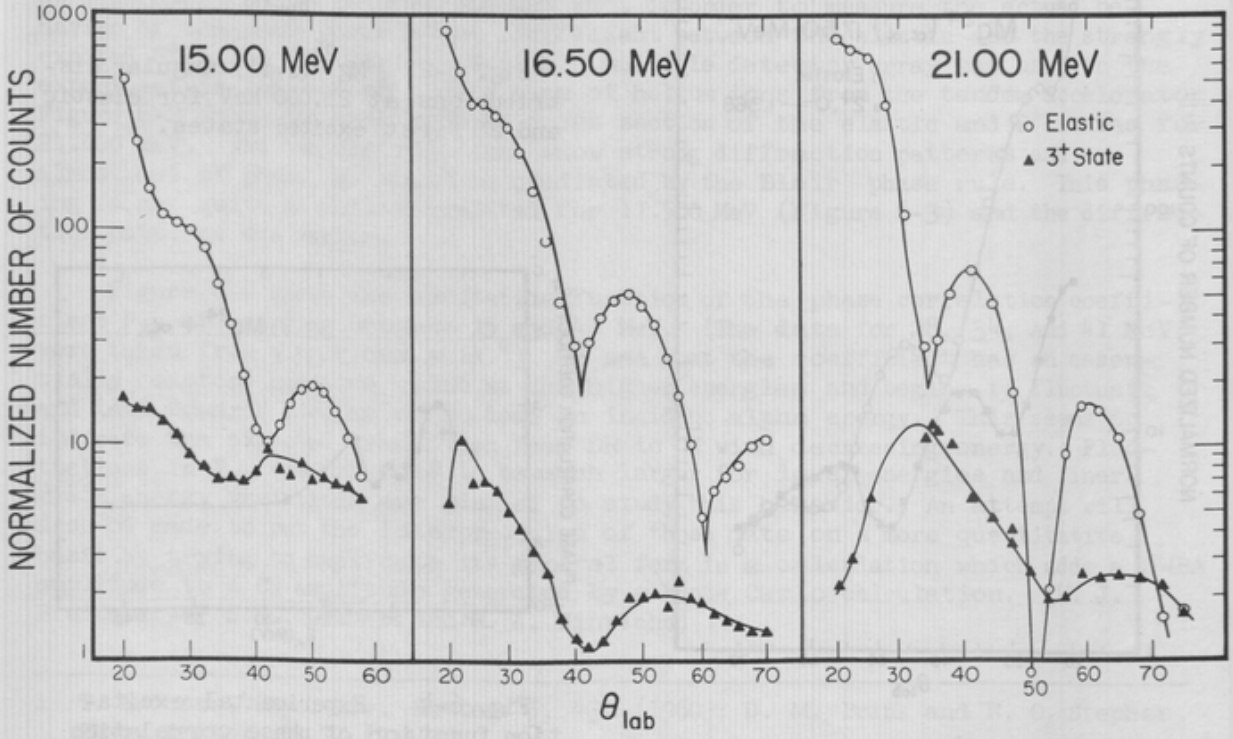

Fig. 7-1 $Mg^{24}(\alpha,\alpha')$ angular distributions of elastic and 3^+ state at 15.00, 16.50, and 21.00 MeV.

The reaction $Mg^{24}(\alpha,\alpha')$ is being studied at energies between 15 and 24.5 MeV. Experimentally, a multiple detector array was used to obtain angular distributions between 20° and 70° in the lab. This choice is indicated by a recent calculation.[4]

Figure 7-1 shows angular distributions for the elastic and 3^+ states for alpha bombarding energies of 15, 16.5 and 21 MeV. The 3^+ distribution shows peaking at forward angles and diffraction pattern maxima-minima. A more complete angular distribution would allow one to say whether this behavior tends to exclude sizeable contributions from compound nucleus processes in the excitation. There is no clear phase relationship between the 3^+ and the elastic distributions. From the analysis done so far, at lower alpha energies the two distributions appear to be in phase for the more forward angles and out of phase as we go back in angle. This relationship tends the other way for higher energies. The work on phase correlations (Section 6) between the elastic and 2^+ angular distributions could also be applied to the elastic and 3^+ inelastic angular distributions. The ill-defined phase relationships between these two states may indicate the predominance of compound processes. The phase correlation function P_{xy} (as defined in Section 6) has values of -0.10 for 21 MeV, -0.32 for 16.5 MeV, and -0.025 for 15 MeV.

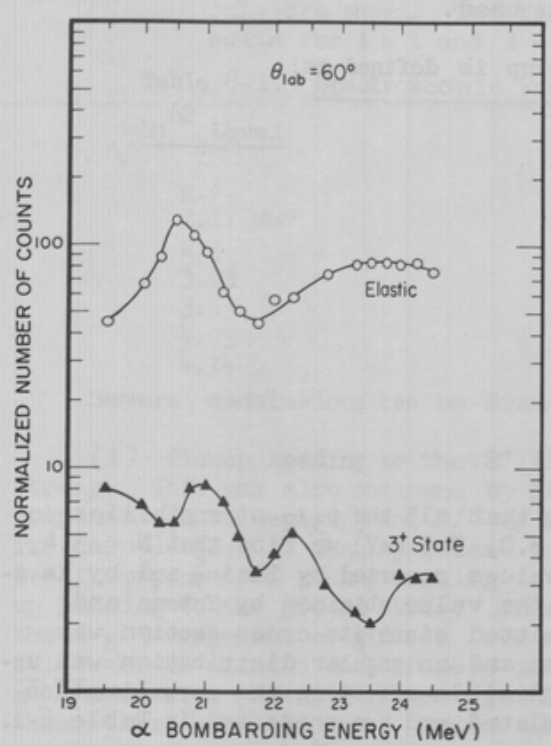

Fig. 7-2 Excitation function of 3^+ state (5.22 MeV) in $Mg^{24}(\alpha,\alpha')$ for bombarding energies between 19.5 and 24.5 MeV at $\theta_{lab} = 60°$.

An excitation function between 19.5 and 24.5 MeV of the elastic and 3^+ states of Mg^{24} measured at a fixed laboratory angle of 60° is shown in Figure 7-2. (Target thickness varies from 290 to 240 keV for the above energy range.) The fairly smooth variation in the elastic values is contrasted with the fluctuations in the 3^+ excitation function. The overall fluctuation width of the 3^+ state is about 1.5 MeV. (W. J. Braithwaite, J. G. Cramer and R. A. Hinrichs)

1 W. W. Eidson and J. G. Cramer, Jr., Phys. Rev. Letters 9, 497 (1962).
2 B. Buck, Phys. Rev. 127, 940 (1962).
3 J. Kokame, K. Fukunaga, N. Ingue, and H. Nakamura, Phys. Letters 8, 342 (1964).
4 T. Tamura (to be published).

II. PICKUP AND STRIPPING REACTIONS

8. The $Cu^{63}(d,He^3)Ni^{62}$ Reaction

Additional data and results have been obtained for the $Cu^{63}(d,He^3)Ni^{62}$ reaction in the region of 3 MeV of excitation.[1] In order to study the He^3 particles with a minimum of background interference it was necessary to use a E-ΔE counter telescope system for detection and a multiplier circuit[2] to discriminate against other particles. An 87 micron thick surface barrier transmission-mounted detector was used as the ΔE detector and an 870 micron thick surface barrier detector as the E detector. The detection system gave a threshold of about 13 MeV. A self-supported, evaporated 250 micrograms/cm^2 thick target of the separated isotope Cu^{63} was used.

Angular distributions for the ground, 1.17 MeV, 2.34 MeV (doublet), 3.03 MeV, 3.53 MeV, 4.03 MeV (complex), and 4.74 MeV (complex) states were taken; the results are shown in Figure 8-1. Distorted-wave Born approximation calculations[3] were made and the results are shown as the solid curves. The deuteron optical model parameters which were used are set D of Perey[4] and the He^3 parameters are those of Blair.[5] A cutoff of 4.87 fermi was used.

The experimental cross section for pickup is defined as:

$$\left(\frac{d\sigma}{d\Omega}\right)_{exp} = \left(\frac{2s_a+1}{2s_b+1}\right) NS_\ell \sigma_\ell \ ,$$

where s_a = spin of He^3,
s_b = spin of deuteron,
S_ℓ = spectroscopic factor,
σ_ℓ = DWBA cross section,
N = normalization constant.

By requiring that $\sum_{\ell=1} S_\ell = 1.0$ and assuming that all the $p_{3/2}$ strength lies in the lowest states (g.s., 1.17, 2.3, 3.0, 3.5 MeV) we find that N = 3.4, which is in reasonable agreement with the values reported by Blair[5] and by Kavaloski, et al.[6], but is in disagreement with the value obtained by Yntema and Satchler.[7] The 0^+ state at 2.05 MeV was omitted since its cross section was much smaller than that of the 3.03 MeV state and an angular distribution was unobtainable. Its omission should have a negligible effect on the normalization constant. Spectroscopic factors were calculated and are presented in Table 8-1.

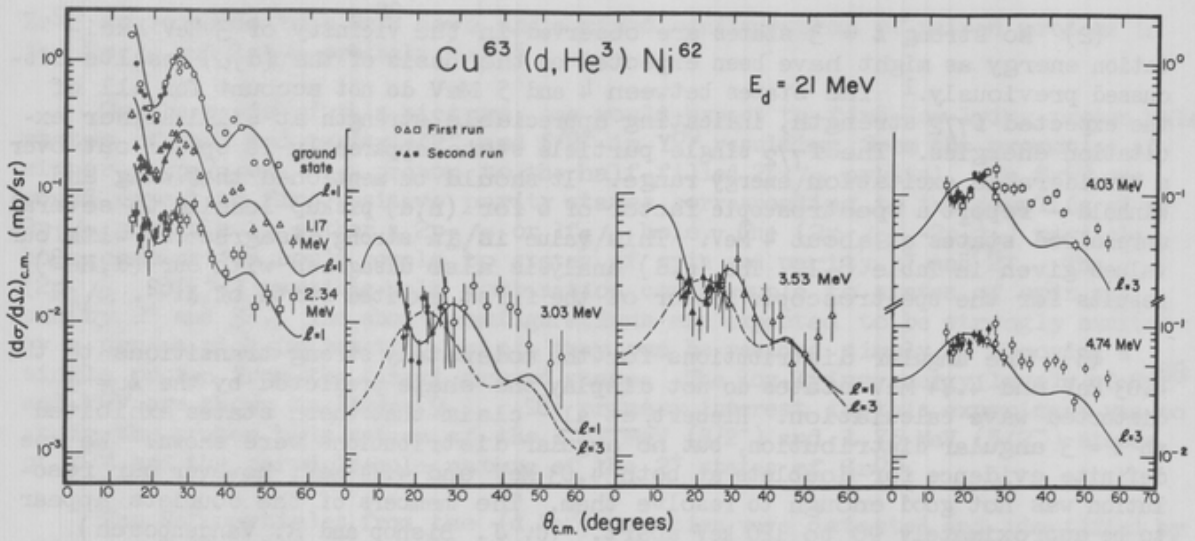

Fig. 8-1 Angular distributions of states in Ni^{62}. Statistical errors only are shown. The full and dashed curves are the DWBA results for $\ell = 1$ and $\ell = 3$ pickup, normalized to the data.

Table 8-1. Spectroscopic Factors for $Cu^{63}(d,He^3)Ni^{62}$ Reaction

Ni^{62} Level	Assumed ℓ	S
g.s.	1	0.70
1.17 MeV	1	0.19
2.3	1	0.067
3.03	1	0.013
3.53	1	0.028
4.03	3	0.17
4.74	3	0.13

Several conclusions can be drawn from the present work.

(1) Pickup leading to the 2^+ first excited state of Ni^{62} is surprisingly strong. This was also observed by Hiebert, et al.,[8] who concluded that the $\ell = 1$ component is between 1/3 and 1/4 as strong as pickup leading to the ground state. The calculations of Thankappan and True[9] predict a ratio of about 1/6 for the $\ell = 1$ component of pickup leading to the first excited state compared with pickup leading to the ground state. There is no conclusive evidence as to whether the $\ell = 3$ component originates from $f_{5/2}$ or $f_{7/2}$ proton pickup. As Hiebert, et al.[8] have pointed out, if $f_{7/2}$ pickup were responsible this would indicate much more $f_{5/2}$ strength in the ground state of Cu^{63} than is indicated in the theoretical calculations.[9] These calculations have assumed an intact $f_{7/2}$ proton shell for the Ni^{62} ground state. (The structure of the 2^+ excited core state is not specified in the calculations). Other evidence for incomplete closure of the $f_{7/2}$ shell has been obtained by Blair[5] who concludes from the $Ni^{62}(He^3,d)Cu^{63}$ reaction that the $f_{7/2}$ shell is 6 per cent empty in Ni^{62}. Earlier qualitative information indicating that the $f_{7/2}$ shell is not a good closed shell has been reported by Yntema.[10]

(2) No strong $\ell = 3$ states are observed in the vicinity of 3 MeV excitation energy as might have been expected on the basis of the (d,α) results discussed previously.[1] The states between 4 and 5 MeV do not account for all of the expected $f_{7/2}$ strength, indicating appreciable strength at still higher excitation energies. The $f_{7/2}$ single particle state apparently is spread out over a considerable excitation energy range. It should be mentioned that Wang and Winhold[11] report a spectroscopic factor of 6 for (n,d) pickup leading to several unresolved states at about 4 MeV. This value is in strong disagreement with our values given in Table 8-1. The (n,d) analysis also disagrees with our (d,He^3) results for the spectroscopic factor of the first excited state of Ni^{62}.

(3) The angular distributions for the moderately strong transitions to the 4.03 MeV and 4.74 MeV states do not display the shape predicted by the $\ell = 3$ distorted wave calculation. Hiebert, et al.[8] claim that these states exhibited an $\ell = 3$ angular distribution, but no angular distributions were shown. We see definite evidence for doublets at both 4.03 MeV and 4.74 MeV; however our resolution was not good enough to resolve them. The members of the doublets appear to be approximately 90 to 120 keV apart. (C. J. Bishop and R. Vandenbosch)

---

1 Nuclear Physics Laboratory Annual Report, University of Washington (1965), p. 31.
2 Ibid., p. 76.
3 R. M. Bassel, R. M. Drisko and G. R. Satchler, Oak Ridge National Laboratory Report ORNL-3240.
4 C. M. Perey and F. G. Perey, Phys. Rev. 132, 755 (1963).
5 A. G. Blair, Phys. Rev. 140, B648 (1965).
6 See Section 9 of this report.
7 J. L. Yntema and G. R. Satchler, Phys. Rev. 134, B976 (1964).
8 J. C. Hiebert, E. Newman and R. H. Bassel, Physics Letters 15, 160 (1965).
9 V. K. Thankappan and W. W. True, Phys. Rev. 137, B793 (1965).
10 J. L. Yntema, Proc. Rutherford Jubilee, Inter. Conf. (1961), p. 521.
11 W. Wang and E. Winhold, Phys. Rev. 140, B882 (1965).

---

9. (d,He^3) Studies on Y^{89} and Zr^{90}

The reactions Zr^{90}(d,He^3)Y^{89*} and Y^{89}(d,He^3)Sr^{88*} have been studied with 21 MeV deuterons in order to investigate the single particle nature of the low-lying states of Y^{89} and Sr^{88}. A previous investigation of the inelastic scattering of alpha particles from Sr^{88} and Y^{89} had suggested that the low-lying positive-parity states in Sr^{88} and the negative-parity states in Y^{89} might correspond to rather simple configurations.[1] Since both of these nuclei have closed neutron shells (N=50), one might expect that their low-lying states could be described mainly by proton configurations only. It was therefore expected that a proton pick-up reaction would be useful in understanding the structure of these states.

In the simple shell model, where only protons are considered, the ground state of Sr^{88} closes the $2p_{3/2}$ subshell. The ground state of Y^{89} corresponds to a Sr^{88} core plus an unpaired proton in the $2p_{1/2}$ orbital. The ground state of

Zr^{90} corresponds to a Sr^{88} core and a mixed configuration of paired protons in the $2p_{1/2}$ and $1g_{9/2}$ orbitals.[2,3,4]

On the basis of this picture, one would expect to find low-lying proton hole states of spin and parity $3/2^-$ and $5/2^-$ in Y^{89} resulting from the promotion of either a $2p_{3/2}$ or $1f_{5/2}$ proton to the half-filled $2p_{1/2}$ orbital. In Sr^{88} one would expect to find positive parity states corresponding to the coupling of a $2p_{1/2}$ particle to either a $2p_{3/2}$ or $1f_{5/2}$ hole. The $(2p_{1/2}\ -2p^{-1}_{3/2})$ particle-hole combination could couple to states of spin and parity 1^+ and 2^+. The $(2p_{1/2}\ -1f^{-1}_{5/2})$ particle-hole combination could couple to states of spin and parity 2^+ and 3^+. The above configurations are expected to be strongly excited by a proton pick-up reaction, since they can be reached simply by removing a single proton from the target ground state. The low-lying energy levels of Sr^{88} and Y^{89} are shown in Figure 9-1. The primary interest in this experiment was to study the proton hole nature of the 1.51 MeV $(3/2^-)$ and 1.75 MeV $(5/2^-)$ states of Y^{89} and the particle-hole nature of the 2^+ states of Sr^{88}.

The He^3 particles from the (d,He^3) reaction were detected and identified by using an E-ΔE solid state detector telescope and an electronic multiplier circuit. A photograph of a typical X-Y scope display of multiplier vs (E+ΔE) outputs for 21 MeV deuterons incident on Y^{89} is shown in Figure 9-2. It may be observed that the He^3 and He^4 groups are clearly separated by the identification system.

Angular distributions were measured for the transitions to the ground state, 0.906, 1.51 and 1.75 MeV states of Y^{89} and to the ground state, 1.84, 3.21, 3.48 and 3.64 MeV states of Sr^{88}. The energies of the 3.48 and 3.64 MeV states of Sr^{88} were measured in this experiment to ±20 keV. They are probably the states

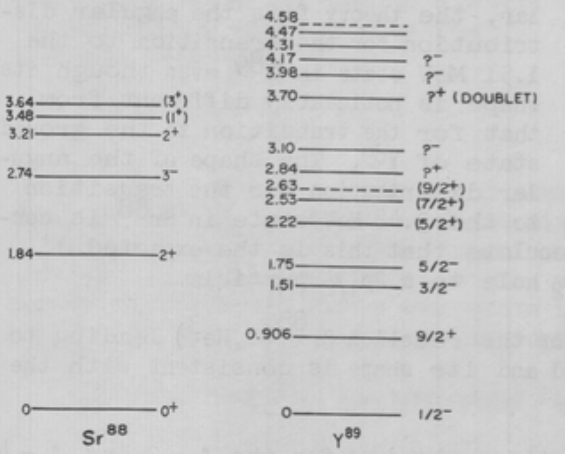

Fig. 9-1 The low-lying energy levels of Sr^{88} and Y^{89}. The energies for all but the 3.64 and 3.48 MeV states in Sr^{88} are from Ref. 1. The spins for the 3.48 and 3.64 MeV states are suggested on the basis of the model discussed in the text.

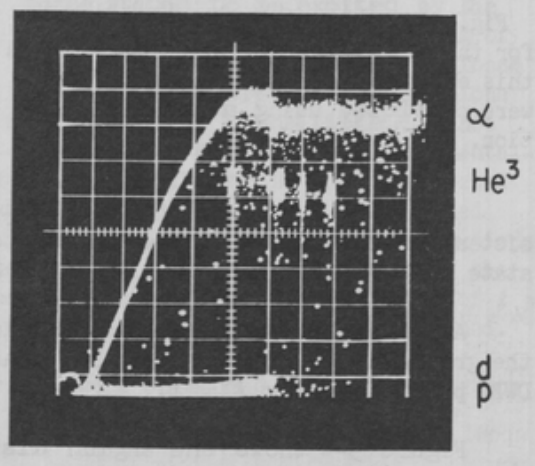

Fig. 9-2 X-Y oscilloscope display of multiplier output (y-axis) versus total energy of particle. Separation of deuteron (extreme bottom of picture), He^3 and He^4 groups is clearly indicated.

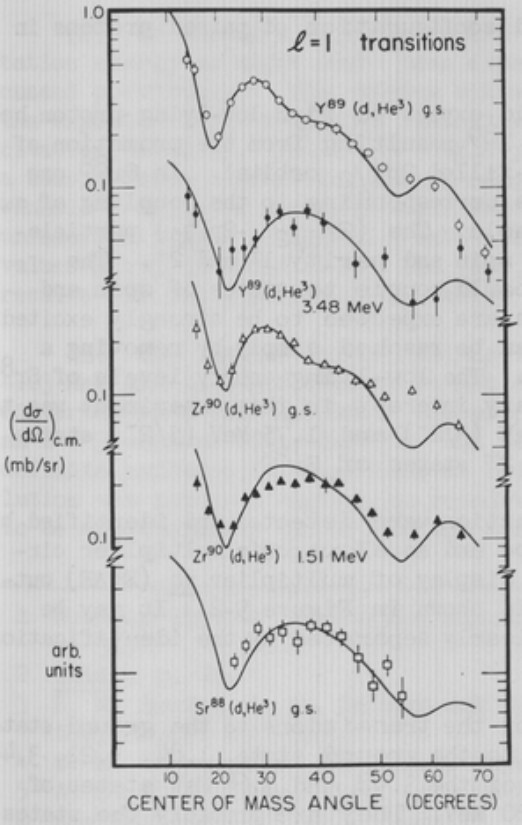

Fig. 9-3 Angular distributions for the $\ell = 1$ transitions observed in this experiment. The solid curves were predicted using a DWBA calculation.

listed in the nuclear data sheets[5] at 3.52 ± 0.05 and 3.68 ± 0.05 MeV.[6] There was no indication of transitions exciting the positive parity states at 2.22 or 2.53 MeV in Y^{89} or the 3^- state at 2.74 MeV in Sr^{88}.

Figure 9-3 shows the angular distributions obtained for the $\ell = 1$ transitions observed in this experiment. The solid curves were calculated using a distorted wave Born approximation (DWBA).[7] Since no optical model parameters were available for this energy and mass region, parameters had to be interpolated from existing studies.[8,9] Because there are several existing sets of parameters which fit elastic scattering data equally well, a choice between them was made by requiring the best fit for the transition to the ground state of Y^{89}. This set of parameters was then used without change for all other transitions. It is seen that the shapes of the angular distributions are fit quite well by the DWBA predictions. In particular, the theory fits the angular distribution for the transition to the 1.51 MeV state in Y^{89} even though its shape is noticeably different from that for the transition to the ground state of Y^{89}. The shape of the angular distribution for the transition to the 3.48 MeV state in Sr^{88} is consistent with pure $\ell = 1$, leading us to speculate that this is the expected 1^+ state arising from the coupling of a $2p_{3/2}$ hole to a $2p_{1/2}$ particle.

A preliminary angular distribution for the reaction $Sr^{88}(d,He^3)$ leading to the ground state of Rb^{87} was also measured and its shape is consistent with the DWBA prediction for $\ell = 1$.

Figure 9-4 shows the angular distributions obtained for the $\ell = 3$ and $\ell = 4$ transitions observed in this experiment. The fits for these transitions are considerably worse than those obtained for the $\ell = 1$ transitions. The poorer quality of the fits will be reflected in an associated uncertainty in the spectroscopic factors which result. On the basis of a comparison to the shape of the known $\ell = 3$ transition to the 1.75 MeV state in Y^{89}, the transition to the 3.64 MeV state in Sr^{88} is assigned $\ell = 3$. The shape of the angular distribution for the 1.75 MeV state in Y^{89} is shown as a dashed curve through the 3.64 MeV data points.

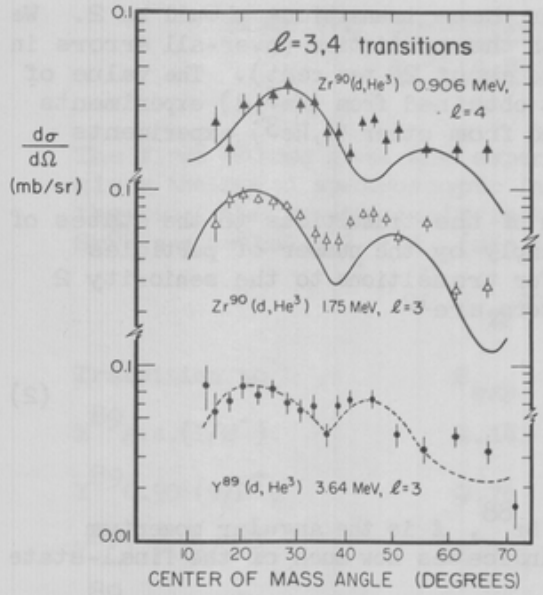

Fig. 9-4 Angular distributions for the $\ell = 3$ and $\ell = 4$ transitions. The solid curves are predictions based on a DWBA calculation. The dashed curve is the experimental shape ($\ell = 3$) of the angular distribution for the transition to the 1.75 MeV state of Y^{89}.

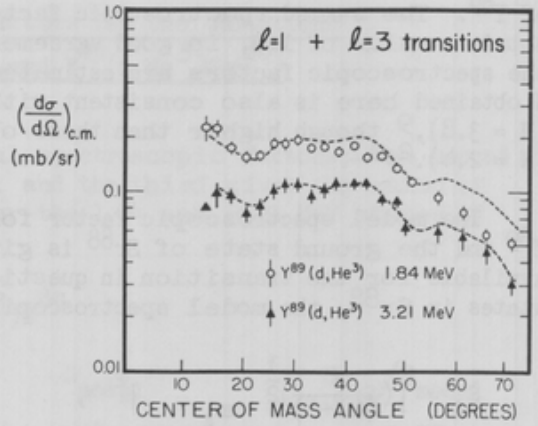

Fig. 9-5 Angular distributions for the mixed $\ell = 1$ and $\ell = 3$ transitions to the 2^+ states in Sr^{88}. The dashed curves are sums of the experimental angular distributions for the $\ell = 1$ and $\ell = 3$ transitions to the excited states of Y^{89}.

Figure 9-5 shows the angular distributions obtained for the transitions to the 1.84 and 3.21 MeV (2^+) states of Sr^{88}. Selection rules allow these states to be excited by the transfer of either 1 or 3 units of angular momentum. As was mentioned above, the theoretical predictions for the $\ell = 3$ transitions did not give a good fit to the experimental data. The summed $\ell = 1$ and $\ell = 3$ theoretical angular distributions reflected this and failed to reproduce these mixed angular distributions. The dashed curves represent sums of the experimental $\ell = 1$ and $\ell = 3$ angular distributions obtained from the transitions to the excited states of Y^{89}. The shape of the summed experimental curves was quite insensitive to the relative amounts of $\ell = 1$ and $\ell = 3$, so that no accurate measure of the mixing ratio could be obtained.

The experimental spectroscopic factors S_ℓ were obtained from the relation

$$\frac{d\sigma}{d\Omega}(d,He^3) = \frac{2}{3} N \Sigma S_\ell \sigma_\ell \quad , \tag{1}$$

where σ_ℓ is the DWBA prediction, ℓ is the angular momentum transfer and N is a constant which contains the overlap of the He^3 nucleus with the proton-plus-deuteron system. If we assume that the transition to the ground state of Sr^{88} has a spectroscopic factor of unity, we obtain N = 3.5. A consistency check of this value is provided by the transitions to the ground and first excited states

of Y^{89}. The summed spectroscopic factors for these transitions should be 2. We obtain a value of 1.9, in good agreement with the prediction (over-all errors in the spectroscopic factors are estimated to be about 20 per cent). The value of N obtained here is also consistent with that obtained from (He^3,d) experiments (N = 3.8),[9] though higher than those obtained from other (d,He^3) experiments (N = 2.4).[2,11]

The model spectroscopic factor for each of the transitions to the states of Y^{89} and the ground state of Sr^{88} is given simply by the number of particles available for the transition in question. For transitions to the seniority 2 states in Sr^{88}, the model spectroscopic factors are[12]

$$S_\ell = \left|\left(\frac{2}{(2J+1)}\right)^{\frac{1}{2}} a_{\ell j_1 j_2}\right|^2 , \qquad (2)$$

where J is the spin of the excited state in Sr^{88}, ℓ is the angular momentum transfer, and $a_{\ell j_1 j_2}$ is a coefficient that indicates how much of the final-state wave function corresponds to a particle-hole pair in the j_1 and j_2 shell model orbitals coupled to a final spin of J. It was assumed that the only particle-hole configurations in the 2^+ states at 1.84 and 3.21 MeV are $(2p_{1/2}, 2p_{3/2}^{-1})$ and $(2p_{1/2}, 1f_{5/2}^{-1})$.

Table 9-1 lists the spectroscopic factors obtained from this experiment. The spectroscopic factors for the transitions to the ground state and the 0.906 MeV state of Y^{89} are in good agreement with those obtained by Yntema[2] who studied these states in a similar experiment. The values obtained imply a 40 per cent admixture of $(1g_{9/2})^2$ configuration in the ground state of Zr^{90}, a value which is consistent with a number of other theoretical and experimental studies.[2,3,4]

The spectroscopic factor for the transition to the 1.51 MeV state of Y^{89} indicates that the configuration of this state is predominantly $2p_{3/2}$ hole in the Zr^{90} ground state. The model spectroscopic factor was calculated assuming that the configuration mixing of the two paired protons between the $2p_{1/2}$ and $1g_{9/2}$ orbitals is the same in this state as in the ground state of Zr^{90}. If this is not true, then the relative amount of proton hole in this state will be increased accordingly. If, for example, there were no configuration mixing between the $2p_{1/2}$ and $1g_{9/2}$ orbitals in the Y^{89} excited state, then the model spectroscopic factor would be 2.4 and the ratio of S_{exp} to S_{model} would be greater than one.

The spectroscopic factor for the 1.75 MeV state indicates that while this state contains a sizeable fraction of the $1f_{5/2}$ hole strength, other configurations are also important.

Since the assumption that the Y^{89}(d,He^3)Sr^{88} transition to the ground state had a spectroscopic factor of unity resulted in an acceptable value for N, it is

Table 9-1. Spectroscopic Factors for the Reactions $Zr^{90}(d,He^3)Y^{89*}$ and $Y^{89}(d,He^3)Sr^{88*}$

The first column gives the experimental spectroscopic factors; the second gives the model spectroscopic factors; and the third gives the ratio of the two. The spectroscopic factors for the 1.84 and 3.21 MeV states of Sr^{88} are actually $S_1 + S_3$ (see text).

$Zr^{90}(d,He^3)Y^{89}$

Transition to	S_{exp}	S_{model}	S_{exp}/S_{model}
Y^{89} g.s.$(1/2^-)$	1.14	2	0.57
Y^{89} 0.906$(9/2^+)$	0.76	2	0.38
Y^{89} 1.51$(3/2^-)$	2.7	4	0.67
Y^{89} 1.75$(5/2^-)$	1.9	6	0.32

$Y^{89}(d,He^3)Sr^{88}$

Sr^{88} g.s.(0^+)	1.0	1.0	1.0
Sr^{88} 1.84(2^+)	2.1	2.5	0.84
Sr^{88} 3.21(2^+)	2.0	2.5	0.80
Sr^{88} 3.48$(1^+?)$	1.6	1.50	1.1
Sr^{88} 3.64$(3^+?)$	1.95	3.5	0.55

concluded that the underlying assumption is reasonable. That is, there is no appreciable configuration mixing involving the $2p_{1/2}$ proton orbital in the ground state of Sr^{88}.

The values for S_1 and S_3 for the transitions to the 2^+ states of Sr^{88} could not be extracted separately with any degree of accuracy, as has been remarked above. However, the sum of S_1 and S_3 was quite insensitive to the relative magnitudes of S_1 and S_3. The value of S_1 plus S_3 given in Table 9-1 indicate that approximately 80 per cent of the wave function for these 2^+ states contain a $2p_{1/2}$ proton coupled to a $2p_{3/2}$ hole or a $1f_{5/2}$ hole.

The spins shown for the 3.48 and 3.64 MeV states of Sr^{88} are suggestions only, based on the predictions of the coupling model proposed here. Other work[13]

suggests that a 2^+ state exists at about 3.6 MeV. Our results cannot rule out the assignment of spin 2 to either of these two states.

The results of the experiments on Zr^{90} and Y^{89} have been reported[14] and a paper is in preparation. Work is continuing on the study of the $Sr^{88}(d,He^3)$ reaction in order to test the conclusions drawn here. (C. D. Kavaloski, J. S. Lilley, D. C. Shreve and Nelson Stein)

1 J. Alster, D. C. Shreve, and R. J. Peterson, Phys. Rev. 144, 999 (1966).
2 J. L. Yntema, Phys. Letters 11, 140 (1964).
3 B. Bayman, A. S. Reiner, and R. K. Sheline, Phys. Rev. 115, 1627 (1959).
4 S. Cohen, R. D. Lawson, M. H. MacFarlane, and M. Soga, Phys. Letters 10, 195 (1964).
5 Nuclear Data Tables compiled by K. Way et al. (Printing and Publications Office, National Academy of Sciences - National Research Council, Washington 25, D.C.), NRC 61-3-51.
6 N. H. Lazar, E. Eichler, and G. D. O'Kelley, Phys. Rev. 101, 727 (1956).
7 R. H. Bassel, R. M. Drisko, and G. R. Satchler, Oak Ridge National Laboratory Report ORNL-3240 (1962).
8 C. M. Perey and F. G. Perey, Phys. Rev. 132, 775 (1963).
9 R. W. Klingsmith, H. J. Hausman, and W. D. Ploughe, Phys. Rev. 134, B1220 (1964).
10 A. G. Blair, Phys. Rev. 140, B648 (1965).
11 J. L. Yntema and G. R. Satchler, Phys. Rev. 134, B976 (1964).
12 S. Yoshida, Nucl. Phys. 38, 380 (1962).
13 M. M. Stautberg, J. J. Kraushaar, and B. W. Ridley, Bull. Am. Phys. Soc. 11, 119 (1966).
14 D. C. Shreve, C. D. Kavaloski, J. S. Lilley and Nelson Stein, Bull. Am. Phys. Soc. 11, 118 (1966).

10. (α,t) Reactions in the Lead Region

The $Pb^{208}(\alpha,t)Bi^{209}$ measurements reported in the 1965 Annual Report[1] have been extended and a distorted-wave Born approximation (DWBA) analysis has been made based on a proton-stripping mechanism to identify the proton states in Bi^{209}.

The experimental procedure followed closely that described earlier.[1] The over-all energy resolution of 130 keV was better than the previously-obtained 170 keV. The elastic α-particle scattering was measured simultaneously with the triton spectra by simply setting the appropriate electronic window to accept 42 MeV pulses. In addition, a Faraday cup and a fixed-angle monitor detector gave continuous checks on the integrated beam hitting the target. All these measurements were consistent and reproducible to between 2 and 3 per cent. This degree of accuracy in the data was needed in order that the weak oscillatory structure in the angular distributions could be shown.

Measurements were also taken for angles less than 30°, where structure characteristic of angular momentum transfer was expected to be more pronounced

than in the 30° to 70° region studied previously. An aluminum degrader was placed before the dE/dx detector at these small angles to stop the intense flux of elastically scattered α-particles. This worsened the resolution to approximately 300 keV, but, knowing the Q-values of the levels excited, it was possible to extract all the peaks of interest from the energy spectra.

Angular distributions were taken at 2 degree intervals between 10° and 62° and then at 70°, 80° and 90°. In the region of overlap excellent agreement was obtained with the earlier data. Comparison of the elastic data with previous measurements[2] of elastic cross sections gave an accurate normalization for the (α,t) results. The levels excited strongly in $Pb^{208}(\alpha,t)Bi^{209}$ are: the ground state ($9/2^-$), 0.90 ($7/2^-$), 1.61 ($13/2^+$), 2.61, 2.84, and 3.15 MeV states of Bi^{209}. Angular distributions are shown in Figures 10-1 to 10-5.

DWBA fits to these distributions were made using "DRC", a computer code originally written by W. R. Gibbs and W. Tobocman. Since the 0.90 MeV state is known to have spin and parity $7/2^-$, we assume it to be the $f_{7/2}$ single proton state with spectroscopic factor S=1. The angular distribution was fit with DRC to obtain a normalization factor and sets of parameters for the bound-state function and triton distorted waves. The binding energy for the bound-state function was taken to be the proton separation energy. No spin-orbit force was used in calculating either the bound-state function or the distorted waves. No lower cut-off was used, although it was noticed that this had little effect up to 8 fermis, which is approximately equal to the nuclear radius. Optical parameters for the incident waves were obtained by fitting the elastic α-particle scattering data. Since triton data are not available the triton parameters were considered free and were varied to give a good fit to the 0.90 MeV results, as shown in Figure 10-1.

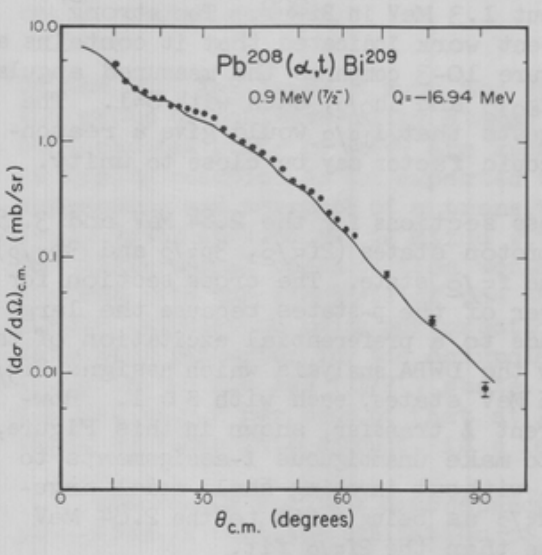

Fig. 10-1 Angular distribution for $Pb^{208}(\alpha,t)Bi^{209}$ to the 0.90 MeV ($7/2^-$) state. Solid curve is a DWBA calculation for transfer of a $2f_{7/2}$ proton.

No further adjustments were made to calculate fits to the ground state, 1.61, 2.84 and 3.15 MeV distributions. The appropriate binding energy, Q-value and quantum numbers for the bound state function were used. All other parameters were held fixed, including the normalization factor given by the $f_{7/2}$ fit.

As can be seen from Figure 10-2, an $h_{9/2}$ calculation gives a good fit to the ground state distribution with a spectroscopic factor of unity. This, together with the fit to the 0.90 MeV differential cross section, is good evidence supporting the validity of a DWBA analysis for these data, since the ground state of Bi^{209} has spin and parity $9/2^-$ and should be well described as a rather pure $h_{9/2}$ proton state.

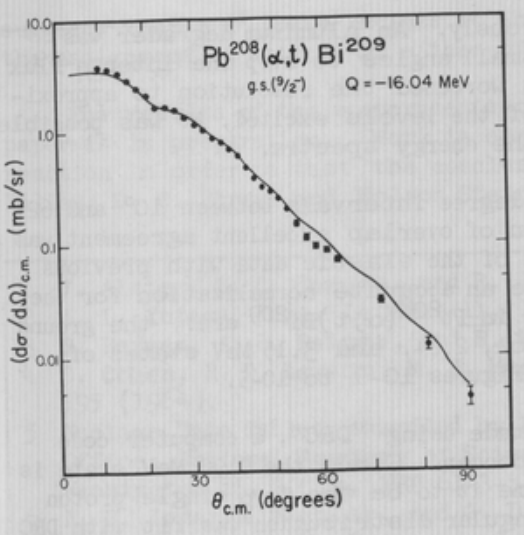

Fig. 10-2 Angular distribution for $Pb^{208}(\alpha,t)Bi^{209}$ to the ground state $(9/2^-)$. The solid curve is a DWBA calculation for transfer of a $h_{9/2}$ proton.

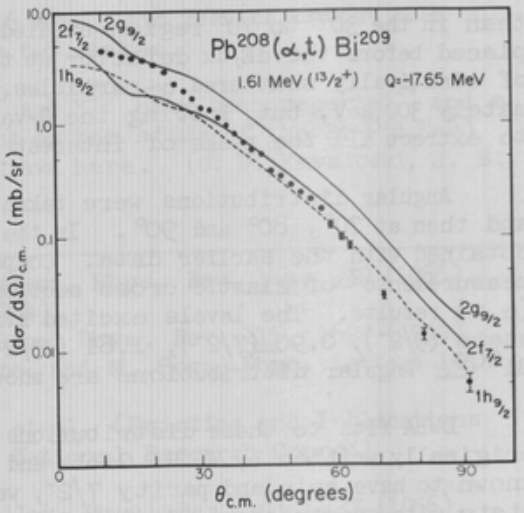

Fig. 10-3 Angular distribution for $Pb^{208}(\alpha,t)Bi^{209}$ to the 1.61 MeV $(13/2^+)$ state. The solid curves are DWBA calculations for transfer of a $2g_{9/2}$, $2f_{7/2}$ and $h_{9/2}$ proton.

Since the DWBA code would not run for an angular momentum transfer $\ell = 6$, it was not possible to confirm that the 1.61 MeV level is the $i_{13/2}$ proton state. This assignment is based on shell model calculations[3] which predict the $i_{13/2}$ state to lie at an excitation energy of about 1.3 MeV in Bi^{209}. The strong excitation of the 1.6 MeV level in the present work indicates that it contains a great deal of single-proton strengths. Figure 10-3 compares the measured angular distribution with calculations for $2f_{7/2}$, $2g_{9/2}$ and $1h_{9/2}$, each with S=1. The increasing steepness with increasing ℓ suggests that $i_{13/2}$ would give a reasonable fit to the data and that the spectroscopic factor may be close to unity.

Figure 10-4 shows the differential cross sections for the 2.84 MeV and 3.15 MeV levels. Of the remaining shell model proton states ($2f_{5/2}$, $3p_{3/2}$ and $3p_{1/2}$), the strong level at 2.84 MeV is probably the $f_{5/2}$ state. The cross section for this is expected to be higher than for either of the p-states because the large momentum mismatch in the (α,t) reaction leads to a preferential excitation of the higher ℓ-states. This is well confirmed by the DWBA analysis which assigns $2f_{5/2}$ and $3p_{3/2}$ respectively to the 2.84 and 3.15 MeV states, each with $S \cong 1$. However, several other calculations for different ℓ transfer, shown in this Figure, illustrate how difficult it is in general to make unambiguous ℓ-assignments to (α,t) angular distributions. For instance, without invoking shell model arguments it would be impossible to rule out $3d_{5/2}$ as being a fit to the 2.84 MeV distribution since it is only slightly worse than the $2f_{5/2}$ fit.

The level excited at 2.61 MeV is not thought to be a single-proton state since the only one unaccounted for is the $3p_{1/2}$ and this is expected to lie above the $3p_{3/2}$ state found at 3.15 MeV. Furthermore, the angular distribution

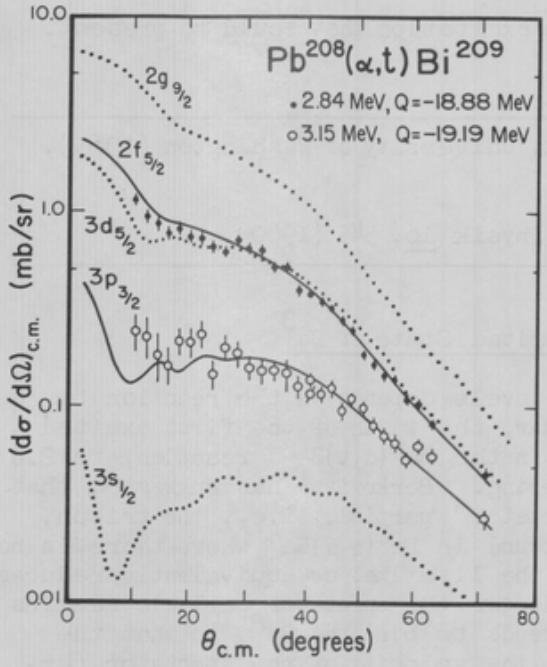

Fig. 10-4 Angular distributions for $Pb^{208}(\alpha,t)Bi^{209}$ to the 2.84 and 3.15 MeV states. Solid and dotted curves are DWBA calculations for transfer of a proton with the indicated quantum numbers.

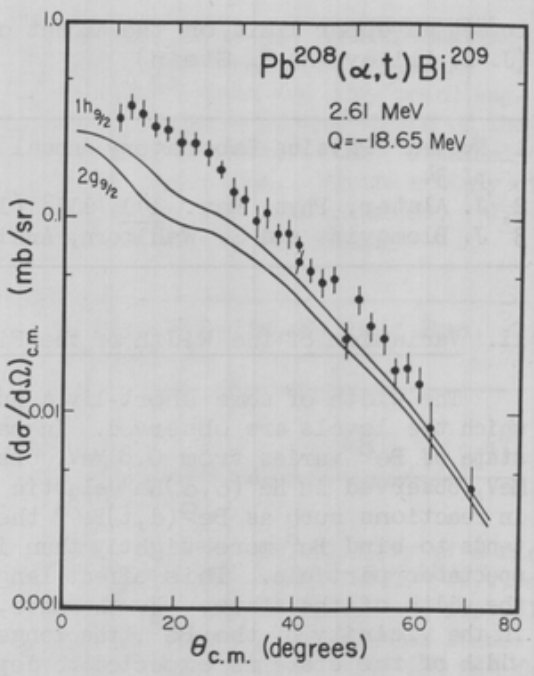

Fig. 10-5 Angular distribution for $Pb^{208}(\alpha,t)Bi^{209}$ to the 2.61 MeV state. The solid curves are DWBA calculations for transfer of a $h_{9/2}$ and $2g_{9/2}$ proton.

of the 2.61 MeV level is much too steep to be fitted by an $\ell = 1$ transition. The group of positive parity states formed by coupling the $h_{9/2}$ proton to the 3^- core-excited state of Pb^{208} are known to lie close together near 2.6 MeV.[2] A stripping reaction is not expected to excite the core strongly. However, the appearance and strength of a transition to 2.61 MeV might be expected if the $i_{13/2}$ level at 1.61 MeV is mixed with the $13/2^+$ component of the 2.6 MeV group. The differential cross section would be characteristic of $\ell = 6$ and this is consistent with the steepness of the observed distribution (See Figure 10-5). A simple calculation using perturbation theory and the known value of β, the deformation parameter for the octupole state, predicts a 14 per cent admixture of $i_{13/2}$ in the 2.6 MeV ($13/2^+$) state. This leads to a relative cross section at 2.6 MeV only 2 per cent of that at 1.61 MeV which, after the dependence on Q-value is taken into account, is a factor of four smaller than the observed ratio.

The reason for this discrepancy is not fully understood. One possible explanation is that the excitation of the core, even though it is weak in this reaction, is enough to account for the missing strength. One would then expect to similarly excite a state in Po^{210} near 2.6 MeV in the $Bi^{209}(\alpha,t)Po^{210}$. Experimentally there is no evidence for a state at 2.6 MeV as strong as that seen in the $Pb^{208}(\alpha,t)Bi^{209}$ reaction. However, strongly excited groups of states partly overlap the region of interest and the data are being carefully reanalyzed

to set an upper limit on the amount of core excitation that could be present. (J. S. Lilley and N. Stein)

---

1 Nuclear Physics Laboratory Annual Report, University of Washington (1965), p. 34.
2 J. Alster, Phys. Rev. 141, 1138 (1966).
3 J. Blomqvist and S. Wahlborn, Arkiv For Physik 16, 545 (1960).

---

11. Variation of the Width of the First Excited State of Be^8

The width of some short-lived nuclear levels depends on the reaction by which the levels are observed. In particular, the width of the first excited state of Be^8 varies from 0.8 MeV, observed in the $Be^9(d,t)Be^{8*}$ reaction, to 2.0 MeV, observed in $He^4(\alpha,\alpha)He^4$ elastic scattering. Berkowitz[1] has suggested that in reactions such as $Be^9(d,t)Be^{8*}$ the "spectator" particle, i.e., the triton, tends to bind Be^8 more tightly than it is bound in $He^4(\alpha,\alpha)He^4$ where there is no spectator particle. This effect lengthens the lifetime, or equivalently reduces the width of the state. Furthermore, the longer the spectator particle remains in the vicinity of the Be^8, the longer it tends to bind the Be^8, so that the width of the state is expected to depend on the velocity of the spectator particle.

To give evidence of this velocity dependence, Berkowitz collected data from ten different reactions, each of which gave Be^{8*} and a spectator particle in the final state. He plotted the asymptotic velocity of the spectator particle versus $1/\Gamma - 1/\Gamma_0$ where Γ is the width observed in the reaction, and Γ_0 is the width observed in $He^4(\alpha,\alpha)He^4$ elastic scattering. The principal features of his graph are shown in Figure 11-1. Solid triangles show the data, and the dotted line suggests the velocity dependence.

In the measurements available to Berkowitz the width of the state had been measured at essentially a single velocity for each reaction. In no case had the spectator velocity for a given reaction been varied over a wide range. An obvious, but simple test of the velocity dependence shown by the dotted line in Figure 11-1 is to determine if the width varies as a function of spectator velocity for a single reaction.

The $Be^9(p,d)Be^{8*}$ reaction was selected as the first reaction to be tested. A thin target of Be^9 was bombarded with 7.5 to 15 MeV protons. Deuteron spectra were obtained with a ΔE-E particle identification system. The spectra, which were taken at a laboratory angle of 30°, showed a broad, well separated peak corresponding to the 2.9 MeV first excited state of Be^8, as well as a narrow ground state group.

Preliminary analysis of the data shows that there is no significant variation in the width of the state, even though the spectator velocity was changed by a factor of 1.6. The open circles plotted in Figure 11-1 give values of $[(1/\Gamma) - (1/\Gamma_0)]$ derived from the data.

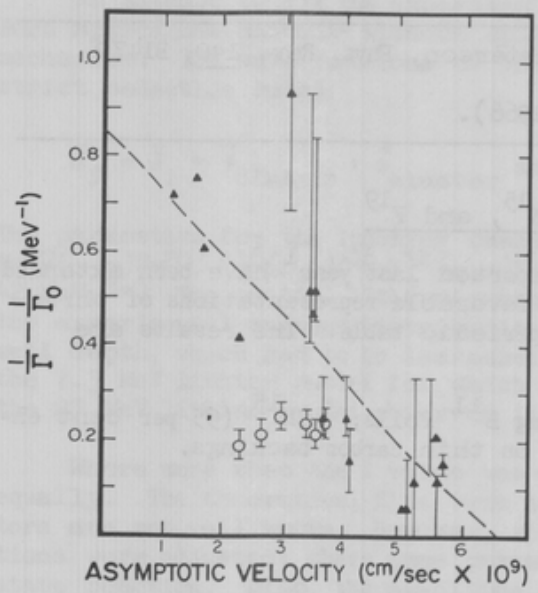

Fig. 11-1 Dependence of the width of the first excited states of Be^8 on the asymptotic velocity of the spectator particle.

with a minor exception the large, negative (oxygen, carbon, and other isotopes of Ca) was the first and second excited states of much of a problem.

There is as yet no explanation for the disagreement between the $Be^9(p,d)Be^{8*}$ data and the trend suggested by values of the width of the first excited state of Be^8 obtained in other reactions. Further study of this problem has been planned. (J. Alster and W. G. Weitkamp)

---

1 E. H. Berkowitz, Nuclear Phys. 60, 555 (1964).

---

12. A Survey of the $Ca^{48}(d,t)\,Ca^{47}$ Reaction

Due to the availability of a rare Ca^{48} target[1] the reaction $Ca^{48}(d,t)Ca^{47}$ was studied. The purpose was two-fold: (1) to investigate the ground state configuration of Ca^{48}, and (2) to make a survey of the energy levels in Ca^{47} that can be excited by a pick-up reaction mechanism. The Q value for this reaction is -3.7 MeV; therefore Q values of prominent contaminants kept the spectra clean. The exception $C^{13}(d,t)C^{12}$, but these did not cause

The target, consisting of 97 micrograms/cm^2 of Ca^{48} (isotopic purity 95.6 per cent) on a 100 microgram/cm^2 carbon backing, was bombarded with 200 to 500 nanoamperes of 16 MeV protons from the Van de Graaff accelerator. The particle detection system consisted of two solid state detectors (an E and a dE/dx detector) with a combined resolution of 140 keV, and the conventional dE/dx-E multiplier arrangement.

The counting rates were very low, resulting in poor statistics. Energy levels were observed at the Ca^{47} ground state, and at 1.99, 2.59, 2.87, 3.29, 3.42, 3.95, and 4.44 MeV. These correspond to levels observed[2] in Ca^{47} in the reaction $Ca^{46}(d,p)Ca^{47}$, where (using 12 keV resolution) levels were seen at ground state, 2.017, 2.58, 2.60, 2.84, 2.87, 3.294, 3.425, 4.019, 4.057, 4.103, and 4.402 MeV. Angular distributions were taken for the transition to the ground state and to the 2.59 MeV level; both showed some structure. An attempt is now being made to fit these angular distributions with an optical model code. The poor statistics prohibited the determination of the ground state configuration mixing in Ca^{48}. (G. Chenevert)

1 The same target used by Peterson [R. J. Peterson, Phys. Rev. 140, B1479 (1965)].
2 T. Belote et al., Phys. Rev. 142, B624 (1966).

13. (α,Li^6) and (α,Li^7) Reactions on B^{11}, N^{15}, and F^{19}

(α,Li^6) and (α,Li^7) reactions on F^{19} reported last year[1] have been extended to N^{15} and B^{11}. All three nuclei should be favorable representations of three nucleon "clustering" in this region of the periodic table. The results are shown in Figures 13-1 through 13-6.

The targets consisted of self-supporting B^{11} foils; KCN^{15} (95 per cent enriched N^{15}) and CaF_2, which were evaporated on thin carbon backings.

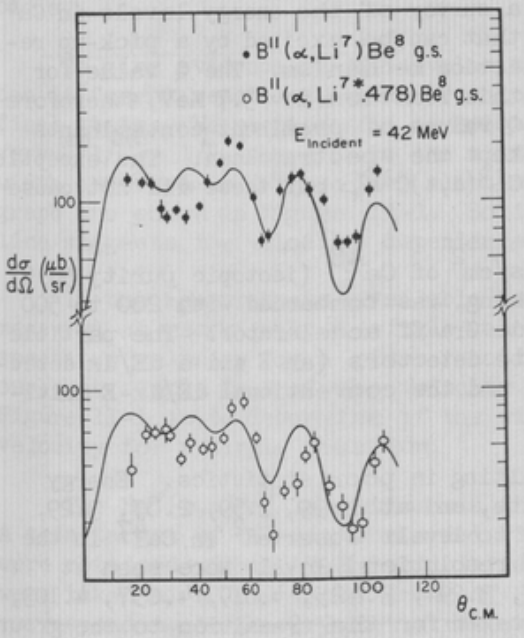

Fig. 13-1 Angular distributions of Li^7 g.s. and Li^7 first excited state from $B^{11}(\alpha,Li^7)$ reactions leading to the ground state of Be^8. The solid curves are the predicted angular distributions using an $\ell = 1$ bound state wave function for the triton.

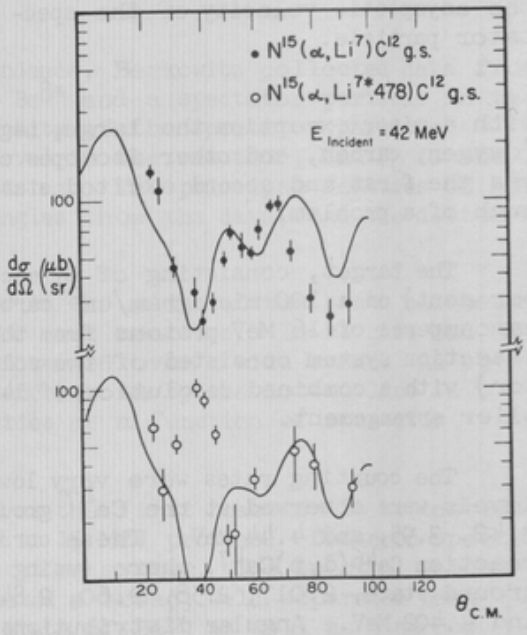

Fig. 13-2 Angular distributions for the reactions $N^{15}(\alpha,Li^7$ g.s.) and $N^{15}(\alpha,Li^7$ first excited state) proceeding to the ground state of C^{12}. The solid curves were calculated for an $\ell = 1$ bound state wave function.

An attempt to fit the experimental data was made using a Distorted Wave Born Approximation code[2] without spin-orbit and assuming a one-cluster pick-up mechanism. The wave functions of the bound clusters were determined by the strict selection rules:

$$\vec{J}_f = \vec{J}_i + \vec{\ell}_{cluster} + \vec{s}_{cluster} \text{ and } \pi_f = \pi_i (-1)^{\ell_{cluster}}.$$

The parameters for the incoming channel were obtained by reasonable fits to $Ne^{20}(\alpha,\alpha)Ne^{20}$, $O^{16}(\alpha,\alpha)O^{16}$, $N^{14}(\alpha,\alpha)N^{14}$, and $C^{12}(\alpha,\alpha)C^{12}$ elastic scattering at 42 MeV.[3-5] The initial lithium parameters[6] had to be adjusted slightly to fit the experimental angular distributions. The largest change was the imaginary well depth, which had to be decreased. This is consistent with the change from the 7.3 MeV lithium nuclei for which the original parameters were calculated to the 25 MeV lithium nuclei observed in these reactions.

Where more than one ℓ value was allowed, the two amplitudes were added equally. The theoretical fits were adjusted by eye because the parentage factors are not well known. However, when the Li^7 ground state angular distributions were adjusted, these same parameters were used for the Li^7 first excited state reaction. Also, the magnitude of the Li^7 first excited state angular distribution was one-half of the Li^7 ground state predicted distribution due to the final spin factor. This assumes the ratio of parentage factors for Li^7 ground state and Li^7 first excited state to be one. This was found to be the case for the two B^{11} reactions. (J. B. Gerhart, P. Mizera and F. Slee)

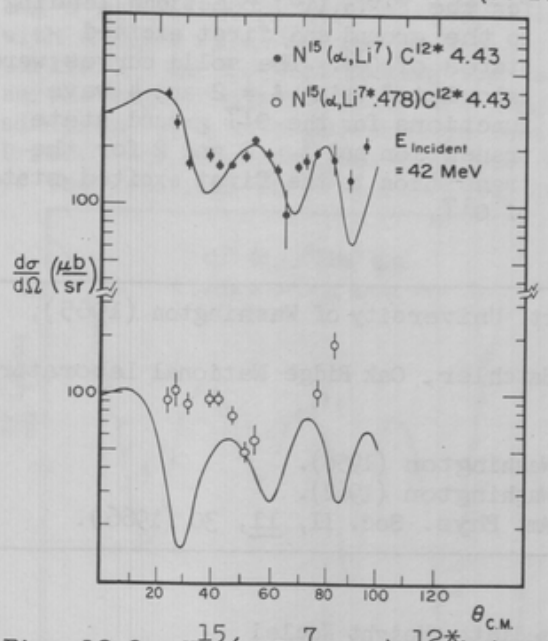

Fig. 13-3 $N^{15}(\alpha,Li^7$ g.s.)C^{12*}4.43 and $N^{15}(\alpha,Li^{7*}0.478)C^{12*}4.43$ angular distributions. The selections rules allow $\ell = 1$ and $\ell = 3$ for the distorted wave calculations as shown in the solid curves.

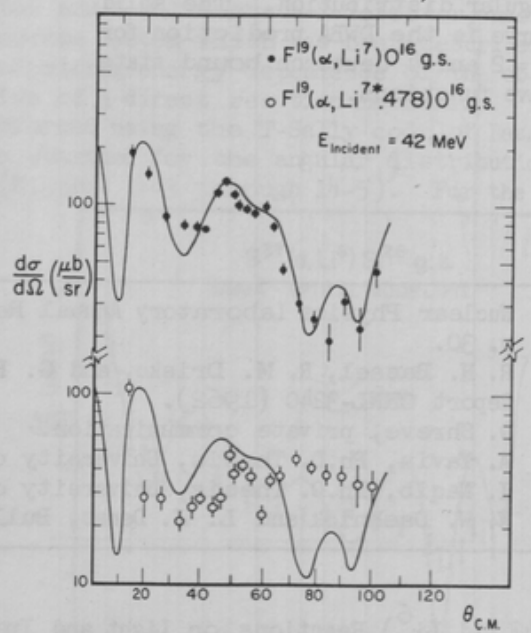

Fig. 13-4 The solid curves are the predicted angular distributions using an $\ell = 0$ bound state wave function for the reactions $F^{19}(\alpha,Li^7$ g.s.) and $F^{19}(\alpha,Li^{7*}0.478)$ proceeding to the ground state of O^{16}.

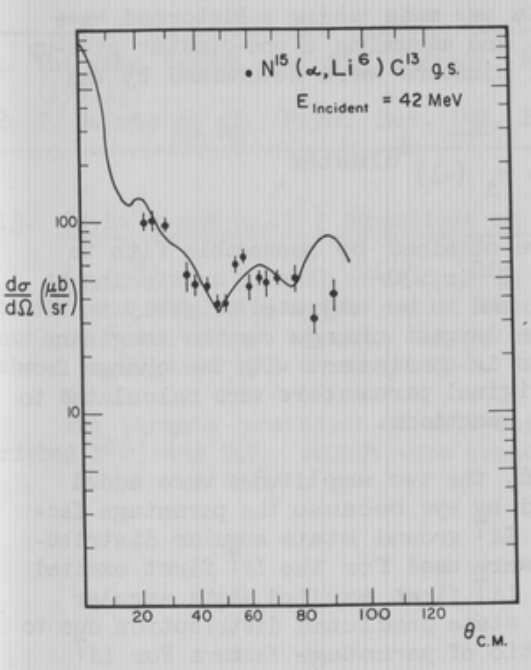

Fig. 13-5 $N^{15}(\alpha,Li^6)C^{13}$ g.s. angular distribution. The solid curve is the DWBA prediction for $\ell = 2$ and 4 deuteron bound state wave functions.

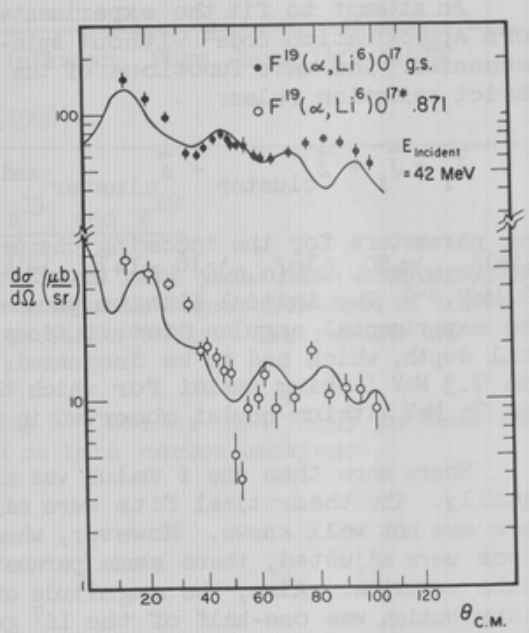

Fig. 13-6 Angular distribution for the $F^{19}(\alpha,Li^6)$ reactions leading to the ground and first excited states of O^{17}. The solid curves were calculated using $\ell = 2$ and 4 wave functions for the O^{17} ground state transition and $\ell = 0$ and 2 for the transition to the first excited state of O^{17}.

1 Nuclear Physics Laboratory Annual Report, University of Washington (1965), p. 30.
2 R. H. Bassel, R. M. Drisko, and G. R. Satchler, Oak Ridge National Laboratory Report ORNL-3240 (1962).
3 D. Shreve, private communication.
4 A. Yavin, Ph.D. Thesis, University of Washington (1958).
5 I. Naqib, Ph.D. Thesis, University of Washington (1962).
6 W. W. Daehnick and L. J. Denes, Bull. Am. Phys. Soc. II, 11, 30 (1966).

14. (d,Li^6) Reactions on Light and Intermediate Weight Nuclei

In our investigation of (d,Li^6) reactions at 21 MeV incident deuteron energy, we have obtained angular distributions for the reactions $Mg^{24}(d,Li^6)Ne^{20}$ and $Ni^{58}(d,Li^6)Fe^{54}$ (Figures 14-1 and -2) in addition to the angular distributions for the reactions $C^{12}(d,Li^6)Be^8$, $O^{16}(d,Li^6)C^{12}$, $F^{19}(d,Li^6)N^{15}$, $S^{32}(d,Li^6)Si^{28}$, and $Ca^{40}(d,Li^6)Ar^{36}$ which have been reported earlier.[1] Particle detection and

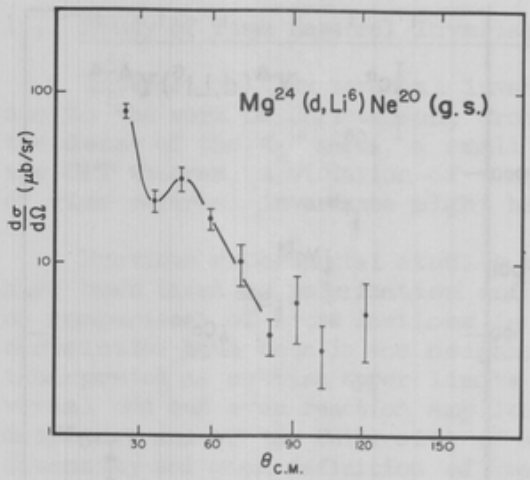

Fig. 14-1 Angular distribution for the reaction $Mg^{24}(d,Li^{6})Ne^{20}$ (g.s.)

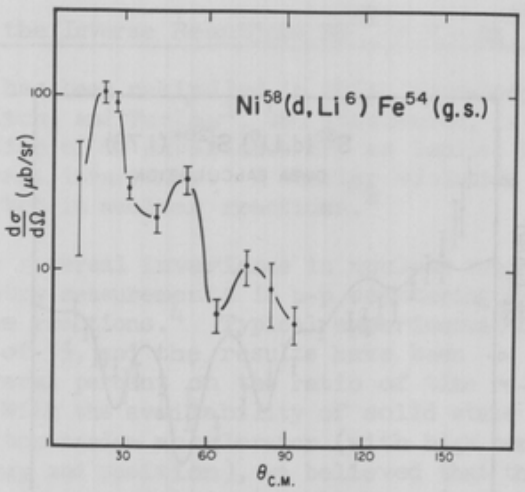

Fig. 14-2 Angular distribution for the reaction $Ni^{58}(d,Li^{6})Fe^{54}$ (g.s.)

identification were accomplished by means of an E - ΔE counter telescope employing a gas-filled proportional dE/dx counter and a solid state E detector, used with a pulse stretcher and an x-y oscilloscope system which has been described earlier.[2] The forward peaking and lack of strong energy dependence of the observed angular distributions are suggestive of a direct reaction mechanism. In addition, DWBA calculations have been performed using the T-Sally code of Bassel, Drisco, and Satchler[3], and fits have been obtained for the angular distributions of the reactions on C^{12} and S^{32} targets (Figures 14-3 through 14-5). For the

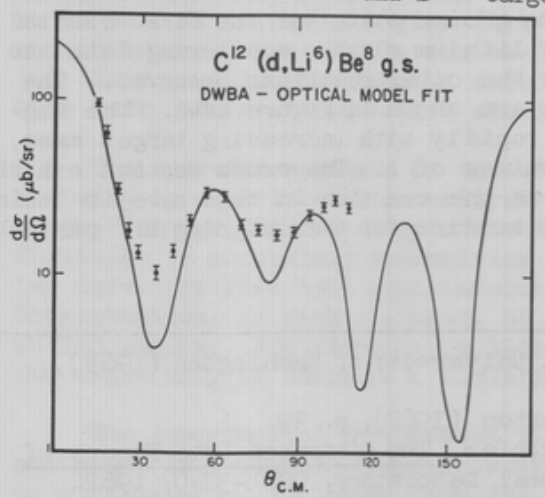

Fig. 14-3 Angular distribution for the reaction $C^{12}(d,Li^{6})Be^{8}$ (g.s.) with DWBA fit.

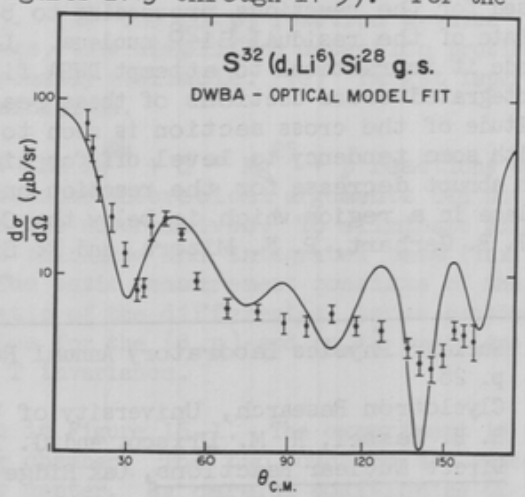

Fig. 14-4 Angular distribution for the reaction $S^{32}(d,Li^{6})Si^{28}$ (g.s.) with DWBA fit.

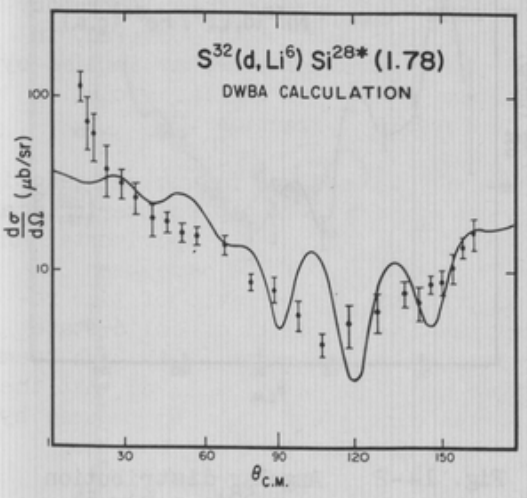

Fig. 14-5 Angular distribution for the reaction $S^{32}(d,Li^6)Si^{28}(1.78)$ with DWBA fit.

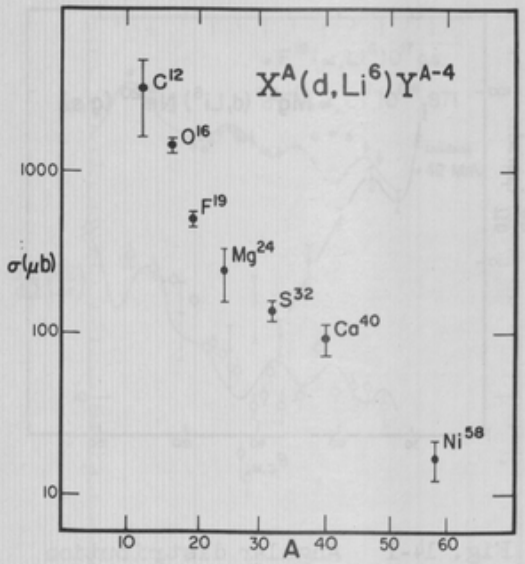

Fig. 14-6 Total cross sections for the (d,Li^6) reactions proceeding to the ground states of the residual nuclei, versus target mass.

case of C^{12}, we used optical model parameters obtained from elastic scattering data for the incoming and outgoing channels. The reasonableness of this fit is taken as strong additional evidence for a direct pick-up reaction mechanism. For the fits to the S^{32} data, only the real and imaginary well depths in the outgoing channel were changed from the case for C^{12}. The same parameters were then used for the reactions proceeding to both the ground state and the first excited state of the residual Si^{28} nucleus. Lack of lithium elastic scattering data has made it impractical to attempt DWBA fits for the other reactions observed. The integrated cross sections of these reactions are shown in Figure 14-6. The magnitude of the cross section is seen to drop rapidly with increasing target mass, with some tendency to level off for higher values of A. The cross section exhibits an abrupt decrease for the reaction on Ni^{58} as the reaction in this case is taking place in a region which is below the Coulomb barrier for the outgoing Li^6 particle. (J. B. Gerhart, P. F. Mizera, and F. Slee)

---

1 Nuclear Physics Laboratory Annual Report, University of Washington (1965), p. 28.

2 Clyclotron Research, University of Washington (1962), p. 39.

3 R. H. Bassel, R. M. Drisco, and G. R. Satchler, The Distorted Wave Theory of Direct Nuclear Reactions, Oak Ridge National Laboratory, ORNL-3240, 1962.

15. Study of Time Reversal Invariance in the Inverse Reactions $Mg^{24} + d \rightleftarrows Mg^{25} + p$

Interest in time reversal invariance has been rekindled in this laboratory due to the work of Christenson, Cronin, Fitch, and Turlay[1], who discovered, in the decay of the K_2^0 meson, a small violation of CP invariance or, as implied by the CPT theorem, a violation of time reversal invariance. A similar violation of time reversal invariance might be expected in nuclear reactions.[2]

Previous experimental studies of time reversal invariance in nuclear reactions have been based on polarization and asymmetry measurements in p-p scattering,[3] and on comparisons of cross sections in inverse reactions.[4] Typical experimental uncertainties have been in the neighborhood of 5%, and the results have been interpreted as setting upper limits of several percent on the ratio of time reversal odd and even reaction amplitudes. With the availability of solid state detectors and of the University of Washington tandem accelerator (with high beam intensity and good definition of beam energy and position), we believed that the experimental uncertainties in the study of inverse reactions could be reduced by a factor of about ten. For this reason such a test of T invariance has been undertaken.

The inverse reactions $Mg^{24} + d \rightleftarrows Mg^{25} + p$, using 10 MeV deuterons and 15 MeV protons, were chosen for this test. If there is no violation of T invariance, then the reaction cross sections, at properly matched energies, should be related by the principle of detailed balance. The choice of a (p,d), (d,p) comparison was based primarily on the availability of intense proton and deuteron beams from the tandem accelerator. The choice of target elements was determined by the following considerations: (a) The first excited states should be well separated from the ground states. (b) The target should be light, to give a large compound nuclear width for Ericson fluctuations, reducing sensitivity to mismatch in the incident beam energies; but, on the other hand, it should be relatively heavy to minimize the change in outgoing energy with angle, permitting similar counters to be used at different angles (see below). (c) The (d,p) reaction Q-value should be small because, in our energy range, this simplifies detection problems. (d) Isotopically pure targets should be readily available. (e) Target impurities with unfavorable Q-values should be minimized.

The specific approach to the study of the $Mg^{24} + d \rightleftarrows Mg^{25} + p$ reactions was dictated by experimental considerations, because theoretical arguments did not suggest any preference among various plausible alternatives. To eliminate difficulties in accurately determining target thickness and integrated beam flux, two detectors were used simultaneously. The basic measurement consists of the determination, in each reaction, of the ratio of the differential cross sections at two angles. A difference in these ratios for the (d,p) and (p,d) reactions can exist only if there is a violation of T invariance.

The experimental arrangement is shown in Figure 15-1. The experiment is performed in a 60-inch diameter scattering chamber. The two counters are placed on movable arms, 10 inches from the target center. By careful positioning of the counters and by use of the same defining apertures in the (d,p) and (p,d) measurements, relative solid angle uncertainties are made quite small. The back-angle counter has half-inch diameter aperture, and the forward-angle counter

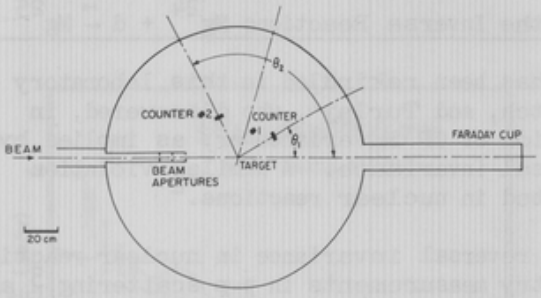

Fig. 15-1 Arrangement of detectors and target in the scattering chamber.

has a quarter inch diameter aperture to reduce the difference in counting rates. The target plane bisects the angle between the two detectors, so that wander of the incident beam produces no change in the ratio of solid angles for the two counters.

The protons in the (d,p) reaction were detected in lithium-drifted silicon detectors prepared in this laboratory. Polyethylene degraders were placed in front of each detector to stop particles heavier than protons. Using conventional electronic techniques, including a biased amplifier to spread the peaks, each of the two proton spectra was displayed in one quadrant of a 512 channel analyzer. The ratio of cross sections was determined, after appropriate corrections, from the ratio of counts in the two ground state peaks.

To permit corrections for dead time and pileup losses, pulses from an electronic pulser were fed into each preamplifier in parallel with the detector pulses. The pulser events were routed into the two remaining quadrants of the analyzer. The electronic efficiency was determined from the loss of events from the pulser peak, and the detector data were appropriately corrected. In order for the pulser efficiency to correctly represent dead time losses, the pulser rates were made proportional to the beam intensity. Typical pulser losses were in the neighborhood of 1%, varying with counting rate and differing at the two angles and in the two reactions.

The deuterons in the (p,d) reaction were detected in conventional ΔE-E telescopes, using fully depleted surface barrier silicon detectors, procured from ORTEC. The overall electronic system, including the use of pulsers for dead-time corrections, was similar to that used in the (d,p) measurements, aside from routine complications arising from the use of a ΔE-E technique. The spectra displayed are for the sums of the pulse heights in the ΔE- and E- detectors of each telescope.

Typical proton spectra for the (d,p) reaction are shown in Figure 15-2. The width of the peaks arises largely from straggling in the degrader. The uncertainty in the determination of the area in the ground state peak, because of overlap with the first excited state peak, is about 0.1%. Typical deuteron spectra for the (p,d) reaction are shown in Figure 15-3. The underlying background is believed to be primarily due to accidental coincidence between two protons. Uncertainties in the background subtraction amount to about 0.1%.

To correct for losses due to nuclear interactions or large angle scattering in the detectors, as well as to uncover defects in the detector, the detector efficiency was measured. This was accomplished by a coincidence method in which the number of (monoenergetic) particles known to enter the detector was compared with the number appearing in the peak of the spectrum. For example, to measure the efficiency of one of the deuteron E-detectors a coincidence d-d elastic

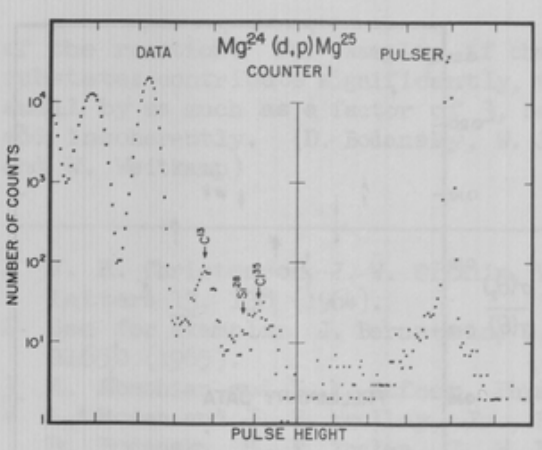

Fig. 15-2 Typical proton spectrum and associated pulser spectrum for the $Mg^{24}(d,p)Mg^{25}$ reaction. Arrows indicate the positions of groups from (d,p) reactions in impurity elements.

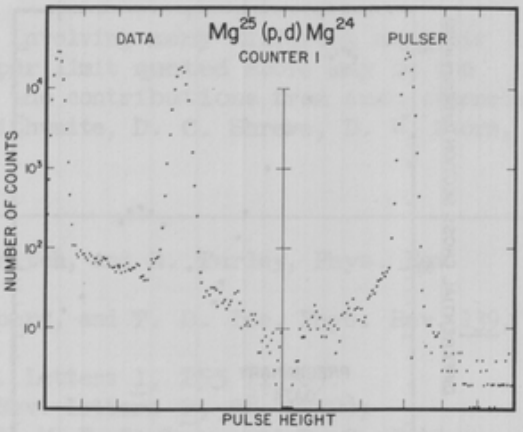

Fig. 15-3 Typical deuteron spectrum and associated pulser spectrum for the $Mg^{25}(p,d)Mg^{24}$ reaction.

scattering measurement was made. Coincidences were formed between deuterons in the two ΔE-detectors, and these coincidences were used to gate the analyzer in which the E-spectrum was displayed. By comparing the number of gating pulses with the number of events appearing in the spectrum, the efficiency of the E-detectors was determined. Similar measurements (with p-p scattering) were carried out for the proton detector by inserting a special thin detector in front of the polyethylene degrader. Typically it was found that the efficiency defects were several tenths of a percent, and could be accounted for by nuclear interactions in the detectors.

A detailed investigation has been made of possible contributions to the peaks from target impurities, but the net contribution proved to be negligible.

Preliminary results consist of angular distributions and excitation functions for the two reactions. The angular distributions, at matched energies, are shown in Figure 15-4. It is seen that the two distributions agree to within an experimental uncertainty of about 2%. The angular distributions have peaks at 29.68° and 119.20° (c.m.). Excitation function studies were made with the counters placed at laboratory angles corresponding to these peaks.

The results of these excitation function studies are shown in Figure 15-5, where the ratio, $R(E) = \sigma(119.20°, E)/\sigma(29.68°, E)$ is plotted as a function of incident energy. To represent the energy on a scale appropriate to the two reactions, the laboratory energies of the incident particles are converted to excitation energies of the Al^{26} system. While the absolute uncertainty in these excitation energies is determined in part by the uncertainty in the Al^{26} mass, the relative uncertainty is determined only by uncertainties of a few keV in the reaction Q-value (5.106 MeV) and in the accelerator energy calibration.

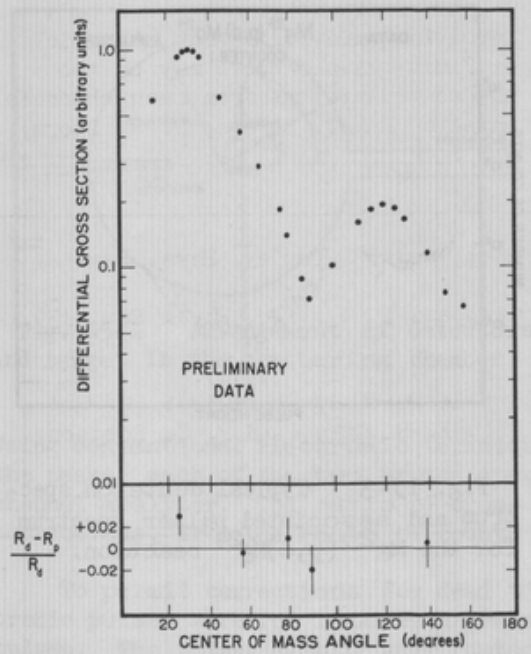

Fig. 15-4 Angular distribution for the $Mg^{24}(d,p)$ reaction at an excitation energy of 20.606 MeV in Al^{26}. The differential cross section is normalized to unity at the top of the forward peak. The lower part of the figure shows the fractional difference between R_d, the cross section ratio measured in the $Mg^{24}(d,p)$ reaction, and R_p, the ratio measured in the $Mg^{25}(p,d)$ reaction.

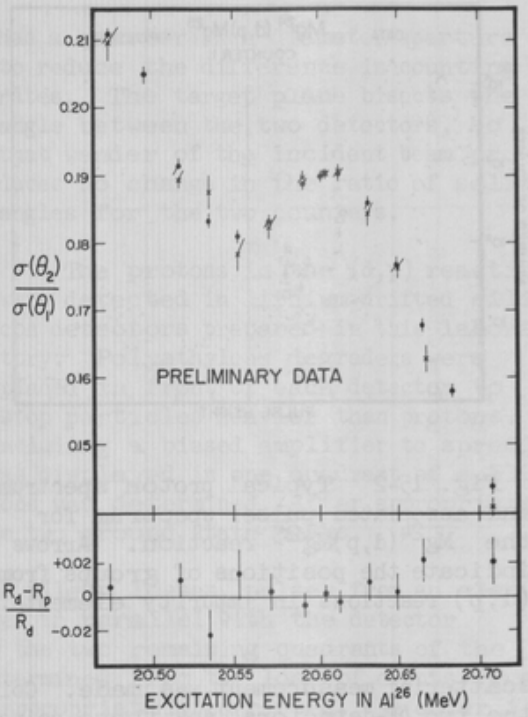

Fig. 15-5 Excitation function for $R(E) = \sigma(119.20°, E)/\sigma(29.68°, E)$ for the reactions $Mg^{24} + d \rightleftarrows Mg^{25} + p$. Dots show values of R_d, the ratio measured in the $Mg^{24}(d,p)$ reaction, and crosses show values of R_p, the ratio measured in the $Mg^{25}(p,d)$ reaction. The lower part of the figure shows the fractional difference between R_d and R_p.

A comparison of the two excitation functions in Figure 15-5 shows good overall qualitative agreement. The most accurate comparison of the ratios has been made at the peak in the excitation function. The energies at the peaks agree, the measured difference in energy being 0 ± 5 keV. It is found that the peak heights differ by 0.1% with a probable error of 0.4%. This can be interpreted as meaning that the difference in the cross section ratios, R(E), is probably less than 0.5%.

It is not clear how this limit may best be translated into an upper limit on the ratio of the time reversal odd and even reaction amplitudes. If the original criterion of Henley and Jacobsohn is applied[5], this upper limit (based on probable errors) is roughly 0.25%. However, determination of an upper limit on the time reversal odd contribution is sensitive to assumptions concerning specific details

of the reaction. For example, if channels involving many different magnetic substates contribute significantly, the upper limit quoted above may be too small by as much as a factor of 3, because the contributions from such channels add incoherently. (D. Bodansky, W. J. Braithwaite, D. C. Shreve, D. W. Storm, and W. Weitkamp)

---

1 J. H. Christenson, J. W. Cronin, V. L. Fitch, and R. Turley, Phys. Rev. Letters 13, 138 (1964).

2 See for example: J. Bernstein, G. Feinberg, and T. D. Lee, Phys. Rev. 139, B1650 (1965).

3 A. Abashian and E. M. Hafner, Phys. Rev. Letters 1, 255 (1958).

4 L. Rosen and J. E. Brolley, Jr., Phys. Rev. Letters 2, 98 (1959); D. Bodansky, S. F. Eccles, G. W. Farwell, M. E. Rickey, and P. C. Robison, Phys. Rev. Letters 2, 101 (1959).

5 E. M. Henley and B. A. Jacobsohn, Phys. Rev. 113, 225 (1959).

III. PHOTONS FROM NUCLEAR REACTIONS

16. Gamma Ray Polarization Measurement

Initial studies indicate that measurements of the sign of gamma ray polarization in inelastic He^4 or proton scattering from 0^+ to 2^+ states, which were discontinued in 1961[1], may now be feasible. It appears that with the dc Van de Graaff beam and some improvements in time resolution obtained by detector cooling[2] it is possible to make such a measurement. It is anticipated that such measurements will be carried out in the near future on the various substates of the 2^+ 4.43 MeV level in Mg^{24}.

The interest in these levels is that in-plane $(\alpha,\alpha'\gamma)$ correlation measurements have been made[3] in an energy range accessible to our Van de Graaff (E_α = 22.5 MeV). These measurements indicate the angles at which the polarization may change sign.[4] The measurements of the signs of these gamma-ray polarizations will thus remove the ambiguities which exist in the previous polarization measurements[3] of the $m = \pm 2$ substates and then allow for a similar type of measurement with protons exciting the $m = \pm 1$ substates. (J. G. Cramer, Jr., T. D. Hayward, W. A. Kolasinski, D. Patterson, and F. H. Schmidt)

---

1 Cyclotron Research, University of Washington (1961), p. 37.
2 Section 33 of this Report.
3 W. W. Eidson, J. G. Cramer, Jr., D. E. Blatchley, and R. D. Bent, Nuclear Phys. 55, 613 (1964).
4 J. G. Cramer, Jr., and W. W. Eidson, Nuclear Phys. 55, 593 (1964).

---

17. The Double Gamma Decay of Ge^{72}

Although the theory of double-photon transitions was first worked out by Mayer[1] in 1931, and since that time many experimental attempts have been made to observe the phenomenon[2], it has never been seen in a nuclear transition[3]. One of the most likely situations for observing a two-photon decay is in an electric monopole transition, i.e., a 0^+ to 0^+ transition, preferably from a first excited to a ground state. Here a normal one-photon transition is not allowed, so the transition must proceed by pair emission, K-electron conversion, or a double-photon transition.

Nature has provided us with only four known examples of even-even nuclei with 0^+ first excited states. These are 0^{16}, Ca^{40}, Ge^{72}, and Zr^{90}. with 0^+ states at excitation energies of 6.05, 3.35, 0.69, and 1.752 MeV, respectively. From this list it is apparent that only Ge^{72} has a 0^+ first excited state at an energy below the 1.022 MeV pair-emission threshold. Because pair-emission is not energetically possible, the state is relatively long-lived, with a lifetime of 0.3 microsec. Thus a double-photon transition has competition only from K electron conversion and may have a reasonable transition probability. A rough calculation indicates that the fraction of double photon transitions in the decay of the first excited state of Ge^{72} may be as high as 5%, although it

also may be several orders of magnitude weaker. Curiously enough, although the O^{16}, Ca^{40}, and Zr^{90} first excited state decays have all been carefully studied for evidence of a double-photon transition[2], such a measurement has never been made on Ge^{72}.

An experiment is now in progress at this laboratory to study this decay. In a preliminary survey measurement a thick target of GeO_2 containing Ge^{72} enriched to 96.4% was bombarded with 5.0 MeV protons from the tandem accelerator. This proton energy is below the threshold for both the $Ge^{72}(p,n)As^{72}$ and the $C^{12}(p,p')C^{12*}$ 4.43 MeV reactions which would produce unwanted background.

Two 3" x 3" NaI(Tl) gamma ray detectors were placed at angles of 60° to the beam, with a lead Faraday cup between them which would catch the beam in its interior and at the same time prevent gamma rays from scattering from one detector to the other. A fast coincidence circuit with a resolving time of about 40 nsec was used to select coincident gamma rays in the two detectors. The signals from the two detectors were summed, and the total signal was gated by the fast coincidence circuit and sent to a 512-channel multichannel analyzer. The spectrum thus accumulated was examined for events having a total gamma ray energy of 0.69 MeV, as would be expected from a double photon transition. A two parameter spectrum of γ_1 energy vs γ_2 energy was also accumulated, using the on-line computer system.

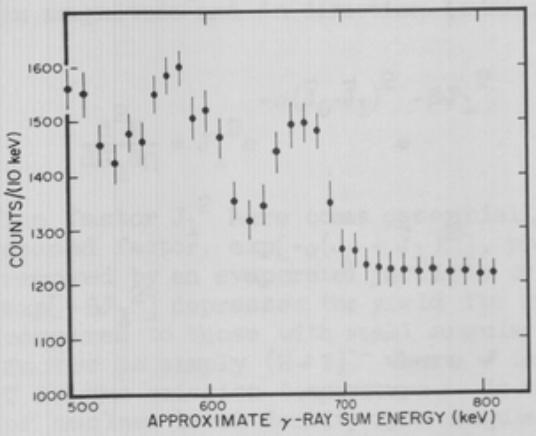

Fig. 17-1 Coincidence spectrum, counts vs. sum energy, for 5 MeV protons on Ge^{72}. (Note the suppressed zero.)

Figure 17-1 shows a portion of the pulse height spectrum which was accumulated in the multichannel analyzer in one 2-hour run. As can be seen from this distribution, there is a small peak approximately in the region where the double-photon peak should appear. If this is indeed the double-photon peak, the cross section for excitation of the Ge^{72} first excited state and decay in this mode is approximately 200 microbarns. A window discriminator was set on this energy region of the sum signal, and this was used to gate the signal from one of the detectors into the analyzer. Thus one of the two components which form this sum peak was examined by itself. The result was that there were no prominent gamma ray peaks present except for the annihilation peak at 0.511 MeV. This is taken as evidence that the peak in the sum spectrum was not produced by adding two well-defined peaks. The two parameter spectrum revealed no new information because the sum peak, when spread over a two-dimensional surface, is lost in the background until a large number of counts is accumulated.

We feel that these data, while not conclusive proof of a double-photon transition in Ge^{72}, are very encouraging. The next step is to take advantage of the very long lifetime of the 0^+ state by pulsing the beam and looking for double-photon transitions only while the beam is switched off. This technique will be put into use in the near future. (W. J. Braithwaite, J. G. Cramer, and C. F. Williamson)

---

1 M. Goepperd-Mayer, Annalen der Physik, 1931; R. G. Sachs, Phys. Rev. 57, 194 (1940).

2 G. J. McCallum, D. A. Bromley, and J. A. Kuehner, Nuclear Phys. 20, 382 (1960); M. Nessin, T. H. Kruse, and K. E. Eklund, Phys. Rev. 125, 639 (1962); D. E. Alburger and P. D. Parker, Phys. Rev. 135, B294 (1964).

3 However, double-photon decays have been observed in atomic processes, c.f. M. Lipeles, R. Novick, and N. Tolk, Phys. Rev. Letters 15, 690 (1965).

---

18. The Distribution Function for Residual Angular Momentum in Decaying Compound Nuclear Systems

As particles and photons are emitted from an assembly of excited compound nuclei, the distribution function for the angular momentum in the residual compound nuclei is modified from the distribution which is originally produced in the bombardment. It is interesting to study these modifications, both in magnitude and in direction of the angular momentum, because of the light such studies may shed on the angular-momentum dependence of the nuclear level density.

It is not easy to sample angular momenta of an assembly of compound nuclei. So far the observations have been mainly restricted to the determination of the production ratio of isomer pairs in a final nucleus, where the yields of both isomers can be determined by radioactivity counting.[1] A more extensive and critical test of the theory of evaporation cascades can be provided by measurements of the relative yields and angular distributions of lines in a ground state rotational band in a distorted nucleus (see Section 19).

To facilitate the comparison of the measurements with the implications of the theory, a simple geometrical model was constructed that permits one to trace the evolution of the angular momentum distribution in a nuclear system. Suppose that to begin with all of the nuclei in a system have the same angular momentum $\vec{J}_0$. If $\vec{J}_1$ is the resultant angular momentum after the evaporation of a single particle (or photon) then it can be argued that the distribution function for J_1 in magnitude and in direction (with respect to that of $\vec{J}_0$) is of the form

$$\frac{d^2N}{dJ_1 d\Omega} = J_1^2 e^{-\alpha(\vec{J}_0-\vec{J}_1)^2} e^{-\beta J_1^2} . \qquad (1)$$

The factor J_1^2 here comes essentially from phase space considerations. The second factor, $\exp[-\alpha(J_0 - \vec{J}_1)^2]$, provides a measure of the rms angular momentum removed by an evaporated particle or photon, namely $3\alpha/2$. The third factor, $\exp[-\beta J_1^2]$ depresses the yield for residual states with large angular momentum compared to those with small angular momentum. It can be shown that β in this factor is simply $(2\mathcal{I}T)^{-1}$ where $\mathcal{I}$ is the effective nuclear moment of inertia and T is the emission temperature. In the familiar expressions for the dependence of nuclear level density upon angular momentum, β is written $(2\sigma^2)^{-1}$. The usefulness of expression (1) rests on the fact that it iterates. That is to say, one can show that the residual angular momentum distribution after a sequence of evaporations can always be cast into essentially the same form as (1). Only two parameters are involved in a distribution of this form. One of them is a fraction, $\gamma\vec{J}_0$, of the original angular momentum, $\vec{J}_0$. $\gamma\vec{J}_0$ measures the average amount of the original angular momentum which is still retained by the nucleus. The rest, $(1 - \gamma)\vec{J}_0$, has been removed by the evaporating particles. The second parameter involved in the general distribution is α_F which measures the rms value of the "random" part of the angular momentum which had been removed in the evaporations. Both α_F and γ are easy to express as a function of the β's and α's which characterize each of the separate emissions.

As a simple exercise in the use of the foregoing formulation, the distribution function for the magnitude of the residual angular momentum, J_R, was computed for the case of slow neutron capture in even-even nuclei. Here one finds that the final distribution has the simple form

$$\frac{dN}{dJ_R} = \frac{4}{\sqrt{\pi}}(\alpha_F)^{3/2} J_R^{\,2} e^{-\alpha_F J_R^{\,2}} . \qquad (2)$$

For slow neutron capture, because of the isotropy of the starting angular momentum, one can set $\vec{J}_0 = 0$ and take the actual value of the angular momentum upon capture into account by attributing it to an extra emission. At any rate the final distribution can be expressed in terms of a single parameter, $\alpha_F^{-1} = 2/3 < J_R^2 >$. In Figure 18-1 we have plotted the observed ratios of high spin to low spin isomers which have been found in slow neutron capture as a function of the average spin of the two isomers.[2] If one assumes that the portion of (2) which feeds the high spin state is the part which lies above the average spin and that feeding the low spin state is the part below the average spin, one can predict the yield ratio as a function of the mean isomer spin, given the value of the single parameter α_F. One would judge from Figure 18-1 that the best value of α_F is about 0.48. By computing values for α_F in terms of α's and β's for the individual photon emissions, it is found that the "best" α_F would be achieved for example if, after neutron capture, three dipole photons are emitted up to the point that the distribution (2) is established. There is no evidence in the fitting of (2) to the available data for the emission of either large numbers or high multipolarities of emitted photons. It is also found that the data are hardly at all sensitive to assumed values of β. These conclusions are in accord with those of Vandenbosch and Huizenga.[1] The scatter of the data about the curves should probably be expected since variations in the particular structure of the two final states can give rise to fluctuations in yield. This sort of scatter should be less when one deals with a set of rotational

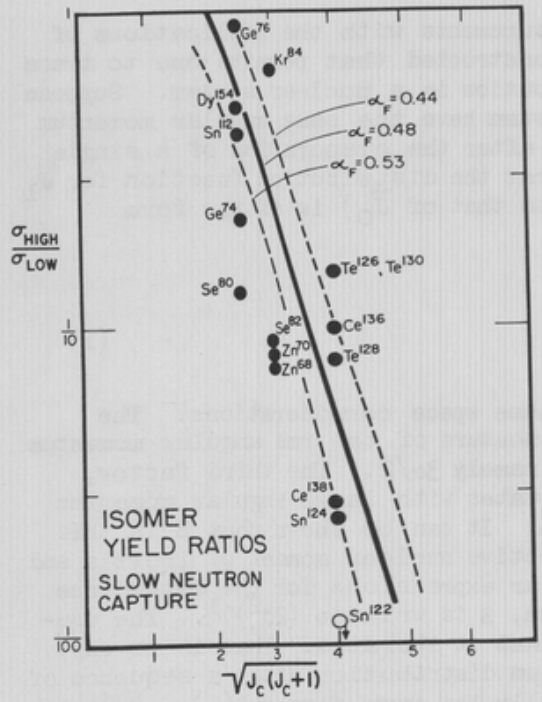

Fig. 18-1 The isomer yield ratio in slow neutron capture by even-even targets as a function of J_c, the average spin of the two isomers. The theoretical curves are based on the one-parameter model described in the text. The mean square angular momentum of the nucleus, $\overline{J(J+1)}$, at the stage sampled by the isomers is given by $1.5\ \alpha_F^{-1}$.

lines since the intrinsic wave functions of these states are all alike. The model described here is really most useful for reactions where the cascade is longer and more complicated than in radiative capture. Generally the distribution for $\vec{J}_0$ is not isotropic and therefore neither is the residual distribution at any stage of the evaporation. Then the model can be used to see if the observed angular distributions together with the observed yields can consistently be understood in terms of an assumed form for the nuclear level density. (I. Halpern, B. J. Shepherd, and C. F. Williamson)

---

1 R. Vandenbosch and J. R. Huizenga, Phys. Rev. 120, 1313 (1960).
2 J. Wing, ANL-6598 (1962) (unpublished).

---

19. Angular and Intensity Distributions of Rotational E2 Gamma Rays Following $(\alpha,3n)$ Reactions

This phase of the program of study of electromagnetic radiation induced by various nuclear reactions was greatly assisted by the purchase of a 1 cm^2 x 4mm Ge(Li) solid-state gamma-ray detector and a field-effect transistor preamplifier which can be operated in vacuum. The combination yields a gamma-ray line width of about 5 keV under actual operating conditions. The intrinsic photopeak efficiency of the detector has been measured absolutely by comparing the full energy peak counting rate for various gamma ray sources to that of a standard 1-1/2 in. x 1 in. NaI(Tl) crystal whose efficiency is known to ± 5%.

The very great improvement in resolution compared with NaI(Tl) is shown in Figures 19-1 and 19-2. Both spectra are for 42 MeV He ions on Dy^{161}. Precise peak areas can now be extracted without resorting to uncertain computer techniques.

The angular distributions of the rotational transitions observed in Yb^{168}, produced by the $(\alpha, 3n)$ reaction on Er^{167}, are shown in Figure 19-3. The intensity distributions for these same transitions are shown in Figure 19-4.

The intensity distributions give a picture of the angular momentum distribution, (dN/dJ), in the assembly of residual nuclei toward the end of the particle-photon evaporation cascade. (Actually (dN/dJ) is the derivative of the curve in Figure 19-4 since the intensity of a given rotational line is the sum of the intensity of the next higher line and the intensities of transitions which lead into the band for the first time at this point.) The angular distribution of any rotational line can be interpreted in terms of the orientation-distribution in space of the $\vec{J}$ of the radiating state.

As was mentioned in Section 18, a simple classical model was developed to help us understand, in a quantitative way, results such as those in Figure 19-3 and Figure 19-4. The theoretical curves in Figure 19-3 are an extreme version of the model curves. They are all of the same form: $W(\theta) = 1 + 1.2 \cos^2\theta - 0.6 \cos^4\theta$, where θ is the angle between the beam and the photon counter. This is the

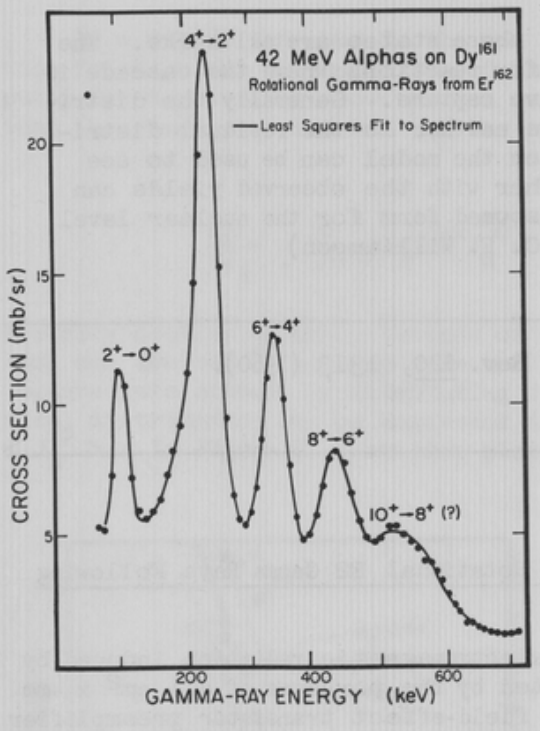

Fig. 19-1 Rotational transitions as observed in Er^{162} excited by the (α, 3n) reaction on Dy^{161}. These data were taken with a 1-1/2 in. x 1 in. NaI(Tl) detector inside an 8 in. x 12 in. NaI(Tl) anti-coincidence annulus. The solid curve is an attempt to fit the data by the method of least squares.

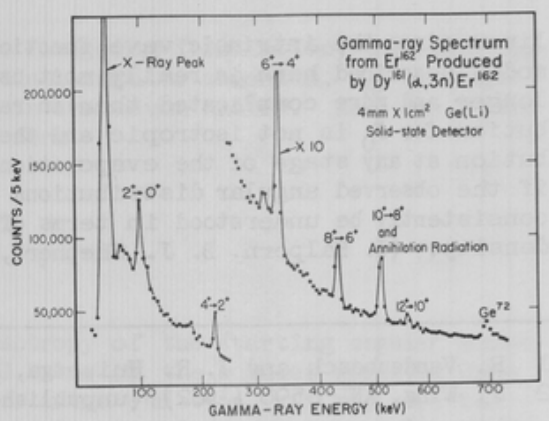

Fig. 19-2 The same spectrum as Fig. 19-1 but recorded by a 1 cm^2 x 4mm Ge(Li) solid-state detector. The solid lines were drawn by hand and are intended only to guide the eye. The improved possibilities for more accurate analysis and observation of higher spin states are obvious.

distribution expected for quadrupole radiation ($J \rightarrow J - 2$) from states with large J and m = 0. It is seen that there must be very little re-orientation during the neutron-photon emission cascade of the angular momentum directions of the original compound nuclei. The $2^+ \rightarrow 0^+$ transition is an apparent exception, but the relatively long lifetime (> 1 nsec) of this state renders possible re-orientation by atomic effects.

The degree of disagreement between the theoretical curves and the data in Figure 19-4 deserves some comment. Roughly put, the experimental J distribution falls off more rapidly with increasing J than any of the theoretical curves. To indicate the sensitivity of this aspect of the calculated curves to various options which one has about the values of calculation parameters, three curves are given in Figure 19-4. For curve A, the angular momentum distribution of the original compound nucleus was assigned on the basis of the optical model calculations of Huizenga and Igo.[1] It was assumed that the emission of the 3 neutrons in the (α, 3n) reaction was followed by the emission of 3 dipole photons and that the effective moment of inertia in the spin cutoff factor was the rigid body moment. It was found that replacing the 3 dipole photons with 3 quadrupole photons hardly changed the curve unless at the same time the effective moment of

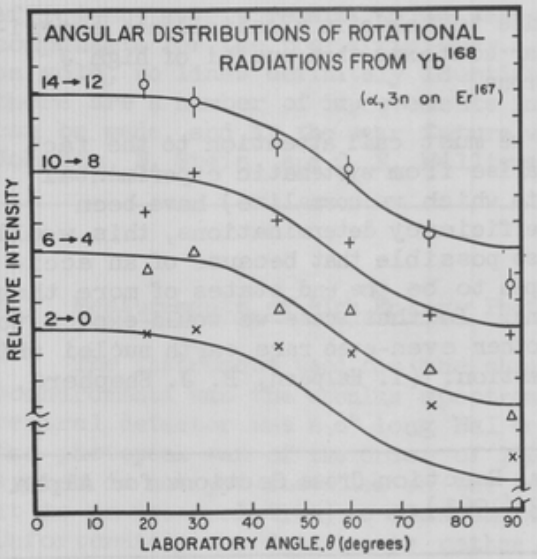

Fig. 19-3 The angular distributions of radiations in the ground state rotational band of Yb^{168} excited by the 42 MeV α bombardment of Er^{167}. The various transitions have been displaced vertically for clarity. The theoretical curves are all meant to correspond to the same value (1.6) for $W(0°)/W(90°)$. (See text.) Unless otherwise indicated, statistical errors are smaller than the data points. Relative errors of normalization between runs are not shown but are believed to be less than ± 4%.

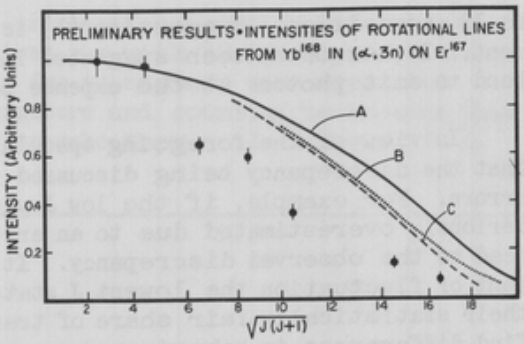

Fig. 19-4 The relative intensities of transitions in the ground state rotational band of Yb^{168} excited by 42 MeV α bombardment of Er^{167}. The abscissa is $\sqrt{J(J+1)}$ where J is the spin of the radiating state. The distinctions between the three theoretical curves A, B, and C are explained in the text. Statistical errors are smaller than the data points; the indicated errors are almost entirely due to uncertainties in the internal conversion coefficients and the relative efficiency of the detector.

inertia was significantly reduced. A reduction of this moment by a factor of 4 leads to curve B. For curve C, we made the same assumptions as in A except that we reduced the optical model value of the initially deposited $\langle J^2 \rangle$ by 20%. Such a reduction might be justifiable if collisions which take place on the outer edges of the nucleus lead generally to assorted direct reactions, instead of to compound nucleus formation and the $(\alpha, 3n)$ reaction. In curve C we have assumed about as much of this effect as we feel is reasonable.

It is clear from an examination of the calculated curves in Figure 19-4 that to improve agreement between the data and the theoretical curves at the high-J points one would want to do one of the following: (1) Increase the assumed number of photons emitted (at least in those events which populate the high-J part of the distribution). (2) Assume a large ratio of quadrupole to dipole radiation for these emissions. (3) Assume a large effective value of $(2\mathcal{J}T)^{-1}$. The larger this quantity, the lower will be the average residual J in each emission.

In principle, suggestions (2) and (3) can be tested by examining the angular distributions of the non-rotational photons in coincidence with, say, the 14^+

to 12^+ transition. Suggestion (1) is likewise testable in a coincidence experiment. It has often been suggested in similar contexts that nuclei of high J tend to emit photons at the expense of neutrons.

In view of the foregoing speculations, we must call attention to the fact that the discrepancy being discussed could arise from systematic experimental errors. For example, if the low J yields (to which we normalize) have been seriously overestimated due to an error in efficiency determinations, this would lead to the observed discrepancy. It is also possible that because of an accident or fluctuation the lowest J states happen to be the end states of more than their statistically-fair share of transitions. In that case we would expect to find differences in behavior as we examine other even-even rare earth nuclei which are produced as residuals in the (α, 3n) reaction. (I. Halpern, B. J. Shepherd, and C. Williamson)

---

1 J. R. Huizenga and G. J. Igo, "Theoretical Reaction Cross Sections for Alpha Particles with an Optical Model" ANL-6373 (1961).

---

20. Radiative Capture

If one wants to study the radiation from nuclei excited to 40 MeV or more, there are two ways that suggest themselves. The first is to study that portion of the radiation spectrum from these nuclei which leads to the ground state and low excited states. The softer part of the spectrum cannot, with certainty, be identified with transitions in the original nucleus. It may come from some of its descendents after particle emission. Apparently few of the very high energy quanta are actually emitted and it has, so far, not been possible to use photon spectral studies in the way described.

The second way to learn about radiation from very highly excited states is to measure the total capture cross section in a bombardment with particles of several tens of MeV. This is possible where the compound nucleus formed decays from its ground (or low lying isomeric) state with a convenient radioactivity. This technique has been fruitfully used many times despite its limitations. The main limitation on the interpretive side is that a measurement of the radioactive yield gives only an integral view of an entire cascade of photon emissions. One can hardly deduce much about the radiations from the initially excited nucleus. On the technical side, the main limitations of these studies arises from the background radioactivities produced by the other reactions (in addition to capture) which occur in the bombardment. These reactions are generally of the order 10^4 times more probable than capture.

Preliminary experiments with a NaI detector showed this latter method was not useful for measuring the small amount of capture activity against a background of other decays. We have begun to explore the feasibility of using Li-drifted germanium counters to measure the yields of radioactivity-associated photons which arise from the capture reaction. The hope is that the very great resolution of these counters will permit us to identify capture radiation in the large background of other radiations. The main drawback of the germanium counter is its low

efficiency and it remains to be seen if the increased resolution can be made to compensate for the poor efficiency. In a first run with 42 MeV alpha particles on gold, no lines definitely identifiable as due to capture were seen, but there are a number of improvements in the exposure and counting techniques that can be made, and in the near future we hope to make them. (I. Halpern, D. L. Johnson, N. Stein, and C. F. Williamson)

---

21. Measurements of High Energy Photons

The instrument used for the observation of high energy photons in nuclear bombardments was the annulus spectrometer described in an earlier report.[1] The central detector was a 6" long NaI crystal of 3" diameter. The resolution of the photopeak was of the order of 10% for quanta of 15 MeV. Since the pulsing system is not yet installed on the tandem accelerator, it was not possible (as it is on the cyclotron) to discriminate against neutrons by using time-of-flight. Unfortunately the detector is rather efficient for neutrons so that photon spectra are significantly contaminated by neutron background below about 12 MeV. It was therefore decided to devote our major attentions to quanta higher than this energy for most of the exploratory runs on the tandem.

A. Photons from bombardment of heavy elements

(1) Alphas on heavy elements

Experiments described in last year's annual report showed that bombardment with 42 MeV alpha particles produced a significant amount of high energy γ rays.[1] For example, in observations at 105° to the beam the cross sections for the production of 16 MeV photons were about 10, 15, and 2.5 μb/sr-MeV for cobalt, silver, and gold respectively. (Note: these results differ from those quoted in last year's report because a different efficiency was used.) A similar experiment was performed using the tandem to produce alpha particles of 18 MeV on a target of natural tin. The cross-section at 90° was less than 0.5 μb/sr-MeV in the region of 16 MeV γ rays. This result, when compared with last year's, suggests that the relative probability for emission of high energy photons increases rapidly with excitation energy.

(2) He^3 on heavy elements

When He^3 is used at the maximum energy currently available at the tandem (~24 MeV), its large Q value leads to excitation energies comparable to those reached with 42 MeV alphas. The following targets (all of natural isotopic mixture) were selected to give a general survey of the mass chart: carbon, aluminum, nickel, cobalt, niobium, tin, holmium, and gold. They were bombarded with 20.88 MeV He^3 ions and the cross sections for photon emission were found comparable to those measured in the experiments using 42 MeV alphas. For example, the cross section for production of γ rays around 16 MeV from tin was about 7 μb/sr-MeV. Beyond 12 MeV the γ-ray spectra drop off slowly with increasing energy as is shown in the two examples of Figure 21-1. The spectra have not been corrected for the crystal response function but have been normalized to give the cross

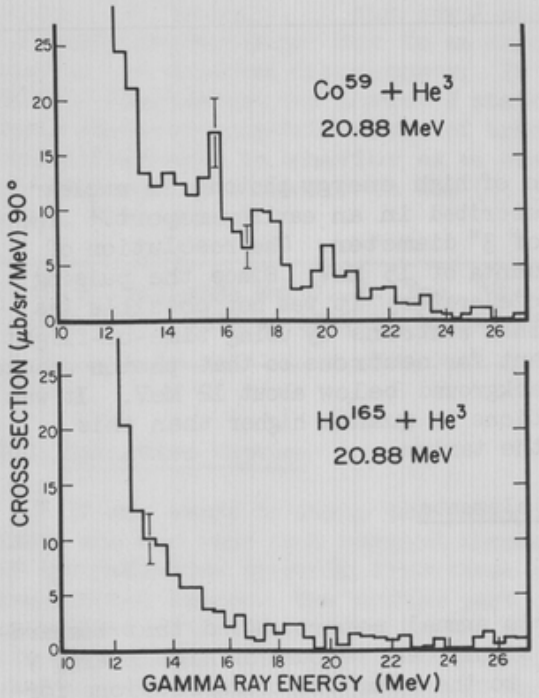

Fig. 21-1 High energy gamma ray spectra from He^3 bombardment of Co^{59} and Ho^{165}.

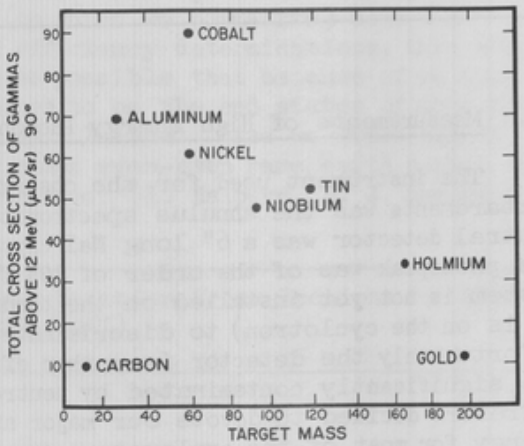

Fig. 21-2 Integral cross sections for the production of gammas above 12 MeV in the He^3 bombardment of various elements at 20.88 MeV.

section in microbarns per steradian per MeV. The efficiency factor needed for these cross-section determinations is only roughly known. It was estimated to be 0.2 for all high energy spectra.

The spectrum obtained at 90° for each target was integrated from 12 MeV on up to provide a measure of the cross section for the production of high energy photons. It was necessary to subtract a small background due to those cosmic rays which leaked through the protective anti-coincidence annulus; the results are shown in Figure 21-2. It is not known why the number of high energy γ rays from carbon is so small relative to the other targets.

(3) Photons from $Sn^{112} + \alpha$

In a recent experiment[2] the total capture cross section of Sn^{112} plus an alpha particle was measured as a function of energy. The excitation function of this reaction shows a broad maximum of 8 mb at E_α = 16 MeV. This unusually large cross section can possibly be attributed to the fact that, statistically, γ rays have a better chance to compete against neutrons in a neutron-poor isotope.

Since this target gives the largest capture cross section yet seen at this energy, it was felt that it would produce many high energy γ rays because a significant fraction of the captures should proceed via such γ rays. An isotopically enriched target of Sn^{112} about 1.5 mg/cm^2 thick was obtained and bombarded with alphas of 16 and 21 MeV. A raw spectrum is shown in Figure 21-3.

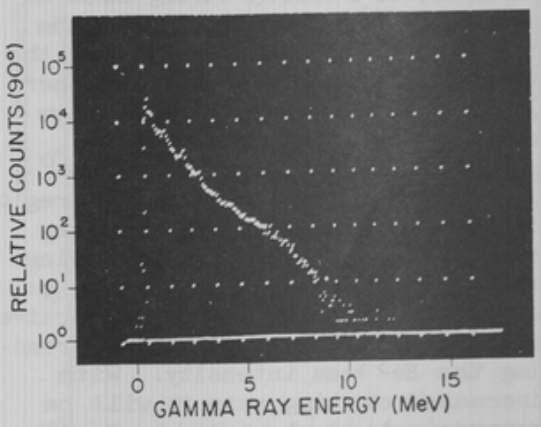

Fig. 21-3 Gamma-ray spectrum from alpha bombardment of Sn^{112} at 21 MeV.

One would like to study the γ-ray spectrum of the initial transitions from a region of high excitation in the compound nucleus. The spectrum of these initial transitions can be studied from the highest γ ray possible ($E_{\gamma\ max} = E^*_{CN}$) down to a region where it becomes possible to get γ rays from sources other than the first transitions in the compound system. These other sources are cascade γ rays in the compound nucleus and γ rays produced by other nuclei after a particle-emission reaction. Because of a possible neutron background we trusted the γ-ray spectra only above 11 MeV. For the two alpha energies used (16 and 21 MeV) γ rays above 11 MeV cannot come from nuclei other than the compound system and cascade γ rays above 11 MeV are highly unlikely since the neutron separation energy is about 10 MeV. Thus we were able to examine the spectrum of initial transitions from 11 MeV up to its maximum, which corresponds to the region from 11 to 16 MeV and 11 to 21 MeV for the 16 and 21 MeV alpha bombardments respectively. If we assume an isotropic angular distribution of all γ rays above 11 MeV we get a total cross section for initial transitions of very roughly 2 mb for both the 16 MeV and the 21 MeV bombardment. It is of interest to compare these cross sections with the previously measured total capture cross sections for these energies. If this is done we get roughly 25% and 100% of the measured values for 16 and 21 MeV. It should be noted that perhaps not all of the initial transitions observed from the 21 MeV bombardment would lead to capture since some ($11 \leq E_\gamma \leq 15$) are transitions to states below the neutron separation energy (~10 MeV) but above the proton separation energy (~ 6 MeV). However, the fraction of transitions to this region that do not lead to capture ought to be small due to the Coulomb barrier. Future experiments are planned to study further the shape and magnitude of these spectra.

B. Photons from bombardment of light elements

(1) $Be^9 + He^3$

The γ-ray spectrum produced by He^3 on Be^9 has been studied by Black et al.[3], at bombarding energies up to 4.5 MeV. In the present work, a 5.1 mg/cm^2 self-supporting Be^9 target was bombarded with He^3 beams of 7, 10,

and 11 MeV. The spectrum at 11 MeV bombarding energy is shown in Figure 21-4.

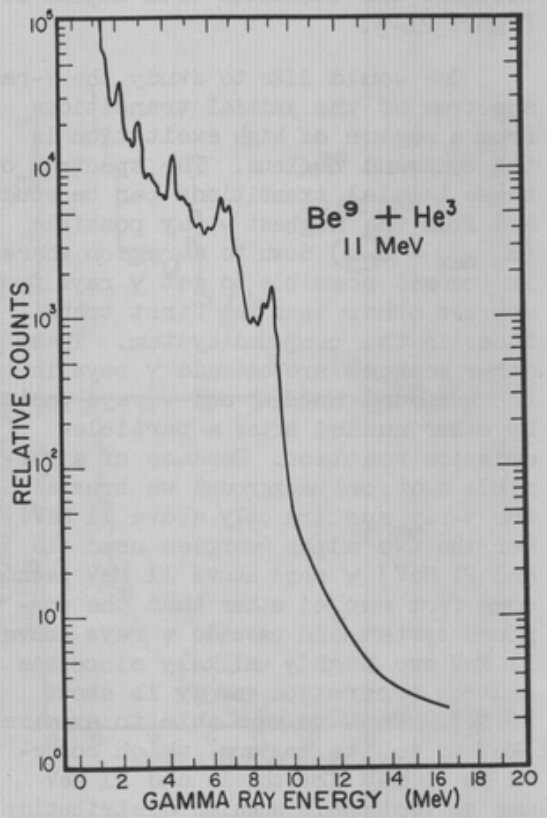

Fig. 21-4 Gamma-ray spectrum from He^3 bombardment of Be^9 at 11 MeV.

Very few γ rays are observed having energies greater than 12 MeV, and the intensity of radiation above is comparable to the residual cosmic ray background which is not eliminated by the anticoincidence annulus. There is observed a fairly strong line at 4.43 MeV which could be due to the reaction $Be^9(He^3, \gamma)C^{12*}$ feeding the first excited state. Several other lines are also observed which have not been definitely identified.

It is planned to study the region of the spectrum above 12 MeV γ ray energy more carefully by increasing the counting rate. This will be accomplished by enlarging the effective solid angle and hopefully by increasing the He^3 beam intensity. With increased counting rate it will be necessary to use techniques of pile-up rejection in the pulse analysis.

(2) Natural B + He^3

The high energy photons produced in natural boron by He^3 bombardment were examined with the only boron target we had. It was unfortunately quite thick (~ 19.5 mg/cm^2). The γ-ray spectrum at a bombarding energy of 20.88 MeV is shown in Figure 21-5. A rather intense peak is observed at an energy of about 16 MeV, along with several lower energy peaks which are probably also attributable to γ ray production in the target.

At a bombarding energy of 18 MeV, the target thickness is such that the excitation function is integrated from 12.8 MeV to 18 MeV. If it is assumed that the angular distribution is isotropic and that the detector efficiency is 20% (both conditions are probably correct to ± 30%), then the integrated total cross section over this energy range is 36 ± 18 microbarns. This assumes the reaction occurs in B^{11}; if it occurs in B^{10} the cross section is 4 times as large. At 10 MeV He^3 energy the target is almost infinitely thick. The same line is still observed at this bombarding energy but diminished in magnitude by about a factor of 7 for the same integrated charge. Thus the threshold for the reaction leading to this γ ray lies below 10 MeV. It is also observed that the energy of the 16 MeV γ ray does not change as the bombarding energy is varied,

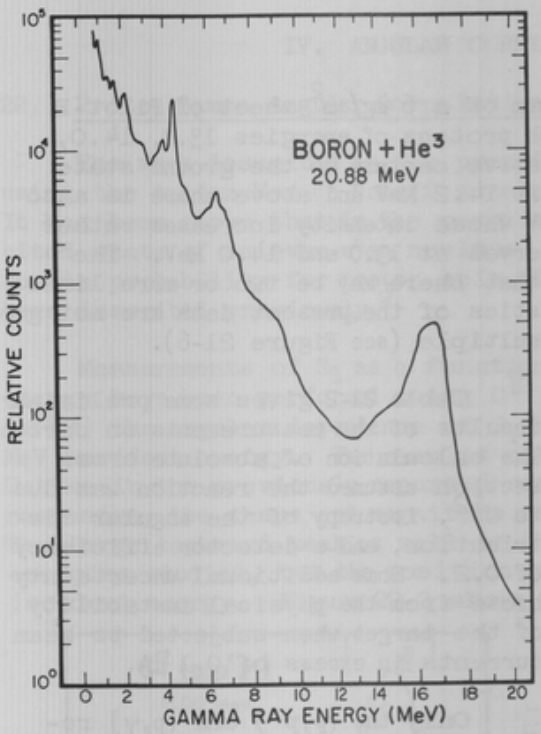

Fig. 21-5 Gamma-ray spectrum from He^3 bombardment of boron at 20.88 MeV.

indicating that it is not due to radiative capture to any state. The shape of the line is such that it could be a γ ray of discrete energy.

It is not yet known if the 16 MeV γ ray is produced from reactions in B^{10} or B^{11}. Table 21-1 lists the 8 reactions that cannot be excluded on energetic grounds. Reactions 3, 7, and 8 are somewhat less likely than the others because the outgoing charged particles would be moving with such low energy that they presumably would be inhibited by the Coulomb barrier. There is observed a rather strong 4.43 MeV line from C^{12}, indicating that reactions 2 and/or 7 are fairly important in the overall picture.

Isotopic targets of B^{10} and B^{11} of about 1 mg/cm^2 have been ordered, and these will be used to find out which isotope produces the 16 MeV γ ray. These targets will also be thin enough to allow study of the excitation function. It is also planned to study the angular distribution of this γ ray in hopes of learning something about its multipole character.

Table 21-1. Possible Reactions that Could Produce the 16 MeV γ Ray Observed in He^3 Bombardment of Natural Boron

	Reaction	Q-Value (MeV)
1	$B^{10}(He^3, \gamma)N^{13}$	21.64
2	$B^{10}(He^3, p)C^{12}$	19.69
3	$B^{10}(He^3, \alpha)B^{9}$	12.14
4	$B^{11}(He^3, \gamma)N^{14}$	20.73
5	$B^{11}(He^3, n)N^{13}$	10.18
6	$B^{11}(He^3, p)C^{13}$	13.18
7	$B^{11}(He^3, d)C^{12}$	10.46
8	$B^{11}(He^3, \alpha)B^{10}$	9.12

(3) Natural Carbon + p

A natural carbon target in the form of a 6 mg/cm^2 sheet of Pilot-B plastic scintillator has been bombarded with protons of energies 13.0, 14.0, 14.2, 14.5, 15.0, 15.5, and 16.0 MeV. Radiative capture to the ground state of N^{13} is observed at all these energies. At 14.2 MeV and above there is also observed a line (or lines) at about 12.7 MeV whose intensity increases rather rapidly with energy. This line was not observed at 13.0 and 14.0 MeV. The width and structure of this line indicates that there may be two or more lines contributing to the strength, but the statistics of the present data are not good enough to say for certain that the line is multiple (see Figure 21-6).

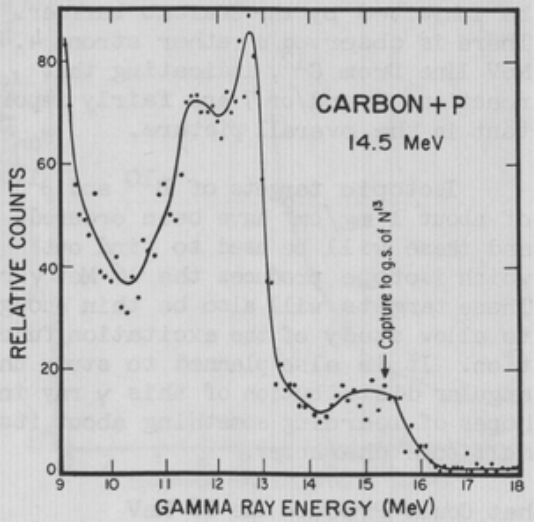

Fig. 21-6 High energy gamma-ray spectrum from proton bombardment of carbon at 14.5 MeV.

Table 21-2 gives some preliminary results of the measurements on carbon. The calculation of absolute cross section assumed the reaction was due to C^{12}, isotropy of the angular distribution, and a detector efficiency of 0.2. Some additional uncertainty arose from the physical instability of the target when subjected to beam currents in excess of 0.1 μA.

Only the (p,p') and (p,γ) reactions have sufficiently positive Q-values to excite a level of about 12.7 MeV in either C^{12} or C^{13}. (A reaction in C^{13} would require a cross section 100 times larger than that in Table 21-2 due to the 1% abundance of this isotope).

Future plans call for the use of self-supporting carbon foils as targets. Coupled with pile-up rejection electronics this will allow larger beam currents and improved statistics.

Table 21-2. Cross Sections for Observed Reactions in C^{12}

Average Proton Energy	Radiative Capture Total Cross Section	12.7 MeV Line Total Cross Section
14.4 ± 0.1 MeV	0.19 ± 0.08 μb	1.5 ± 0.8 μb
14.9 ± 0.1 MeV	0.12 ± 0.08 μb	1.7 ± 0.9 μb
15.4 ± 0.1 MeV	0.15 ± 0.08 μb	2.9 ± 1.5 μb

(S. M. Ferguson, I. Halpern, D. L. Johnson, N. Stein, and C. F. Williamson)

1 Nuclear Physics Laboratory Annual Report, University of Washington (1965), p. 55.
2 D. E. Khulelidze et al., J.E.T.P. 20, 259 (1965).
3 J. A. Black et al., Nuclear Phys. 54, 689 (1964).

IV. ANGULAR CORRELATIONS IN NUCLEAR REACTIONS

22. Proton-Gamma Angular Correlations and Spin Flip

The work described in the preceding issue of this report[1] has been continued using the tandem Van de Graaff accelerator which became operational in June, 1965. It has been shown that in the reaction of the type $X(p,p')X^*$ leading to a 2^+ excited state of an even-even nucleus, the $m = \pm 1$ substate population S_1 is equal to the probability for proton spin flip. The method used for measuring S_1 has been described previously.[2]

Measurements of S_1 as a function of proton scattering angle and incident energy have been performed using C^{12} and Ni^{60} targets. In the reaction $C^{12}(p,p'\gamma)C^{12}$ (4.43) the angular dependence of S_1 has been investigated at 12, 13, 14, and 15 MeV incident energy. The results obtained at 13.0 MeV are shown in Figure 22-1. Unlike in the previously reported results[2] in the neighborhood of the 10.5 MeV resonance, the shape and magnitude of S_1 do not change drastically with energy. The large backward peak as well as the smaller forward one are observed at all energies studied, but the position of the backward peak changes considerably with incident energy. Figure 22-2 shows the energy dependence of S_1 and the differential

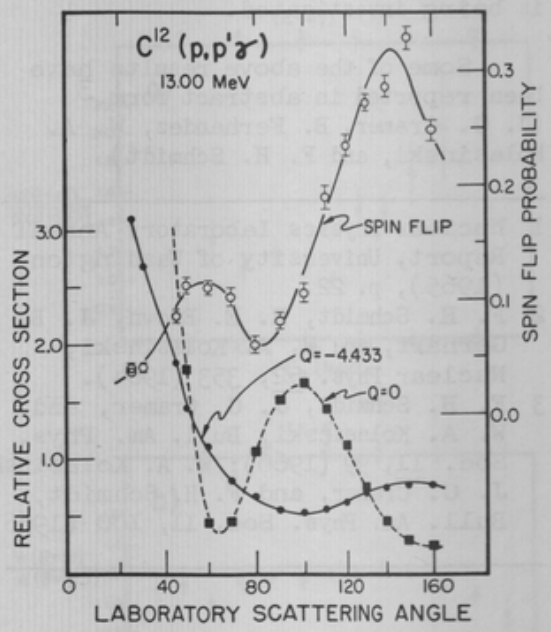

Fig. 22-1 Proton spin-flip probability in the reaction $C^{12}(p,p')\ C^{12*}(4.43)$; relative differential cross sections for the reactions $C^{12}(p,p)\ C^{12}$ and $C^{12}(p,p')\ C^{12*}(4.43)$, as functions of scattering angle.

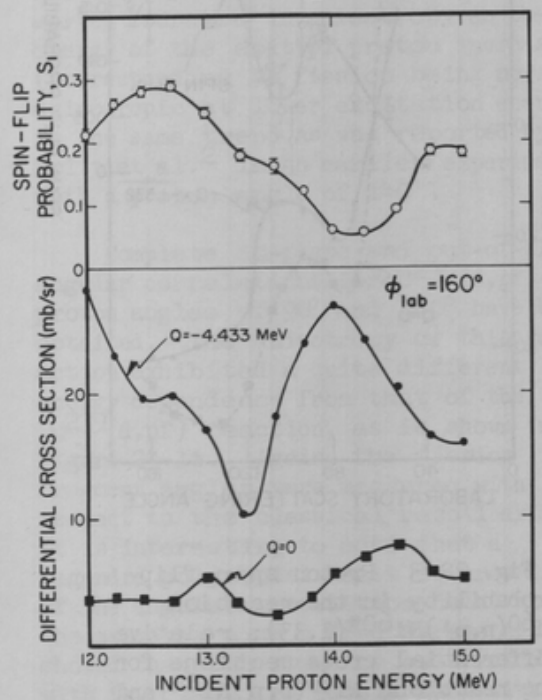

Fig. 22-2 Proton spin-flip probability in the reaction $C^{12}(p,p')\ C^{12*}(4.43)$; differential cross sections at φ_{lab} of 160° for the reactions $C^{12}(p,p)\ C^{12}$ and $C^{12}(p,p')\ C^{12*}(4.43)$, as functions of incident proton energy.

cross sections for elastic and inelastic (Q = -4.43 MeV) scattering of protons at 160 deg. in the laboratory frame. The observed energy dependence of S_1 is largely due to the change of the backward peak position with the incident energy.

The study of the reaction $Ni^{60}(p,p'\gamma)Ni^{60}(1.33)$ was undertaken with the idea in mind that the relatively low p-n threshold and high excitation energy in the compound nucleus would tend to reduce the compound nuclear contribution to the inelastic scattering process. Unfortunately, the relatively small scattering cross section and the large number of γ rays from competing reactions, coupled with the fact that the counting rate in the γ detector had to be limited to $\approx$ 10,000 counts/sec, drastically increased the data collection time. Consequently, the statistical errors in the results are much larger than in the case of C^{12}. In Figure 22-3 are shown results obtained at 10.5 MeV incident energy. The angular dependence of S_1 is similar to that in C^{12}, showing a peak at backward angles. At 14.0 MeV, S_1 exhibits essentially the same angular dependence, but the magnitude is roughly a factor of two less than at 10.5 MeV. At present, the reaction $Ni^{64}(p,p'\gamma)Ni^{64}$ is being investigated.

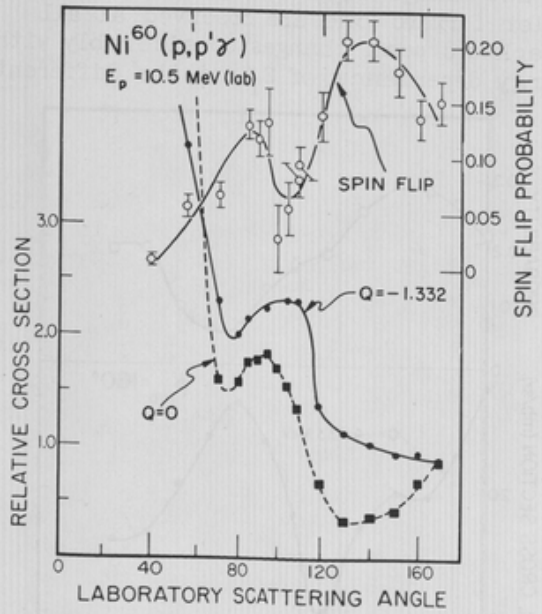

Fig. 22-3 Proton spin-flip probability in the reaction $Ni^{60}(p,p')Ni^{60*}(1.33)$; relative differential cross sections for the reactions $Ni^{60}(p,p)Ni^{60}$ and $Ni^{60}(p,p')Ni^{60*}(1.33)$ as functions of scattering angle.

Some of the above results have been reported in abstract form.[3] (J. G. Cramer, B. Fernandez, W. A. Kolasinski, and F. H. Schmidt)

---

1 Nuclear Physics Laboratory Annual Report, University of Washington (1965), p. 22.

2 F. H. Schmidt, R. E. Brown, J. B. Gerhart, and W. A. Kolasinski, Nuclear Phys. 52, 353 (1964).

3 F. H. Schmidt, J. G. Cramer, and W. A. Kolasinski, Bull. Am. Phys. Soc. 11, 99 (1966); W. A. Kolasinski, J. G. Cramer, and F. H. Schmidt, Bull. Am. Phys. Soc. 11, 100 (1966).

23. Angular Correlations in (d,pf) Reactions

The motivation and results of a preliminary experiment using the $U^{235}(d,pf)$ reaction were reported last year.[1] The scope of these studies has been broadened and now includes $U^{235}(d,pf)$ and $Pu^{239}(d,pf)$ reactions both in and out of the plane defined by the beam and the proton.

The experimental apparatus is the same as previously described[1] except for a few refinements such as a particle identification system to distinguish stripped protons from scattered deuterons. Also, a 15 MeV deutron beam from the tandem accelerator was used.

Preliminary work has been done using the $Pu^{239}(d,pf)$ reaction. An in-plane correlation with a proton angle of 90° relative to the beam was obtained, but further experiments could not be performed because deterioration of the plutonium oxide target created a very serious health hazard.

Figure 23-1a shows the fission fragment anisotropy as a function of proton energy at a proton angle of 90°. The angle θ is measured with respect to the classical recoil axis. The observed increase in anisotropy as the energy of the emitted proton increases (corresponding to fission being more anisotropic at lower excitation energy) is the same trend as was reported by Britt et al.[2] in an earlier experiment with a proton angle of 140°.

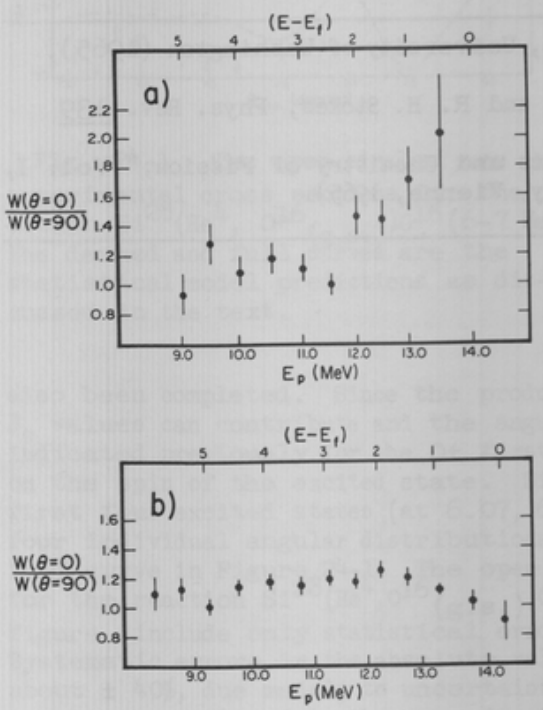

Fig. 23-1 In-plane anisotropy for (a) Pu^{239}, and (b) U^{235}. The lower abscissa scale on each Figure gives the proton energy in the laboratory system, and the upper scale gives the excitation energy in excess of the fission threshold.

Complete in-plane and out-of-plane angular correlations for $U^{235}(d,pf)$ at proton angles of 90° and 140° have been obtained. The anisotropy of this reaction exhibited a quite different energy dependence from that of the $Pu^{239}(d,pf)$ reaction, as is shown in Figure 23-1b. Again, the fission fragment angles were measured with respect to the classical recoil axis. It is interesting to note that a Legendre polynomial least squares fit of the angular correlation data, with the symmetry axis a free parameter, showed that the symmetry axis coincided with the classical recoil axis within experimental error.

The decrease in anisotropy at high proton energies (corresponding to fission becoming more isotropic at low excitation energies) is in qualitative agreement with results obtained

from the U^{234}(t,pf) reaction[3] which also involves the U^{236} compound nucleus. However, the explanation which we think most likely for the U^{235}(d,p) result does not account for the U^{234}(t,p) observation. We tentatively attribute the difference between the U^{235}(d,p) and the Pu^{239}(d,p) anisotropies close to threshold to a target spin effect. As the excitation energy decreases the higher members of the rotational band become partially closed and the lower members with low angular momentum contribute more on a relative basis. For U^{235}, which has a large target spin randomly oriented with respect to the beam axis, the angular momentum vectors are more weakly aligned than for Pu^{239}. The disorientation effect becomes less important for higher values of the total angular momentum because the orbital angular momentum transfer of the direct reaction becomes the largest contributor to the total angular momentum of the fissioning nucleus.

The out-of-plane anisotropy shows a rather puzzling characteristic of remaining approximately constant from fission threshold to the lowest proton energy measured.

Future plans include completion of the investigation of the Pu^{239}(d,pf) reaction employing the SDS 930 on-line computer for more efficient data collection. (W. Loveland, R. Vandenbosch, and K. Wolf)

---

1 Nuclear Physics Laboratory Annual Report, University of Washington (1965), p. 22.

2 H. C. Britt, W. R. Gibbs, J. J. Griffin, and R. H. Stokes, Phys. Rev. 139 B354 (1965).

3 D. Eccleshall and M. J. L. Yates, "Physics and Chemistry of Fission," Vol. I, p. 77 (International Atomic Energy Agency, Vienna, 1965).

V. COMPOUND NUCLEAR REACTIONS

24. Investigation of the $Si^{28}(He^4, O^{16})O^{16}$ Reaction

In a continuation of the study of this reaction reported last year[1], the angular distribution of O^{16} fragments formed in their ground states by decay of S^{32} compound nuclei, resulting from bombardment of Si^{28} with 42 MeV helium ions, has been measured. The angular distribution, shown as the open circles in Figure 24-1, exhibits considerably more structure than that previously obtained when one of the O^{16} fragments is formed in an excited state. This structure results from the fact that if both O^{16} nuclei are produced in their ground states they are identical particles and only even angular momentum compound states can contribute. The magnitude of the oscillations observed implies that compound states with a few even J_c values contribute. Statistical model calculations of the type described previously[2] suggest that $J_c = 14$ predominates with some contribution from $J_c = 16$ and 18. The relative shape of this calculated angular distribution is shown by the dashed line in Figure 24-1 (see below for a description of the normalization).

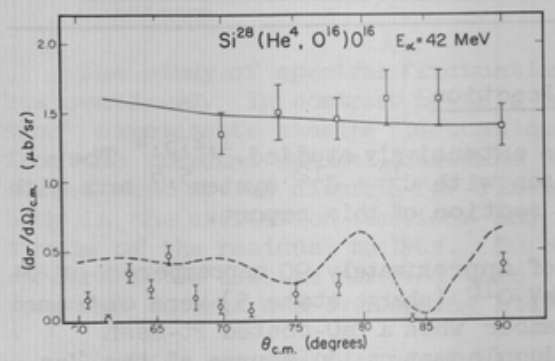

Fig. 24-1 The open circles are the experimental cross sections for the reaction $Si^{28}(He^4, O^{16}_{(g.s.)})O^{16}$(6-7 MeV). The dashed and full curves are the statistical model predictions as discussed in the text.

Statistical model calculations of the expected angular distributions for formation of one O^{16} fragment in the ground state with the other in one of the first four excited states have also been completed. Since the products are no longer in identical states, odd J_c values can contribute and the angular distributions are rather featureless, as indicated previously for the 0+ first excited state. There is little dependence on the spin of the excited state. Since our experiment does not resolve the first four excited states (at 6.07, 6.13, 6.93, and 7.13 MeV), we have added the four individual angular distributions together and plotted the result as the full curve in Figure 24-1. The open squares are the experimental cross sections for the reaction $Si^{28}(He^4, O^{16}_{(g.s.)})O^{16}$ (6-7 MeV). The errors indicated in the figure include only statistical errors in the total number of events recorded. Systematic errors in the absolute value of the cross sections are believed to be about ± 40%, due mainly to uncertainty in the target thickness. The full curve has been normalized to the experimental value at 90° (center-of-mass angle).

The dashed curve is the calculated curve for $O^{16}_{(g.s.)}$, $O^{16}_{(g.s.)}$ with the same normalization as the full curve. The fact that the predicted value of the cross section is somewhat larger than the observed value may reflect the expectation[3] that the reduced width for forming the ground state, with a rigid closed shell configuration, is less than the reduced width for forming the more easily

deformable excited nucleus. Another possibility for explaining the discrepancy is that the energy dependence of the O^{16} - O^{16} penetrabilities are not given correctly by the optical model which was used. A study of the inverse reaction, where the center of mass energy in the O^{16} - O^{16} system can be more easily varied, will help in clarifying this problem. (C. J. Bishop, J. Norman, and R. Vandenbosch)

---

1 Nuclear Physics Laboratory Annual Report, University of Washington (1965), p. 42. (Figure 21-2 of this reference is erroneously labeled mb/sr instead of μb/sr).
2 Ibid., p. 44.
3 Cyclotron Research, University of Washington (1964), p. 41.

---

25. Investigation of the $O^{16}(O^{16},He^4)Si^{28}$ Reaction

The reaction $C^{12}(C^{12}, He^4)Ne^{20}$ has been extensively studied.[1,2,3,4] The O^{16} + O^{16} system is of interest for comparison with C^{12} + C^{12} system[5,6] and with the $Si^{28}(He^4, O^{16})O^{16}$ data of the preceding section of this report.

In preliminary experiments, a maximum of approximately 90 nanoamperes of 54 MeV O^{16} (charge state 6) and 150 na of 36 MeV O^{16} (charge state 5) were obtained in the Faraday cup of the 60" scattering chamber when a BaO-coated Pt-mesh filament and hydrogen gas were used in the duoplasmatron ion source of the Van de Graaff accelerator. The 36 MeV O^{16} beam was used to bombard a 170 microgram/cm^2 thick NiO target. Several lithium-drifted silicon detectors, covered by 1.4 mils of aluminum foil to stop the scattered oxygen beam, were used to detect the alpha particles produced in the reaction $O^{16}(O^{16}, He^4)Si^{28}$. A multichannel analyzer and the on-line computer were used to record the energy spectrum from each detector. Peaks in the particle spectra attributable to alpha particles leading to formation of Si^{28} in the ground state, 1.8 MeV first excited state, and the 4.62 and 4.98 MeV second and third excited states (unresolved) were observed. These results indicated that the average differential cross section varies from approximately 10μb/sr for formation of the Si^{28} in the ground state to 60μb/sr for formation of the Si^{28} with 4-5 MeV of excitation energy.

Experiments are in progress to measure the angular distribution with 36 MeV O^{16} ions, and at several other energies up to 54 MeV (which corresponds to formation of the S^{32} compound nucleus with the same excitation energy as in the reaction of Si^{28} with 42 MeV He^4). A search for the fine structure in the energy dependence will also be performed in several energy regions. Methods of obtaining larger O^{16} beam currents and more stable beams are currently being investigated. (C. J. Bishop, J. Norman, and R. Vandenbosch)

---

1 E. Almqvist, J. A. Kuehner, D. McPherson, and E. W. Vogt, Phys. Rev. 136, B84 (1964).
2 E. W. Vogt, D. McPherson, J. A. Kuehner, and E. Almqvist, Phys. Rev. 136, B99 (1964).

3 J. Borggreen, B. Elbek, and R. B. Leachman, Mat. Fys. Medd. Dan. Vid. Selsk. 34, no. 9 (1965).
4 J. P. Bondorf and R. B. Leachman, Mat. Fys, Medd. Dan. Vid. Selsk. 34, no. 10 (1965).
5 Cyclotron Research, University of Washington, p. 41 (1964).
6 J. O. Rasmussen, Proceeding of the Third Conference on Reactions Between Complex Nuclei, Ed. by A. Ghiorso, R. M. Diamond, and H. E. Conzett, University of California Press, Berkeley (1963), p. 447.

---

26. Spectral Fluctuations in the $Al^{27}(d,p)$ Reactions Proceeding to the Continuum

The study of spectral fluctuations, discussed in the 1965 Annual Report[1], has continued. In contrast to this present study, conventional Ericson fluctuation[2] experiments examine fluctuations in the excitation function for transitions from the compound nuclear continuum to discrete final states. However, the final states need not be discrete for fluctuations to occur; fluctuations will occur both in the excitation functions and in the spectra for transitions from the continuum of the residual nucleus. To complete the symmetry, fluctuations in the spectra would also be observed were it possible to have discrete states in the compound nucleus and overlapping states in the residual nucleus.

Leaving out the last case, which in practice is unattainable, we can distinguish three types of fluctuation processes and the coherence widths, Γ, obtained from each: (1) Excitation function fluctuations with transitions to discrete states (the conventional case). Here one learns about the compound nucleus width, Γ_{CN}, with a sample size determined by Γ_{CN} and the energy region spanned in the excitation function. (2) Spectral fluctuations at one incident energy. Here one learns about the residual nucleus width, Γ_R, with a sample size determined by Γ_R and the spectral interval examined. (3) Excitation function fluctuations with transitions to the continuum. Here one learns about Γ_{CN} and Γ_R simultaneously. In particular, Γ_{CN} can be deduced with a large sample size, determined essentially by the spectral interval, even for only a few incident energies, while Γ_R can be determined as in (2) above. (Conversely, but less usefully, the width Γ_R can be determined with a large sample size if one observes at many incident energies several narrow intervals of the spectrum, each interval corresponding to a fixed residual excitation energy; Γ_{CN} can be deduced as in (1) above.)

The design of the experiment determines which of these cases one observes. But they are in principle similar, and the basic formalism and terminology of conventional fluctuation treatments are applicable to all three cases. In the present experiment the original interest lay in the observation of spectral fluctuations. However, in the attempt to identify these, it was natural to examine spectra at several energies and thus information was also gained about Γ_{CN}.

It is to be expected that the magnitude of the spectral fluctuations will be small, due to the incoherent addition of contributions from channels involving

different magnetic substates and to a background from protons emitted in the second or third stage of the emission cascade. To identify spectral fluctuations the following criteria may be applied: (1) The magnitude of the fluctuations should decrease as the observation angle is moved from 180° (or 0°) to 90°, because there will be more magnetic substates contributing incoherently to the cross section. (2) At the same incident energy, the particle spectra should be uncorrelated at angles that are separated by more than one angular coherence width.[5] (3) The particle spectra taken at two different incident energies become uncorrelated as ΔE is made greater than Γ_{CN}.

The $Al^{27}(d,p)Al^{28*}$ reaction was chosen for the initial study because, in addition to the ready availability of pure targets, the combination of high Q (5.50 MeV) and intermediate A leads one to expect a relatively high ratio of width to level spacing = Γ_R/D_R ($\sim$ 20 at a residual excitation energy, U_R, of 12 MeV). Therefore the fluctuation criterion[3,4] $\Gamma/D \gtrsim 2$ will be well satisfied for $U_R > 12$ MeV.

At a typical residual excitation energy, U_R = 15 MeV, Γ_R is estimated to be about 25 keV. The main instrumental problem encountered in this experiment is the need for a particle detection system with an energy resolution $< \Gamma_R$ capable of distinguishing protons from deuterons over an energy region from 2-10 MeV. A considerable effort was spent toward achieving this resolution. A ΔE-E system, incorporating a conventional multiplier circuit was chosen for particle identification. The detectors used were ORTEC fully depleted silicon surface barrier detectors with thicknesses of 47 microns and 1030 microns and sensitive areas of 25 mm^2 and 50 mm^2 respectively. Both detectors were selected for low noise characteristics. Thermoelectric cooling (to about -20° C) was provided to further reduce noise arising from leakage current. In the actual data taking configuration, an anticoincidence detector is mounted behind the ΔE-E telescope to reject protons which pass through the E detector.

Tests of energy resolution with alpha-particles from radioactive sources typically gave values of $\sim$ 20 keV (FWHM) for the E detector and $\sim$ 24 keV for the ΔE detector. The ΔE-E configuration (adding signals after the preamplifier stage) typically gave values of $\sim$ 32 keV. Energy resolution checks using 7 MeV elastically-scattered protons from thin Au targets gave a slightly better value. Under typical data taking conditions, however, the resolution achieved was somewhat worse ($\sim$ 40 keV) apparently due to a count pileup effect which persisted even at the lowest tolerable counting rate.

Initial runs indicated that buildup of C^{12} on the Al target was a severe problem because the $C^{12}(d,p)C^{13*}$ reactions yielded discrete proton groups in the energy region where fluctuations are expected. Installation of a liquid nitrogen cold trap around the target reduced the carbon buildup rate by a factor of 2.5. Because this rate still amounted to 1.5 ± 0.5 $\mu g/cm^2/hr$ under charged particle bombardment, targets were used for only several hours and then replaced with fresh ones. This reduced the $C^{12}(d,p)$ contributions to the proton spectra to an acceptable amount.

The Al targets used were typically 5.5 keV thick for the 16 MeV incident deutrons and 11.6 keV thick for 3 MeV protons. The incident beam energy spread was limited by defining slits to be less than 16 keV.

Figure 26-1 displays preliminary proton spectra at 170° and 90° at a bombarding energy of 16.48 MeV. The 170° spectrum was taken with the detector at 5 in. from the target whereas the 90° spectrum was taken at R = 9 in. in order to reduce kinematic broadening effects at 90°.

The 170° spectrum shows structure that is outside of the statistical uncertainties, qualitatively suggesting the existence of the fluctuations we seek. The fluctuations are less pronounced at 90° than at 170°, in further agreement with expectations. In addition, the positions of the peaks and valleys are uncorrelated for the 170° and 90° spectra. To put these features in quantitative terms, we have calculated the self- and cross-correlation coefficients for the two spectra. The cross-correlation coefficient is defined as:

$$C(\theta,\theta') = \left\langle \left(\frac{\sigma(\theta,U_R)}{\bar{\sigma}(\theta,U_R)} - 1.0\right)\left(\frac{\sigma(\theta',U_R)}{\bar{\sigma}(\theta',U_R)} - 1.0\right)\right\rangle_{U_R}, \qquad (1)$$

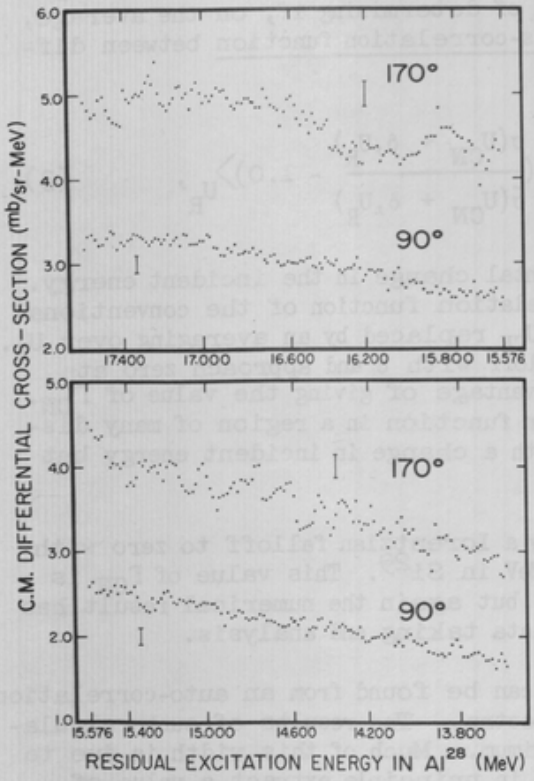

Fig. 26-1 Proton spectra from the $Al^{27}(d,p)Al^{28}$ reaction at 170° and 90° (Lab). The proton energies (Lab) range from about 3 MeV to 7 MeV. The incident deuteron energy is 16.48 MeV. Note the suppressed zero on the ordinate scale. The standard deviations are typically about 3% at each point. Several representative values are shown.

where the average is performed over the residual excitation energy U_R. The average cross section is assumed to have a simple functional form

$$\bar{\sigma}(\epsilon_p) = A(\epsilon_p - V)\, e^{-\epsilon_p/T}, \qquad (2)$$

where ϵ_p is the emitted particle energy and the parameters A, V, and T were determined by least-squares fitting to the data points of the individual spectrum concerned. The self-correlation coefficient is essentially Eq. (1) with $\theta' = \theta$.

The results of these calculations gave a self-correlation coefficient of 2.3×10^{-3} for the 170° spectrum and 0.6×10^{-3} for the 90° spectrum, confirming that fluctuations in the 90° spectrum are indeed dampened. A value of 0.01×10^{-3} was calculated for the cross correlation between the two spectra. The fact that the cross correlation is much smaller than either self correlation suggests that the two patterns are uncorrelated, as expected for angles separated by more than an angular coherence width. Proton spectra were also taken at several intermediate angles at the same

incident energy. Self-correlation coefficients for these angles display a smooth falloff between 170° and 90°.

The magnitudes of these self-correlation coefficients are considerably smaller than the values to be expected on the basis of the effective number of magnetic substates contributing incoherently to the cross section. However, little significance can be attached to the absolute magnitudes until one takes into account effects of imperfect instrumental resolution, of contributions from later stages of the emission cascade, of discrete proton groups (from reactions on lighter elements or from sequential emission between discrete levels), and of finite sample size. As yet, this has not been done.

To establish further that the peaks arise from transitions to the continuum and not to discrete levels, one would wish to demonstrate that the peaks (at the same U_R) disappear if the incident energy is changed by $\Delta E > \Gamma_{CN}$. However the small magnitude of the fluctuations causes serious difficulties in identifying and following individual peaks. Neither the present data nor the analysis techniques currently used are as yet adequate to enable one to trace individual peaks with incident energy. An alternative method of determining if, on the average, the peaks disappear is to make use of a cross-correlation function between different bombarding energies, i.e.,

$$XC(\Gamma_{CN},\delta) = \left\langle \left(\frac{\sigma(U_{CN},U_R)}{\bar{\sigma}(U_{CN},U_R)} - 1.0\right)\left(\frac{\sigma(U_{CN}+\delta,U_R)}{\bar{\sigma}(U_{CN}+\delta,U_R)} - 1.0\right)\right\rangle_{U_R}, \qquad (3)$$

where δ is the absolute value of the incremental change in the incident energy. This function is equivalent to the auto-correlation function of the conventional fluctuation theory, with the averaging over U_{CN} replaced by an averaging over U_R. It therefore should exhibit a Lorentzian falloff with δ and approach zero at large δ. This method of analysis has the advantage of giving the value of Γ_{CN}. It is to be noted that this cross-correlation function in a region of many discrete residual levels would also decrease with a change in incident energy but would not approach zero at large δ.

The uncorrected cross correlations show a Lorentzian falloff to zero with $\Gamma_{CN} \sim 70$ keV at the excitation energy of 33 MeV in Si^{29}. This value of Γ_{CN} is somewhat lower than expected from other data, but again the numerical result has little significance at the present stage of data taking and analysis.

The residual nucleus coherence width Γ_R can be found from an auto-correlation function analysis of the individual proton spectra. The results of such calculations yielded a value of ~ 45 keV at half maximum. Much of this width is due to the detection resolution. Although one could in principle extract a value of Γ_R even if the resolution is worse[6,7] than Γ_R, at present this has not been attempted.

In conclusion, it appears probable that the spectra exhibit the predicted fluctuations. This tentative conclusion is supported by the difference in self-correlation coefficients at 90° and 170°, the absence of correlation between spectra at 90° and 170°, and the approach to zero of the incident energy cross-

correlation function at large energy separations. As yet, however, neither the data nor the analysis is adequate for the extraction of meaningful values of Γ_{CN} or Γ_R. (D. Bodansky, N. Cue, and C. D. Kavaloski)

1 Nuclear Physics Laboratory Annual Report, University of Washington (1965), p. 46.
2 T. Ericson, Phys. Rev. Letters 5, 430 (1960); Ann. Phys. (N.Y.) 23, 230 (1963); D. M. Brink and R. O. Stephen, Phys. Letters 5, 77 (1964).
3 P. A. Moldauer, Phys. Letters 8, 70 (1964).
4 P. J. Dallimore and I. Hall, University of Oxford, NPL Report Ref: 176/65 (1965).
5 D. M. Brink, R. O. Stephen, and N. W. Tanner, Nuclear Phys. 54, 577 (1964).
6 W. R. Gibbs, LASL Report No. LA-3266 (1965).
7 D. W. Lang, Nuclear Phys. 72, 461 (1965).

VI. NUCLEAR FISSION

27. Competition between Neutron Emission and Fission at Moderate Excitation Energies

Neutron emission and fission are the two main modes of de-excitation of heavy nuclei excited above the thresholds for these processes. Although a fair amount is known about the dependence of the competition between neutron emission and fission on the atomic number and mass number of the fissioning nucleus, the energy dependence of this competition is not well understood. Analysis[1] of fission and spallation cross section data for heavy elements at moderate excitation energies generally indicates little variation of the ratio of fission to neutron emission (Γ_f/Γ_n) with excitation energy E*. An experiment by Harding and Farley[2], however, implied that Γ_f/Γ_n decreases markedly with E*.

An analysis according to statistical theory would predict that the dependence of Γ_f/Γ_n on E* would be of the following form:

$$\Gamma_f/\Gamma_n = f(E^*)\, e^{-(B_n - B_f)/T(E^*)},$$

where B_n and B_f are the thresholds for neutron emission and fission and where f is a function whose form is sensitive to assumptions made about the nature of the fission process. The function f depends on B_f, B_n, and on E*, but the dependence is expected to be slower than that of the exponential except where $B_n - B_f \cong 0$. The fact that this happens to be the case in the uranium region makes this region particularly suited to studies of f.

In the proposed experiment, values of Γ_f/Γ_n will be determined by the method of Harding and Farley. In this method one measures the angular correlation between neutrons and fission fragments. Neutrons emitted before fission are essentially uncorrelated in direction with the fission fragments. On the other hand, neutrons emitted after fission are strongly correlated in direction in the laboratory system because they are emitted from moving fragments. One can thus hope to deduce a ratio of post-to pre-fission neutrons from an angular correlation study. This in turn allows one to estimate the average excitation energy at which the fissions under study are occurring. It is hoped that by studying a variety of fissioning species at a series of energies it will be possible to deduce a simple function f that consistently accounts for the observations.

The experiment will include some important differences from the original Harding-Farley work while using the same basic technique:

(1) The present experiment will be performed at lower bombarding energies than the earlier work (10-22 MeV rather than 147 MeV). Fewer direct interactions, which can result in incomplete momentum transfer, are expected at the lower bombarding energies. It may also allow the use of an iterative procedure to deduce Γ_f/Γ_n at the higher excitation energies in our range. The point here is that the correlation measurements always provide some average Γ_f/Γ_n down the decay chain. In order to deduce $\Gamma_f/\Gamma_n(E^*)$ from such measurements, one must develop a consistent unfolding procedure, starting with low-energy values of Γ_f/Γ_n.

procedure, starting with low-energy values of Γ_f/Γ_n.

(2) In the present measurement neutron energy spectra will be recorded. (This was not done in the earlier work.) This will be accomplished by using a time-of-flight technique. The importance of spectral measurements is two-fold:

(a) They permit us to make the rather large correction for the falloff in neutron detection efficiency with laboratory neutron energy.

(b) They permit us to check to what degree the neutron spectra seen at different angles with respect to the fragments can be consistently interpreted as identical spectra in the center of mass system of the emitting fragments.

Some calculations of expected spectra and angular distributions have been made to permit us to better design our experiment.[3]

The neutron detection system consists of a photo tube with a one inch thick plastic scintillator, a time pick-off unit, and a time-to-pulse height converter. The efficiency calibration of the system will be carried out using Cf^{252}, a convenient source for which the spectrum is very well known.[4] A typical time-of-flight spectrum for Cf^{252} using this system is shown in Figure 27-1.

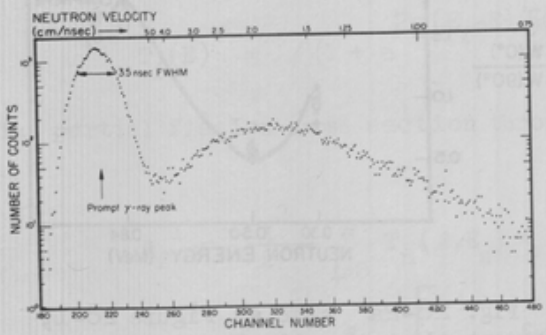

Fig. 27-1 Cf^{252} Neutron Time-of-Flight Spectrum. Flight Path = 30 cm.

The two fission fragment kinetic energies will be measured simultaneously by a pair of solid state detectors. For each event the neutron time-of-flight and the two fragment energies will be stored in the equivalent of a three-dimensional array using the SDS 930 on-line computer. This will provide fragment velocity information for each event, facilitating comparisons involving transformations between the laboratory and fragment center-of-mass systems. It will also permit determination of the dependence of neutron emission on mass asymmetry and total kinetic energy release.

A thin-walled chamber and beam tube[5], especially designed for low neutron background, has been constructed and installed on one of the University of Washington Van de Graaff beam lines. (C. J. Bishop, I. Halpern, C. D. Kavaloski, R. W. Shaw, and R. Vandenbosch)

---

1 R. Vandenbosch and J. R. Huizenga, Proceedings of the Second United Nations Conference on the Peaceful Uses of Atomic Energy, Geneva, 1958 (United Nations, Geneva, 1958), Vol. 15, p. 284.
2 G. N. Harding and F. J. M. Farley, Proc. Phys. Soc. LXIX, II-A, 853 (1956).
3 We are indebted to A. Bushkin for performing these calculations.
4 H. R. Bowman, S. G. Thompson, J. C. D. Milton, and W. J. Swiatecki, Phys. Rev. 126, 2120 (1962).
5 See Section 42 of this report.

28. Channel Analysis of Cross Sections and Anisotropies for Neutron-Induced Fission

The primary motivation for this analysis arose from an observation of an apparent inconsistency between two features of neutron-induced fission, namely the rounded shape of the total fission cross section excitation function[1,2] in the vicinity of the barrier, and the rapid variation of the anisotropy of the fragment distribution with neutron energy (see Figures 28-1 and 28-2).[2,3] The former observation implies a fission barrier with large enough curvature so that

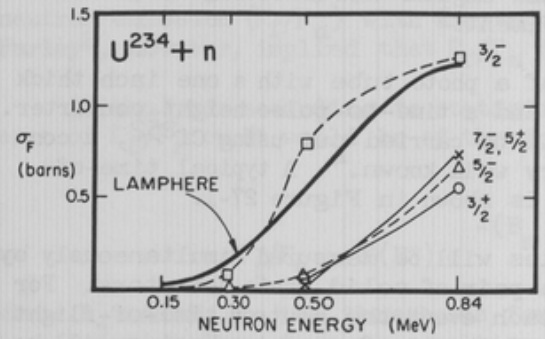

Fig. 28-1 The heavy line represents the total fission excitation function as measured by Lamphere. The various calculated curves are for parameters obtained from a fit to only the anisotropy data.

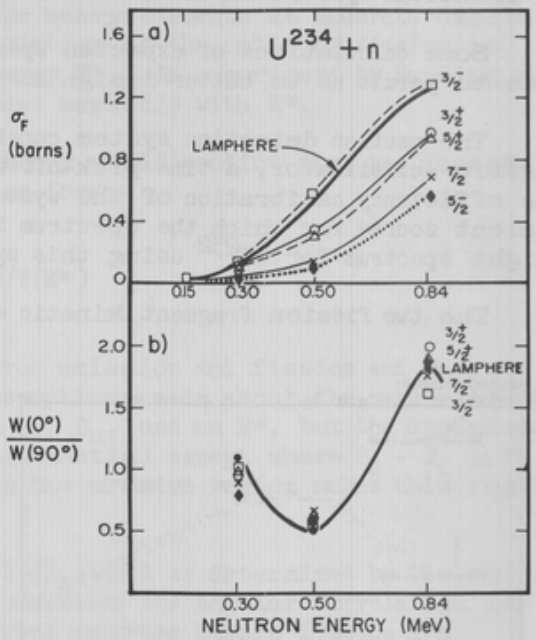

Fig. 28-2a Same as Figure 28-1, except that the calculated curves are for parameters obtained from a fit to both the antisotropy and cross section data.

Fig. 28-2b The full curve is the experimental anisotropy as reported by Lamphere. The various symbols represent the calculated values for parameters obtained from a fit to both the anisotropy and cross-section data.

appreciable penetration occurs below the barrier and also appreciable reflection occurs above the barrier. The angular anisotrophy however, fluctuates quite rapidly with neutron energy, which would seem to imply that new barrier states come in rather suddenly. A further motivation for this analysis came from a desire to explore the uniqueness of previous K-band assignments and to assess the possibilities for further assignments in other nuclei.

These remarks are primarily concerned with even-even target nuclei whose fission threshold is larger than the neutron binding energy. The compound nucleus formed by capture of a neutron of sufficient energy may either de-excite by re-emission of a neutron or may fission through one of the available nuclear states

at the saddle point. These saddle-point states of the highly distorted odd-mass-number nucleus can be identified as the Nilsson states of a deformed potential. For purposes of discussing cross sections and angular distributions, these states are characterized by the total angular momentum I, the projection of the angular momentum I along the symmetry axis, K, and the parity π. Each Nilsson state with a particular K (or Ω in Nilsson's nomenclature) presumably has built on it a rotational band. The most important qualitative dependence of the anisotropy on K can be summarized by the fact that $W(0°)/W(90°)$ is 1.0 or larger for $K = \frac{1}{2}$ and zero for $K \neq \frac{1}{2}$. The dependence of the anisotropy on energy for neutron-induced fission of U^{234}, illustrated by the full curve in Figure 28-2b, indicates that at the lowest bombarding energy fission is occurring primarily through a $K = \frac{1}{2}$ state; at 0.5 MeV neutron energy a state with $K > \frac{1}{2}$ is contributing importantly; and at 0.84 MeV neutron energy $K = \frac{1}{2}$ states dominate again. Lamphere[2] has analyzed these data at several incident neutron energies assuming a sequence of K, π states: $\frac{1}{2}^+$, $\frac{3}{2}^-$, $\frac{1}{2}^-$. Neutron competition from each I,π state of the compound nucleus was included in this analysis, and the relative contributions of the different K states were deduced from the anisotropy at each incident neutron energy. No attempt however, was made to relate the K-band fission probabilities at one incident neutron energy to that at another incident energy. This we have attempted to do by defining the barrier height E_f and the barrier curvature $\hbar\omega$ for each fission channel. The[4] fission barrier was assumed to be parabolic, enabling use of the Hill-Wheeler penetrability expression:

$$T_f(E) = 1/(1 + e^{2\pi(E_f - E)/\hbar\omega}).$$

The partial fission cross section through a particular K-band i is given by

$$\sigma_f^{\,i} = \frac{\pi\lambda^2}{2} \sum_{\ell=0}^{\infty} T_n(\ell, E_n) \times \sum_{J=1/2}^{\infty} \left[\frac{\epsilon_{j\ell}\, {}^{J}(2J+1) T_f^{\,i}(J,E)}{\sum_i T_f^{\,i}(J,E) + \sum_{E'\ell'} \epsilon_{j'\ell'}\, {}^{J}T_n(\ell', E')} \right]$$

following the notation of Rae et al.[5]

An exploratory analysis of the U^{234} fission cross section and anisotropy data, assuming a $\frac{1}{2}^+$, $\frac{3}{2}^-$, $\frac{1}{2}^-$ sequence and equal barrier curvature for all states, showed that the variation of cross section with energy implied a value of $\hbar\omega \gtrsim 400$ keV, whereas the anisotropy data implied a curvature of $\hbar\omega \lesssim 250$ keV. The computer code used in the analysis was then generalized to allow other K states, inclusion of a decoupling constant for describing the rotational states for $K = \frac{1}{2}$ bands, and the possibility of associating different barrier curvatures with different K states. Various types of calculations were then performed in an attempt to clarify the sensitivity to the various parameters. Five sets of

barrier states which seemed the most promising for explaining the results were chosen for further explorations. These are given on the first line of Table 28-1.

Table 28-1. Best set of parameters obtained by simultaneous fitting of cross section and anisotropy data for the $U^{234}(n,f)$ reaction. The barrier heights, E_f (relative to the neutron binding energy of 5.24 MeV) and the curvatures, $\hbar\omega$, are expressed in KeV. The decoupling constants α are also given although they are not well-determined by the analysis.

	Set I			Set II			Set III		
K	$3/2^+$	$1/2^-$	$1/2^+$	$3/2^-$	$1/2^-$	$1/2^+$	$5/2^+$	$1/2^+$	$1/2^-$
E_f	350	740	780	510	650	670	350	660	680
$\hbar\omega$	150	12	810	350	12	630	120	750	30
α	-	6.2	9.0	-	0.8	8.9	-	- 9	6.6

	Set IV			Set V		
K	$7/2^-$	$1/2^+$	$1/2^-$	$5/2^-$	$1/2^+$	$1/2^-$
E_f	60	750	900	200	680	1,260
$\hbar\omega$	125	19	950	60	60	1,470
α	-	0.6	9	-	0.9	9.0

In the first of these explorations, the barrier heights, barrier curvatures and decoupling constant parameters were varied[6] to fit only the anisotropy (with no reference to the absolute cross sections) at 0.3, 0.5, and 0.84 MeV. The most interesting result of this search is that although good fits to the anisotropy were obtained for all five sets of parameters, only the set with the $\frac{3^-}{2}$ K state gave a qualitatively correct fit to the cross section, as is illustrated in Figure 28-1. This result is sensitive, however, to the particular optical model parameters employed.

In a second exploration, the same parameters were varied to fit both the anisotropies and the total fission cross sections at the above-mentioned energies together with an additional cross-section value at 0.15 MeV where no anisotropy information is available. The barrier curvatures $\hbar\omega$ were arbitrarily restricted to values larger than 12 keV, and the absolute value of the decoupling constants were restricted to values of 9 or less. The fits to the anisotropies (see

Figure 28-2b) were not quite as good as previously when only the anisotropy was fitted, while the fits to the cross section improved somewhat, as can be seen by comparing Figure 28-2a with Figure 28-1. The parameters obtained are given in Table 28-1. These parameters were also used to compute complete angular distributions at 0.5 and 0.84 MeV neutron energies. The resulting angular distributions are shown in Figure 28-3. As Figure 28-3b illustrates, of the five sets chosen only two of them gives an angular distribution qualitatively different from the others. One must remember that the angular distribution is not simply a function of the K and I values of the available barrier states, but it also depends on the spin and parity distribution of the compound states found at a particular neutron energy and also on the final states to which neutron emission can occur. The sensitivity to the parity of the $K = \frac{3}{2}$ state arises from the fact that there is a fairly strong maximum in the p-wave strength function, so that at certain neutron energies $\ell = 1$ neutron capture dominates over $\ell = 0$ and $\ell = 2$. For similar reasons it can be seen from Table 28-1 that the ordering of K states is not what might be expected from the anisotropy pattern. This reflects the fact that at 0.3 MeV neutron energy the spins and parities of the compound states favor fission through a $K = \frac{1}{2}$ state even though the $K \neq \frac{1}{2}$ state has a lower barrier.

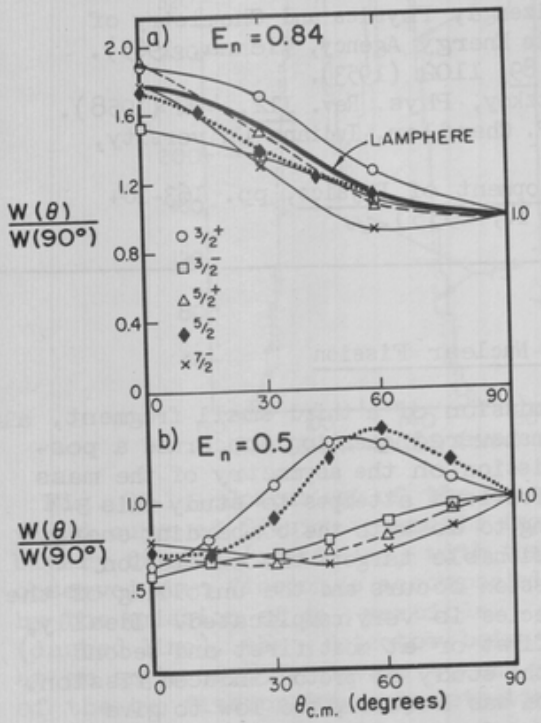

Fig. 28-3 Angular distributions at (a) $E_n = 0.84$ MeV and (b) $E_n = 0.5$ MeV. The calculated curves are for parameters obtained from a fit to both the anisotropy and cross section data.

With respect to the question of the barrier curvature, one sees from Table 28-1 that we have been able to account for both the sub-barrier fission behavior and the rapidly varying anisotropies by having varying curvatures. The states with large curvature account for the first effect, and the state with small curvature permits sharper changes in the anisotropy with energy. The indication that the barrier curvatures are different for different K states does not seem physically unreasonable. As the odd-mass number fissioning nucleus is deforming, it must conserve angular momentum and parity, so that many of the crossings on the Nilsson diagram cannot be exploited. This effect has been discussed by Wheeler[7] in terms of a specialization energy in connection with spontaneous fission. We are currently exploring the Nilsson diagram to see if one can understand the barrier curvatures in more detail. If the varying curvatures do indeed reflect the details of the single particle states of the deformed nucleus, one can understand why some target nuclei like U^{234} and Th^{232}

(both of which form compound nuclei with 143 neutrons) exhibit large variations of the anisotropy with energy, while other target nuclei such as U^{236}, U^{238}, and Pu^{240} do not. (R. Vandenbosch)

1 D. J. Hughes and R. B. Schwartz, United States Atomic Energy Commission Report BNL 325, 2nd Edition (1958).
2 R. W. Lamphere, Nuclear Phys. 38, 561 (1962); R. W. Lamphere, Physics and Chemistry of Fission, Vol. I, 63 (International Atomic Energy Agency, Vienna, 1965).
3 R. Vandenbosch, J. P. Unik, and J. R. Huizenga, Physics and Chemistry of Fission, Vol. I, 547 (International Atomic Energy Agency, Vienna, 1965).
4 D. L. Hill and J. A. Wheeler, Phys. Rev. 89, 1102 (1953).
5 E. R. Rae, B. Margolis, and E. S. Troubetzkoy, Phys. Rev. 112, 492 (1958).
6 The search routine was obtained from J. P. Chandler, Indiana University, private communication.
7 J. A. Wheeler in Niels Bohr and the Development of Physics, pp. 163-184 (McGraw-Hill Book Co., Inc., New York, N. Y., 1955).

29. Doubly Charged Particle Emission During Nuclear Fission

Studies of fission accompanied by the emission of a third small fragment, almost always an α particle, have continued. One unanswered question concerned a possible correlation of the probability of α emission on the asymmetry of the mass split of the two heavy fission fragments.[1] Previous attempts to study this question were inconclusive, for reasons having to do with the bombarding energy. In helium ion induced fission of readily fissionable targets the excitation energies are so high that multiple chance fission occurs and the unfolding of the contributions from the several fissioning species is very complicated. Ideally, one would like to study a system where only first or at most first and second chance fission are possible. This suggests the study of proton-induced fission. The proton energy available from the cyclotron was however, too low to give enough fission events. The experiment was therefore performed with 13 MeV protons from the tandem with a U^{235} target. The bombarding energy is high enough to give an appreciable amount of symmetric fission yet below the threshold for 3rd-chance fission.

The experiment consisted of measuring the two fission fragment kinetic energies in coincidence with an α particle. Because the direction of emission of the α particle relative to the two heavy fragments is correlated with their asymmetry, in order to study the dependence of α emission on mass asymmetry it is necessary to measure the cross section as a function of angle. We chose to use two α detectors, each subtending a rather large solid angle, one centered at 90° relative to the two fission fragment detectors (which were 180° apart), the other at 75° to one of the fragment detectors. In the latter case the fragment detector tended to detect mainly the light fission fragment.

From the fission fragment kinetic energies the mass split in α accompanied fission was computed and compared with the spectrum obtained for binary fission. Figure 29-1 shows the results obtained for coincidence with the α detector placed

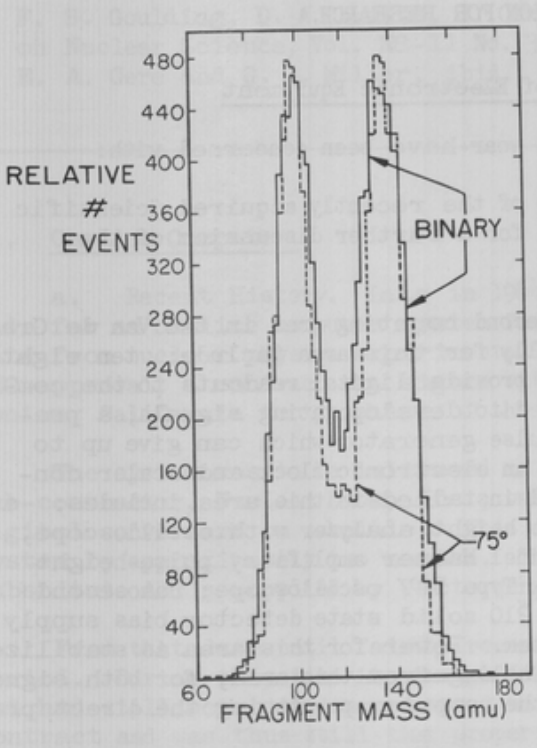

Fig. 29-1 Comparison of the mass-yield curve of fission fragments from binary fission (solid line) with that observed when fission is accompanied by the emission of an α particle (dashed line), the α detector being at an angle of 75° relative to one of the two fission fragment detectors.

at 75°. In this configuration there is a slight favoring of asymmetric over symmetric fission in α accompanied fission. All the data were analyzed with a suitable weighting to allow for the solid angle subtended by each α detector and the overlap between them. Taking the fission yields of fragments in a 9-unit mass range in the light fragment peak as a measure of the yield of asymmetric fission and a 9-unit mass range in the valley between as a measure of the yield of symmetric fission, the average peak-to-valley ratio for α accompanied fission for 13.0 MeV protons on U^{235} is 2.86 ± 0.35, compared with 2.29 ± 0.09 for the same ratio in binary fission. Thus asymmetric fission appears to be favored over symmetric fission by a factor of 1.25 ± 0.16.

This experiment is still far from ideal for answering the question which was asked. If there is such a thing as a symmetric fission "mode," it is not easily observed in studies of the mass valley of U^{235} fission. Most of the events are due to the edges of the asymmetric mass distribution. A much better target for such a study would be Ra^{226}, which under proton bombardment gives well-separated symmetric and asymmetric mass yields.[2] Because of its unique health and contamination hazards we have hesitated to perform experiments with radium in the multi-purpose scattering chamber. Instead, we have constructed a small scattering chamber with a thin membrane to isolate it from the main vacuum system. The experiment will be repeated using the chamber and the computer for on-line data reduction. (A. W. Fairhall, I. Halpern, W. D. Loveland, and D. G. Perry)

---

1 Nuclear Physics Laboratory Annual Report, University of Washington, (1965), p. 57.

2 Fission of Ra^{226} by 11 MeV Protons, R. C. Jensen, and A. W. Fairhall, Phys. Rev. 109, 942 (1958).

VII. INSTRUMENTATION FOR RESEARCH

30. Design, Development and Construction of Electronic Equipment

Major programs pursued during the past year have been concerned with:

a. Installation and trouble-shooting of the recently acquired Scientific Data Systems 930 Computer. (See Section 31 for a further discussion of the computer.)

b. The placement in operation of a second counting area in the Van de Graaff counting room. Items constructed specifically for this area include: ten eight-decade scalers, with output decode lines to provide digital readouts to the computer; a 4-channel slow coincidence unit used to develop gating signals; a precision pulse generator; a general purpose pulse generator which can give up to eight simultaneous (or delayed) pulses; and an electronic clock and scaler controller. Commercial equipment purchased and installed in this area includes: a Nuclear Data Model ND-130 multichannel pulse height analyzer with oscilloscope, paper tape and typewriter readouts; a 4-channel Hamner amplifier, pulse-height analyzer and coincidence system; a Tektronix Type 547 oscilloscope; nanosecond fast coincidence circuitry; two ORTEC model 210 solid state detector bias supply units; and an ORTEC Model 220 amplifier system. Power for this area is stabilized by a General Radio 5 kVa line stabilizer. Cabling from this area, for both signals and scaler readouts, has been installed to the computer permitting the direct presentation of data to the computer.

c. The design and construction of equipment for the Van de Graaff beam bunching system. (See Section 44 for further details.)

d. The construction of a particle identifier system, based on the design of Goulding et al.[1] Prints and negatives were purchased from the Lawrence Radiation Laboratory. The circuits are housed in standard "AEC compatible" plug-in units, to allow for operational flexibility. Testing of this system has begun.

Other construction projects have included: a pulse division circuit based on the design of Gere and Miller[2] (standard plug-in); three adder-mixer units (standard plug-in); a pulse pile-up rejection unit (standard plug-in); a unit used in checking solid state detector fabrication; an 0-800 volt power supply and a resistivity probe for solid state detector fabrication; a counter giving an audible output proportional to the Van de Graaff beam intensity; a fanout system for the beam monitoring output; and numerous small amplifiers, metering circuits, attenuators and terminators.

Commercial equipment purchased for general laboratory use, beyond that mentioned above, includes: two ORTEC Model 220 amplifier systems; three ORTEC Model 260 Time Pickoff Units; an ORTEC Model 210 solid state detector bias supply unit; a Northern Scientific Model NS-601 multichannel pulse height analyzer, with a teletype readout; a Moseley point plotter used in conjunction with the multichannel analyzers; a Nuclear Data Model ND-501 analog dual buffer storage unit; and several charge sensitive preamplifiers for use with solid state detectors. (L. H. Dunning, H. Fauska, K. H. Lee, G. Monge, and N. Ward)

1 F. S. Goulding, D. A. Landis, J. Cerny III, and R. H. Pehl, IEEE Transactions on Nuclear Science, Vol. NS-11 No. 3 (1964), pp. 388-396.
2 E. A. Gere and G. L. Miller, ibid., pp. 382-387.

---

31. On-Line Computer

a. Recent History. Late in 1964 the AEC authorized this laboratory to take bids for an on-line computer system for real-time acquisition and processing of data from nuclear physics experiments. On the basis of these bids and further AEC approval, a contract was signed with Scientific Data Systems, Inc. of Santa Monica, California for purchase of the system.

The system was to be delivered no later than October 6, 1965. However, a sub-contractor, Nuclear Data, Inc., was unable to supply the specified analog-to-digital converters on schedule. This delayed delivery of the entire computer system by approximately two months. The actual deliver date of the system, with substitute ADC's supplied by Victoreen, Inc., was December 15, 1965.

From that date until fairly recently the system has been in the acceptance period. During this time it was partially available for use by this laboratory, but had still not been demonstrated to meet the technical specifications of the contract and was thus still the property of SDS. Because the acceptance period was rather lengthy, the laboratory personnel had an excellent opportunity to test the system against specifications, requirements, and expectations. By April the system was performing in accordance with specifications. On April 6, 1966 the system was accepted from SDS, and final payment (less $14,000 for items in dispute) was made by the University and the AEC to SDS.

b. Description of the System. The on-line computer system is built around an SDS 930 computer with 8,192 words of 24 bit, 1.75 μsec core memory, two input/output channels, twelve levels of true priority interrupts, and a real time clock. Standard SDS peripheral equipment includes two 75 in/sec triple-density magnetic tape transports; a 100 card/min card reader; a 100 card/min card punch (IBM 523); a 300 line/min 132 column line printer with 48 standard characters and 16 special plotting symbols (for plotting at a density of 18 x 20/in); and a keyboard printer (Teletype 35 ASR) with paper tape read/punch at 10 characters/sec. Figure 31-1 shows two views of the computer.

Two special sub-systems, a data-input multiplexer and an oscilloscope display unit, were manufactured by SDS to our specifications. The data-input multiplexer is designed to operate up to 8 analog-to-digital converters (the present system has 4 ADC's) which will accept pulses from particle detectors, etc. Each ADC input contains a redundant register which can accept the ADC input as soon as conversion is complete, thereby de-randomizing the counting rate to some extent. A format register in the multiplexer, which may be read by the computer, keeps track of which ADC's are active. Any ADC or group of ADC's can be connected to a priority interrupt line to initiate data storage. Any ADC can be set to operate either independently, as in the accumulation of a single parameter pulse-height

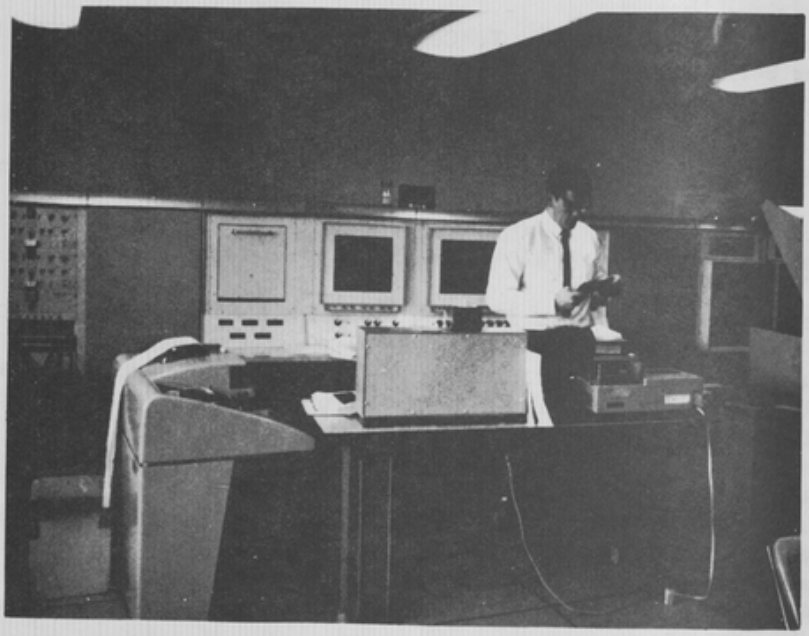

Fig. 31-1 Two views of the SDS 930 computer.

spectrum, or with other ADC's as in a coincidence experiment.

In addition, the data-input multiplexer provides the capability of reading in any of 30 8-decade (32 bit) external data signals such as scalers or clocks, 40 1-bit switch position signals, and 10 10-bit external data signals from position encoders, etc. Ten of the 8-decade inputs are now permanently connected to laboratory scalers in Van de Graaff counting room 4. The control console also contains 5 six-digit thumbwheel switches for numerical entries, and a bank of 10 7-decade Nixie display registers for presenting numbers entered by the computer.

The display unit is designed to provide two- or three dimensional presentations of collected data with a minimum overhead of computer time. The unit is connected to the Y-buffer (I/O channel) of the computer and receives digital signals which represent the x, y, and z coordinates of points in three dimensional space. This digital information is converted by means of D/A converters to analog voltages. These voltages are then transformed to horizontal and vertical oscilloscope deflections by means of a special purpose analog computer contained in the display unit. This unit can form any linear combination of voltages x, y, and z, perform coordinate rotations by turning a knob, take the logarithm of a given analog voltage, and blank, intensify, or trigger an interrupt when an analog voltage falls in a present voltage range. The particular operations to be performed by the display analog computer are controlled by wiring a removable patch panel and by control switches and dials at the display console. (Further details of these special sub-systems may be found in the Technical Specifications of the Computer System.)

c. Progress in the Use of the System. In implementing the use of the on-line computer system, two approaches are possible: to make the operation of the system resemble as much as possible the operation of more familiar apparatus, such as multi-channel analyzers, through special hardware and a few rigid master data collection programs; or to provide building-block subroutines which allow the experimenter to prepare his own data-collection programs in a familiar programming language (e.g., REAL-TIME FORTRAN) and still use the full flexibility of the computer system. The former approach makes the transition to using an on-line computer as easy as possible for the physicist but sharply limits the use of the system. The latter approach puts the principal programming burden on the experimentalist but gives him full flexibility in the use of the system. The latter approach was chosen as more in keeping with the principal role of this laboratory, the education and training of graduate students, and also more in line with the general style of the laboratory. Furthermore, the development of REAL-TIME FORTRAN (RTF) by SDS has provided an excellent and semi-familiar programming language for preparing data collection programs. RTF facilitates communication with the special hardware, such as the data-interrupt multiplexer and the oscilloscope display unit, by providing the capability of in-line machine language instructions and response to priority interrupts.

Building-block subroutines for use with RTF have been written for operating the analog-to-digital converters; for operating the oscilloscope display unit with full control of light pen, characters, and vectors; for reading in the external scalers in Counting Room 4 and reading the digit switches; and for setting and fast updating of the nixie readout units. Some of these routines are now incorporated into the RTF library on magnetic tape, and all are in use.

These building-block subroutines have been used in writing several RTF data collection programs for a variety of experimental applications, including one parameter pulse-height analysis of data from up to four independent sources simultaneously; two parameter analysis accumulated in a 32 x 64 array in memory; and three parameter analysis to be written on magnetic tape for sorting and summing at a later time. A data analysis program is now in use which displays off-line data on the oscilloscope display and permits background subtraction and peak integration using the light pen to specify background and integration limits. A two-parameter particle identification program has been written which allows specification with the light pen of an arbitrary number of boundaries. Events falling in different regions between these boundaries are stored in different areas of memory.

At this writing the computer system has been employed on-line in three experimental projects (Sections 16, 17, and 25), and has proved a valuable asset in each of these experiments. Now that most of the preliminary testing and programming have been accomplished, we expect that it will play a much larger role in experiments at this laboratory in the near future. (D. Bodansky, J. G. Cramer, H. Fauska, J. B. Gerhart and R. Vandenbosch)

---

32. Particle Identification by Pulse Shape Discrimination

A theoretical investigation of the feasibility of particle identification by pulse shape discrimination in lithium-drifted solid state detectors has been performed. The investigation was carried out for protons, deuterons, and alpha particles in the energy range from 3 MeV to 16 MeV.

The basis for this type of particle identification is that the rise time of the pulse from the detector is dependent upon the range of the particular particle in the detector.[1] The range, in turn, depends upon the charge, mass, and energy of the incident particle. Theoretical equations have been derived which predict the time dependence of the pulses derived from solid state detectors.[1] These equations were inverted using the SDS 930 digital computer recently acquired by this laboratory. In this way the dependence on the incident energy and particle type of the time required for a pulse to reach various energy discriminator levels was determined. Using this information one can generate theoretical two-dimensional spectra which display the separation one might expect to obtain under experimental conditions. Figure 32-1 is one such spectrum.

The calculations indicate that in order to get reasonable separation at the lower energies of interest one should arrange the detector so that the particles are incident on what is normally the back side. It is also desirable to have the detector as thick as is possible and the detector bias as low as possible and still totally deplete the detector. It is felt that by using a 1mm thick transmission detector with 100 V bias that one should be able to separate protons, deuterons, and alpha particles with energies down to about 4.5 MeV and perhaps down to 3 MeV.

This type of particle identification system has the obvious advantage over the standard (dE/dx)-E system in that only one detector is required and all the

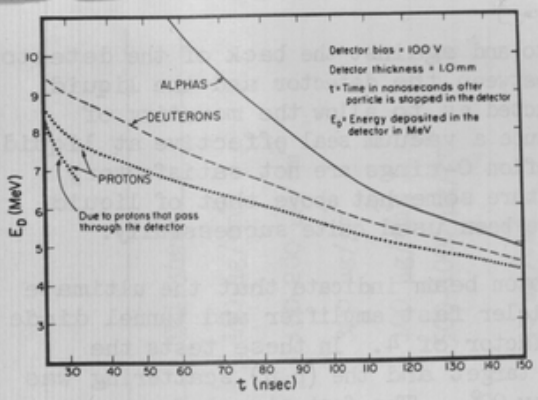

Fig. 32-1 Timing spectra of pulses expected for protons, deuterons, and alpha particles incident from the back of a lithium-drifted detector for a 3.0 MeV energy discriminator.

information is obtained from a single signal. In principle, one should be able to get the rise time information into a usable form using two energy discriminators and a time-to-pulse height converter. The signal from the time-to-pulse height converter and the standard energy signal are fed into some type of two-dimensional analyzer to produce the separated spectra.

It is planned to try this technique in the near future. (T. Hayward and D. Patterson)

1 C. A. J. Ammerlaan, R. F. Rumphorst, and L. A. C. Koerts, Nuclear Instr. and Methods 22, 189 (1963).

33. Liquid Nitrogen-Cooled Solid State Detectors

During the last year we have constructed, tested, and operated in vacuum two liquid nitrogen-cooled holders for solid state detectors for use in the laboratory's 60-in. scattering chambers (Figure 33-1). They were constructed in an attempt to improve the time resolution in an experiment on gamma-ray polarization in inelastic scattering discussed in Section 16.

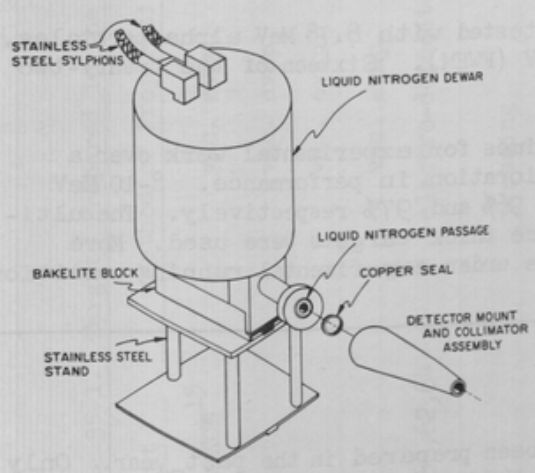

Fig. 33-1 Liquid Nitrogen-Cooled Detector Holder.

These holders consist of a brass dewar which can be mounted in the scattering chamber and filled through stainless steel sylphon lines from outside the vacuum. The dewars have a capacity of approximately 1.5 liters, and with a single filling maintain a detector at nearly liquid nitrogen temperatures for about 4 hours. They are equipped with automatic fillers which sense the liquid nitrogen level by means of thermistors, and can thus be used without periodic manual filling.

Thermal insulation is accomplished by mounting a dewar on a bakelite block supported by a stainless steel stand that can be rigidly mounted on one of the scattering chamber arms.

Liquid nitrogen is allowed to flow up to and against the back of the detector mounting to insure maximum thermal contact between the detector and the liquid nitrogen. Since the apparatus is so constructed as to allow the mounting of different detectors, it is necessary to produce a vacuum seal effective at liquid nitrogen temperatures. It was found that teflon O-rings are not satisfactory for this purpose as they freeze at a temperature somewhat above that of liquid nitrogen; however, annealed copper seals have been used quite successfully.

Initial tests with the Van de Graaff proton beam indicate that the ultimate time resolution obtainable with a Williams-Nieler fast amplifier and tunnel diode discriminator can be improved by at least a factor of 4. In these tests the proton beam was scattered from a polystyrene target and the (p,p) scattering was observed with a pair of detectors separated by 90°. The fast signal from one tunnel diode discriminator was used as the "start" signal for a time to pulse height converter. The "stop" signal was derived from the fast signal of the tunnel diode discriminator associated with the second detector. The output of the time-to-pulse height converter was analyzed in a 512-channel analyzer. The detectors which were used were commercial 200 mm^2 × 1 mm thick lithium-drift detectors. Uncooled, the time resolution at 150 volts bias was about 2 nanoseconds; when cooled to liquid nitrogen temperature the resolving time was about 0.5 nanoseconds. (T. D. Hayward and D. M. Patterson)

---

34. Lithium Drifted Silicon Detector Fabrication

The detector fabrication program has been in effect one year, but only since February, 1966 has it been on a full-time basis. Thirty-two detectors, eight 1 mm thick and twenty-four 2 mm thick, have been fabricated. The active areas range from 45 to 250 mm^2.

Twenty-two of the detectors have been tested with 8.78 MeV alpha particles. These had resolutions between 28 and 100 keV (FWHM). Sixteen of the twenty-two had resolutions below 60 keV (FWHM).

Two 2 mm detectors were used several times for experimental work over a period of six months with no apparent deterioration in performance. 8-10 MeV protons were detected with an efficiency of 96% and 97% respectively. The ultimate resolution has not been determined since thick targets were used. More careful measurements of detector performance under experimental running conditions are in progress. (J. Sauer)

---

35. Target Preparation

The targets listed in Table 35-1 have been prepared in the past year. Only the targets that differ from those prepared the previous two years[1,2] have been listed. (J. Sauer)

Table 35-1. Targets Prepared in the Past Year

Target	Method of Preparation	Backing*	Thickness
N^{15} as KCN^{15}	vac. evap.	75 & 100 $\mu g/cm^2$ carbon	150 $\mu g/cm^2$
Mg^{24}	vac. evap.	75 $\mu g/cm^2$ carbon	100-200 $\mu g/cm^2$
Mg^{25}	vac. evap.	s.s. & 70 $\mu g/cm^2$ Al	300 $\mu g/cm^2$
Ca^{48}	vac. evap.	40 $\mu g/cm^2$ carbon	100 $\mu g/cm^2$
$Ni^{58,60,62,64}$	electro-deposition	Cu which was removed chemically to give s.s. foils	500-1000 $\mu g/cm^2$
Ge^{72}	pressing	s.s.	30 mg/cm^2
$Sn^{112,114,116,117}$ $Sn^{118,119,120,122,124}$	electro-deposition	Cu which was removed chemically to give s.s. foils	200-2000 $\mu g/cm^2$
Ba as $BaCl_2$	molec. plating[3]	100 $\mu g/cm^2$ Ni	100 $\mu g/cm^2$
Ce	vac. evap. & electron bomb.	40 $\mu g/cm^2$ carbon	100-400 $\mu g/cm^2$
Pb^{204}	electro deposition	Cu which was removed chemically to give s.s. foil	600-800 $\mu g/cm^2$
$Pb^{206,207,208}$	vac. evap.	s.s.	500-900 $\mu g/cm^2$
Th as $Th(NO_3)_4$	molec. plating	100 $\mu g/cm^2$ Ni	100 $\mu g/cm^2$
U as $UO_2(NO_3)_2$	molec. plating	100 $\mu g/cm^2$ Ni	100 $\mu g/cm^2$
U^{235} as UO_2	vac. evap.	40 $\mu g/cm^2$ carbon	200-250 $\mu g/cm^2$

*s.s. refers to self-supporting targets

1 Nuclear Physics Laboratory Annual Report, University of Washington (1965), p. 73.
2 Cyclotron Research, University of Washington (1964), p. 62.
3 W. Parker, Methods in Preparation of Radioactive Material, Elanders Boktryckeri Aktiabolag, Göteborg (1965), p. 47.

VIII. ACCELERATOR RESEARCH AND DEVELOPMENT

36. The Three-Stage Van de Graaff Accelerator

The responsibility for all operation and maintenance of the tandem Van de Graaff accelerator was assumed by the University of Washington Nuclear Physics Laboratory in early May, 1965 although the machine had not yet passed acceptance tests nor met the design specifications. Operating time for the next few months was divided about equally between attempts to improve the performance and stability of the beam from the accelerator and operation for research purposes. In addition an extensive training program to develop operating and maintenance personnel was carried out as rapidly as possible.

The injector stage of the three stage Van de Graaff system is still in the High Voltage Engineering Corporation plant undergoing final specification tests. Delivery of the injector, which was originally scheduled for December, 1964, has been delayed due to failure to achieve the required beam intensity and energy. The required values of these parameters are now at least marginally obtainable and it is expected that disassembly for shipment of the components will start not later than the last week of May, 1966.

Plans for installation of the injector are as complete as possible with the information available and some preliminary wiring installation has been completed. It is anticipated that operation of the tandem stage will not be severely curtailed during installation of the injector.

The tandem stage of the accelerator system, together with most of the auxiliary components which have been delivered and installed, were accepted by the University of Washington on January 17, 1966. The machine met performance specifications (except at the 10 MeV points) during tests made the last week of September 1965. The first research data obtained with the beam from the tandem accelerator were taken on May 13, 1965.

Numerous improvements, modifications and additions to the accelerator and its accessory equipment have been made during the past year in order to make the machine more useful and more easily operable. Following is a partial list of such changes:

(1) Addition of a high speed vacuum roughing system connected to all sections of the accelerator vacuum system.

(2) Installation of a dc supply and arc current regulator for the ion source filament current.

(3) Modification of the exchange voltage power supply to reduce ripple and improve regulation.

(4) Construction of a gas switching system for the ion source and exchange gas supplies.

(5) Substitution of motor driven needle valves for manually operated valves in the ion source and exchange gas supplies.

(6) All negative ion source controls were moved from the vicinity of the ion source to the control room.

(7) Automatic liquid nitrogen trap fillers were installed on all traps which required filling more than once per 24 hours.

(8) Addition of a small electromagnet to provide vertical steering of the beam as it emerges from the ion source.

(9) A remotely controlled beam stopper and monitor has been installed to allow access to the experimental areas without interrupting or disturbing the operation of the machine.

(10) Many modifications and additions to the existing safety interlock system for the protection of personnel and equipment.

(11) Partial installation of a Geissler-operated interlock system for protection of the vacuum system.

(12) Spark shields to protect the belt drive motor and electrical leads have been installed.

(13) Leaks in cooling water lines inside the pressure tank have been eliminated and the finned cooling coils have been reconnected in order to increase their efficacy.

(14) Removal of the down charge screen.

(15) Addition of a fine control to the belt charge control system.

(16) Beam limiting aperature installed before low energy deflector plates to reduce aberration in off-center beam.

(17) Safety lights have been placed in strategic locations with appropriate interlocks.

(18) Filters were installed in both condenser and chilled water systems.

(19) A ground system alarm has been installed to detect the presence of multiple return paths of the power system neutral current. In addition, a system of "clean" power outlets has been added to caves 1 and 2, operating off a separate isolation transformer with a single point ground.

(20) Remote power distribution centers were added to caves 1 and 2 including 10 kW of stabiline regulated power.

(21) Several minor refinements include audio indication of beam flap position; NMR audio tuning indication; belt frequency oscilloscope for ripple monitoring; chilled water failure alarm; and an audible beam intensity indicator.

The Van de Graaff tank has been opened 18 times in the past year for the following listed reasons:

(1)	4/27/65	To install new stripper tube.
(2)	5/20/65	To align stripper and install wire grid at stripper entrance.
(3)	6/3/65	Unstable operation - caused by piece of emery paper on beam tube.
(4)	6/10/65	Belt drive motor burned out, caused by faulty circuit breaker and inoperable safety circuits.
(5)	7/28/65	To install new corona points. Also installed shorts on the first 23 sections of the high energy tube to check steering effects. These shorts were later removed without opening the tank.
(6)	8/13/65	To install stripper bias battery in terminal.
(7)	8/17/65	To repair leaks in cooling coils.
(8)	9/1/65	To repair leaks in cooling coils.
(9)	9/7/65	To repair leaks in cooling coils and revise system.
(10)	11/4/65	Drive motor burned out.
(11)	11/6/65	Short in control wiring to stripper gas valve.
(12)	11/9/65	Clutch spring failed in stripper gas valve.
(13)	12/9/65	Sparking caused by loose tube-to-column connector springs.
(14)	12/11/65	Arcing near high energy end of tank (no obvious cause). First three planes at terminal toward high energy base were connected to terminal.
(15)	2/17/66	To replace leaking safety valve on pressure tank.
(16)	3/19/66	Burned out low energy column resistor.
(17)	4/14/66	To put timing mark on belt.
(18)	4/16/66	Machine very unstable. Changed belt, cleaned columns, checked belt guides, tested and regraded column resistors.

The two longest operating periods occurred between #9 and #10 (about 2 months), and between #14 and #15 (about 2 months).

Table 36-1 summarizes the statistics of Van de Graaff operation during the period from June 8, 1965 to May 15, 1966. (J. S. Heagney, T. J. Morgan, J. Orth, G. J. Rohrbaugh and F. H. Schmidt)

Table 36-1. Statistics of Van de Graaf Operation During the Period from June 8, 1965 - May 15, 1966

Division of Van de Graaff Time Among Activities:

Activity		Time (hrs.)	Per Cent
Normal Operation:	Research	3475.0 hrs.	69
	Machine & Component Tests	362.0	7
Scheduled repairs, modifications, & maintenance		557.0	11
Unscheduled repairs (incl. going into tank)		425.0	8.5
Teaching		45.0	1
Experimenter's set-up time		184.0	3.5
	Total	5048.0 hrs.	100%

Division of Normal Operation Among Projectiles:

Protons	2054.3 hrs.	55.8%
He^4	937.5	25.4
Deuterons	525.2	14.2
O^{16}	153.1	4.2
He^3	17.6	0.4
Total	3687.7 hrs.	100.0%

37. Cyclotron

The 60-inch Cyclotron continued operations for research on a nearly full schedule throughout the year. Due to a temporary lack of sufficient numbers of qualified operators for both the cyclotron and the Van de Graaff, the operation schedule on the cyclotron was reduced from 17 hours per day, 6-1/2 days/week to 17 hours per day, 5 days/week. Responsibility for maintenance of the cyclotron has been assumed almost entirely by the graduate students.

One major, and long overdue, improvement was installed during the year; viz., a fully transistorized main magnet regulator incorporating 60 series power transistors and using the existing motor generator as a rough regulator-power supply. Design features include regulation to one part in 20,000, with maximum open circuit protection afforded by zener diode, parallel diode and relay circuitry.

Other improvements, modifications, and major repairs made during the year include the following:

An extensive program was instigated to locate and remove ground loops in the building and machine power system. A current transformer installed in the transformer station's ground system now indicates any violation of ground conditions.

A redesigned copper ion source has been installed in place of the former one, resulting in a substantial reduction in sparking and an increased beam output.

Various minor alterations to the beam positioning equipment were made. Wiring to ladder and wheel type target positioners with binary readout have been completed. A movable mirror has been added to the duct slit system; this allows viewing of the mechanism without removal. A new TV monitor was purchased.

Major repairs to the machine include rewinding the 250 hp motor and turning the commutator of both the main and analyzer magnet generators. A new hydraulic motor and pump was installed to replace the old leaking one.

A cable network was run to connect the cyclotron counting rooms with the Van de Graaff counting area.

Table 37-1 summarizes the statistics of cyclotron operation during the period from May 16, 1965 to May 15, 1966. (J. Orth)

Table 37-1. Statistics of Cyclotron Operation from May 16, 1965 to May 15, 1966.

Division of Cyclotron Time Among Activities	Time	
Activity	Hours	Per Cent
Normal Operation	2976.9	53.9
Set-up of Experiments	532.2	9.6
Cyclotron Testing	355.5	6.4
Scheduled Repairs and Modifications	740.7	13.4
Unscheduled Repairs	605.2	11.0
Failure of Equipment	--	
Unsatisfactory Cyclotron Operation	51.1	0.9
Experiments Using No Beam	--	
Unrequested Time	257.2	4.7
Visitors	8.0	0.1
Total	5517.8	100.0
Division of Normal Operation Time Among Projectiles		
Alpha Particles	2016.3	67.9
Protons	284.6	9.6
Deuterons	667.0	22.5
Total	2967.9	100.0

Bombardments for Outside Investigators

	Hours
University of Oregon	23.3
Oregon State University	147.0
Western Washington State College	10.0
Simon Fraser University	7.1
Hanford Radiation Laboratory	18.3
Department of Physics - Professor McDermott	57.0
Total	315.7

38. The Charge Distribution of O^{16} Ions from a Tandem Accelerator

In an effort to obtain information about the acceleration of heavy ions in tandem accelerators the charge state distribution of oxygen ions accelerated in the University of Washington FN tandem accelerator was measured as a function of terminal voltage and stripper pressure. The results of these measurements are summarized in Figure 38-1, which shows Z_{av}, the average charge state versus

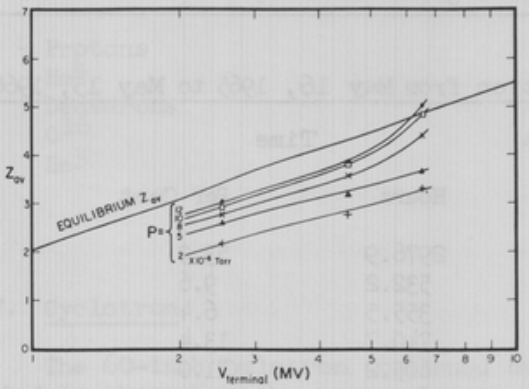

Fig. 38-1 Average charge state as a function of terminal voltage and stripper pressure. Calculated average equilibrium charge is shown for comparison.

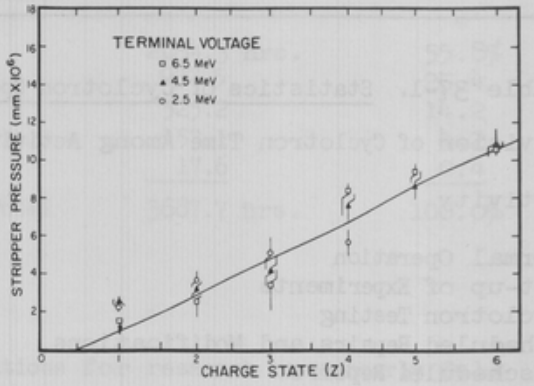

Fig. 38-2 Stripper pressure at maximum yield of a particular charge state as a function of charge and energy. Flags indicate pressure range over which 90% of maximum yield is maintained.

terminal voltage, for five different pressures. The striking feature of these data is that Z_{av} generally falls below the value of the average equilibrium charge, but at the highest voltage and pressure Z_{av} actually exceeds the equilibrium value. This is attributed to the re-focusing of ions in the higher charge states by the high-energy acceleration tube while the ions in lower charge states are lost by collisions with the tube electrodes.

A useful empirical result of this work is shown in Figure 38-2. It was found that the optimum pressure for the production of a given charge state, Z, is

relatively insensitive to terminal voltage and rises fairly linearly with Z. (A detailed report of this work will soon be submitted to the Review of Scientific Instruments.) (J. G. Cramer and E. Preikschat)

---

39. Equilibrium Charge Distributions of 8 MeV Carbon Ions in Various Media

The conventional stripper material in tandem accelerators has been a diatomic gas. More recently solid foil strippers have been introduced for heavy ions because they produce a higher mean ionic charge. It has been known for some time from the work of Lassen[1] with fission fragments that the mean ionic charge was significantly less in low pressure gases than in solids. Litherland et al.[2] have shown that the equilibrium mean ionic charge for Cl, Br, and I ions is appreciably higher in foils than in gases. This dependence of the equilibrium charge distribution on the state of condensation is attributed to the fact that for an ion traversing a gas the time between collisions is long compared to the lifetime for de-excitation of excited states, whereas in a solid it is likely that an ion excited in one collision can undergo another collision while still excited. If it is assumed that an electron in an excited state is more easily stripped than an electron in a ground state, a solid will produce a higher mean ionic charge. Halpern[3] has suggested that it might be possible to increase the average ionic charge in a gas exchanger by using a polyatomic gas which would exhibit local regions of "condensed" matter. To test this idea we decided experimentally to compare the charge state distributions for a diatomic gas, a polyatomic gas, and a metallic foil.

A schematic diagram of the experimental apparatus is shown in Figure 39-1. The 42 MeV helium ion beam from the University of Washington 60-inch cyclotron was elastically scattered from carbon to produce approximately 8.4 MeV carbon recoils. A detector intercepting a solid angle of 0.0016 sr was placed at +48 deg with respect to the incident α-particle beam to detect the elastically scattered α-particles. The carbon recoils (appearing at -59 deg in the laboratory system) had an average energy loss[4] of 0.4 MeV in the 100 $\mu g/cm^2$ carbon target. After leaving the target the carbon recoils traveled through the collimating and charge-exchanging system and were then magnetically separated into the different charge states and analyzed by a position-sensitive detector. The gas exchange target was obtained by employing the simple technique of using the vapor in equilibrium with an excess of a moderately volatile solid.

The results of the measurements to compare the relative stripping of a diatomic gas, a polyatomic gas, and a solid foil are shown in Figure 39-2 and Table 39-1. The errors assigned to the populations of the various charge states are somewhat larger than the statistical errors because an estimate of the additional uncertainty associated in resolving the various charge state peaks has been included in the stated errors. The solid foil is clearly superior to either of the vapor strippers in producing the highest proportion of higher charge states. The polyatomic naphthalene vapor does exhibit an increased effectiveness compared to the diatomic gas in producing higher charge states, although the effect is not as large as might have been hoped.

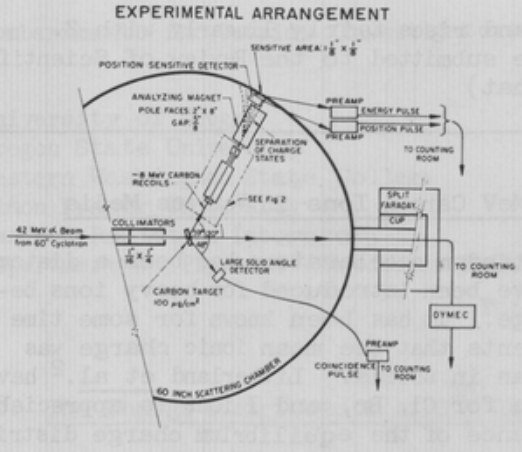

Fig. 39-1 Schematic diagram of the experimental arrangement. The 42 MeV α-beam is scattered off a 100 $\mu g/cm^2$ thick carbon target and the 8 MeV carbon recoils (in coincidence with the elastically scattered α-particles) pass through an exchange material and a collimating system and are then magnetically analyzed and detected.

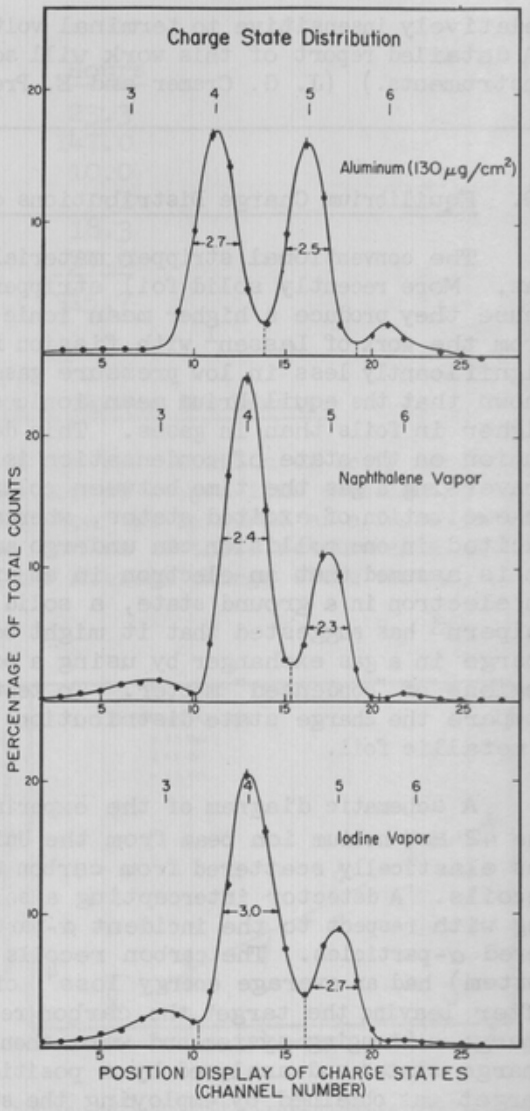

Fig. 39-2 Charge state distributions for aluminum foil, naphthalene vapor, and iodine vapor.

The fact that naphthalene does not produce nearly as large an increase in the average charge as does the solid can be largely attributed to the geometrical structure of the naphthalene molecule. This molecule is planar, and therefore the naphthalene molecule must be oriented favorably with respect to the incident ion direction in order for the incident ion to undergo a collision with two successive atoms of the molecule. A rough estimate based on the interatomic spacings in naphthalene and an interaction radius as deduced from estimates of the value of charge-exchange cross sections suggests that less than half of the naphthalene molecules will be oriented in such a way that two collisions will occur within the same molecule. This suggests that a more spherically shaped complex molecule would be appreciably more effective in producing a higher average equilibrium charge.

A more complete report on this work has been submitted to Nuclear Instruments and Methods. (E. Preikschat and R. Vandenbosch)

Table 39-1. Charge State Populations (in percent) for Various Stripper Materials

Stripper Material	Emergent Energy (MeV)	Charge State 3	4	5	6
Aluminum ($130\ \mu g/cm^2$)	7.4	1.8±.2	51.6±1.1	40.6±1.0	6.0±.6
Naphthalene ($10\ \mu g/cm^2$)	7.4	7.2±.6	64.7±1.2	26.5±.9	1.6±.2
Iodine ($60\ \mu g/cm^2$)	7.35	11.3±.8	65.2±1.2	22.5±.8	1.0±.2

1 N. O. Lassen, Dan. Mat. Fys. Medd. 25, No. 11 (1949).
2 Litherland, Almqvist, Andrews, Broude, and Kuehner, Bull. Am. Phys. Soc. II, 8, 75 (1963).
3 I. Halpern, private communication.
4 C. F. Williamson, Cyclotron Research, University of Washington (1963), p. 33.

40. Precise Calibration of the Tandem Van de Graaff Energy Scale

The neutron threshold reactions listed in Table 40-1 have been employed to convert the proton magnetic resonance gaussmeter frequencies of the analyzing magnet to absolute beam energies. This was accomplished in the usual manner by measuring the threshold for production of neutrons at zero degrees with respect to the proton beam. The neutrons were detected by a BF_3 proportional counter surrounded by several inches of paraffin moderator. A typical experiment is shown in Figure 40-1. The proton resonance frequency corresponding to the threshold could easily be measured to a precision of ± 1kc.

The energy of the beam is related to the proton resonance frequency by the formula

$$k^{1/2} f Z M^{1/2} = [E(1 + E/2Mc^2)]^{1/2}, \qquad (1)$$

where

f ≡ proton magnetic resonance frequency at threshold,
Z ≡ charge state of incident particle,
M ≡ mass of incident particle,
E ≡ energy of incident particle,
k ≡ conversion constant to be evaluated by threshold measurements.

Values of the magnet constant k as determined by the various threshold measurements are given in Table 40-2. There is some slight indication of systematic variation of k with energy which could be attributed to uneven saturation

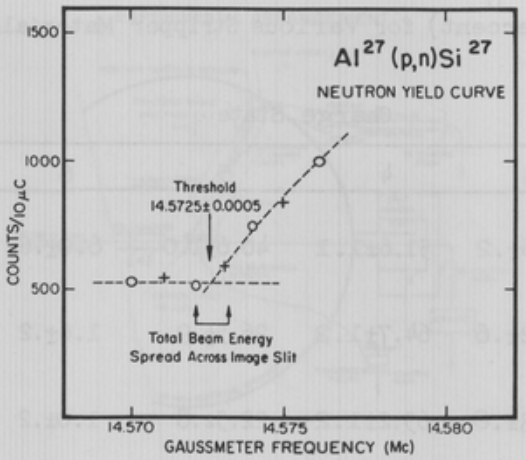

Fig. 40-1 Typical neutron yield curve obtained in the energy calibration runs. The image slits of the analyzing magnet were set at 0.010" opening and the object slits were set at 0.020" opening. Circles are data taken with increasing magnet current; crosses are data taken with decreasing magnet current.

properties of the magnet. However, measurements of higher energy thresholds would be necessary to determine if this is a real effect. The value of k as determined from the $Al^{27}(p,n)Si^{27}$ reaction has been chosen as the basis of our energy calibration.

It was determined very early in the measurements that the frequency for the apparent threshold of the $Al^{27}(p,n)Si^{27}$ reaction could vary as much as 15 kc depending on the past history of the analyzing magnet. Erasing the "memory" of the magnet is normally accomplished by increasing the current through the coils until the iron is saturated. Magnet settings are then approached from above. However, this procedure is impossible here because the power supply furnished with our analyzing magnet is incapable of delivering the requisite current. It was found, however, that the "memory" of the analyzing magnet could be erased completely by cycling the current from 0 to 300 amperes twice, and then approaching the proper setting from zero current. It has been established as standard procedure so to cycle the magnet three times when the Van de Graaff is first turned on each day, or if the energy must be lowered by more than 20 keV. With these precautions it has been found possible to repeat the $Al^{27}(p,n)Si^{27}$ threshold to within 0.5 keV on successive days.

Accurate calibrations at higher equivalent proton energies could be accomplished if needed by using alpha particle and heavy ion neutron thresholds. Some useful reactions are listed in Table 40-3. Measurement of these thresholds would probably require the use of the fast-slow counter ratio technique because the large angular momentum transfers preclude an important s-wave contribution and its resultant sharp threshold. (C. F. Williamson)

Table 40-1. Thresholds Used in the Energy Calibration

Reaction	Threshold Energy
$F^{19}(p,n)Ne^{19}$	4.245 ± 0.005
$Al^{27}(p,n)Si^{27}$	5.803 ± 0.003
$N^{14}(p,n)O^{14}$	6.359 ± 0.003

Table 40-2. Magnet Constants Derived from the Threshold Measurements

Reaction	Threshold Frequency [mc]	Magnet Constant, $k \frac{[MeV]}{[mc]^2}$
$F^{19}(p,n)Ne^{19}$	12.445 ± 0.002	$(2.7594 \pm 0.0028) \times 10^{-2}$
$Al^{27}(p,n)Si^{27}$	14.5725 ± 0.0005	$(2.7625 \pm 0.0026) \times 10^{-2}$
$N^{14}(p,n)O^{14}$	15.251 ± 0.002	$(2.7646 \pm 0.0021) \times 10^{-2}$

Table 40-3. Reactions Suitable for Magnet Calibrations at High Equivalent Proton Energies

Reaction	Charge State of Incident Ion	Threshold Energy	Equivalent Proton Energy
$C^{12}(\alpha,n)O^{15}$	1+	11.35	45.40
$C^{12}(\alpha,n)O^{15}$	2+	11.35	11.35
$O^{16}(\alpha,n)Ne^{19}$	1+	15.20	60.80
$O^{16}(\alpha,n)Ne^{19}$	2+	15.20	15.20
$H^{2}(O^{16},n)F^{17}$	3+	14.54	19.40
$H^{2}(O^{16},n)F^{17}$	4+	14.54	14.54
$H^{2}(O^{16},n)F^{17}$	5+	14.54	11.64

41. Voltage Stabilization of the Tandem Van de Graaff

Even under the best of operating conditions the terminal potential of our Van de Graaff fluctuates by at least 500 to 1000 volts. These variations are too rapid for the corona regulator system (which cannot operate faster than in about 0.2 second). At 10 MeV, the dispersion of the analyzing magnet causes a motion of about 0.001 inch per 250 eV. Thus, a terminal fluctuation of 1 kV moves the proton beam about 0.008". Since a typical operating image slit width is 0.020", the beam intensity changes by about 50% due to this terminal voltage fluctuation.

Under less favorable conditions, the terminal voltage fluctuations are larger and in fact can become so bad that the machine is unusable. On several occasions we have been forced to "go down to air." We have always regarded this instability as the worst feature of our machine, but until recently the cause remained unknown. We now believe the trouble lies primarily in uneven charging of the belt and uneven charge removal from the belt. By exercising extreme care in aligning the belt charge and terminal collector screens, we have succeeded in reducing the fluctuations to tolerable levels, although this still leaves much to be desired.

Recently, by means of the terminal shorting rod, we have made oscilloscope studies of the current delivered to the terminal. Photographs of single oscilloscope traces show that the current fluctuations, though very complex, and at first sight noise-like, are actually periodic and recur at a frequency equal to that of the belt. The maximum per cent fluctuation ranges from 50 at low average charging current (100 μa) down to 10 or 15 at higher average current (300 μa). The periodicity, however, remains unchanged even when the belt position or tightness is altered. During one belt period ($\sim$ 0.35 sec) the current fluctuates with various frequency components. A prominent component is near, but not equal to, 60 cps.

The unshorted terminal potential exhibits a similar periodicity. The amplitude is, of course, very much reduced due to the RC filtering action of the terminal. Oscilloscope studies of the output from the differential amplifier connected to the beam image slits shows that the beam itself is moving back and forth in a complicated manner, but that the same belt period cycle again appears.

The existence of the belt period structure in the terminal potential has led to a proposal for a novel type of regulator. The basic idea is to sense the voltage fluctuations, and delay by an appropriate length of time a correcting signal fed to the belt charge system. The correcting signal is recorrected, redelayed, and refed to the belt charging system. The recorrecting operation must be done exactly once each belt cycle. The time delay between sensing the terminal voltage and applying a correcting signal equals the time required for the belt to go from the terminal charge take-off screen to the up-charge screen. (We have removed the so-called down-charge screen.)

Since the time delays involved are rather excessive for electrical delay lines, we propose to use magnetic tape. A commercial high fidelty stereo tape recorder fitted with an extra read head can be modified for this application. Figure 41-1 shows a schematic diagram of the regulator system. Its operation is

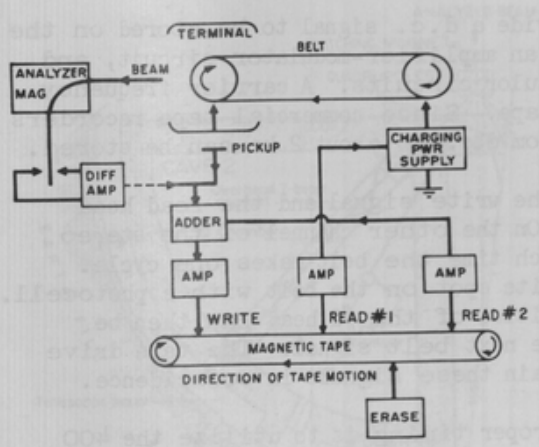

Fig. 41-1 System for eliminating voltage fluctuations in the terminal due to irregularities in the charging belt.

as follows: the terminal voltage fluctuations are sensed by the pick-up electrode. This signal passes through the adder, is amplified, and recorded on the magnetic tape via the write head. At a time when the part of the belt which initially caused the fluctuation has reached the charging screen, the information is read off the tape (Read #1) and fed as a correcting signal to the charging power supply. This then corrects in part for the next fluctuation before it occurs. At the time when the partially corrected charge reaches the terminal, the original signal from the tape is read off (Read #2) and sent to the adder. Simultaneously, the new (reduced) fluctuation is also sent to the adder. The combined correction signal is thus stored on the tape. When the correction signal has reached the required level, no terminal variation occurs, and the magnetic tape continuously stores, reads, re-stores the correct information. The effect is thus to charge the belt with a variable surface charge density which is just that required to deliver a uniform current to the terminal.

Of course small changes will occur in the required pattern stored on the tape. The signal from the terminal voltage can continuously alter the signal stored on the tape each cycle. The system is predicated upon the fact that these changes are apparently small compared with the dominant periodic pattern.

The tape is erased after read #2 so that a continuous length of tape can be used.

The read #2 amplifier should be very stable and its gain, together with that of the adder and write amplifier, should be such that the signal re-read into the tape is almost, but not quite, as strong as the original signal.

The correcting signal can also be derived from the differential amplifier which reads the ratio of the two beam currents striking the image slits after the analyzer magnet. To first order this signal is proportional to the momentum change in the beam, and thus proportional to the square root of the terminal voltage. The signal recorded on the magnetic tape is thus initially not the correct analog. However, after a number of belt cycles the combined re-write and new correcting signal will generate the proper form of correcting signal.

With the system shown the magnetic tape cannot store a d.c. correcting signal, and a slow-speed correction must still be derived from the image slits. This signal may be used as at present to control the corona current, or it may be fed through a buffer directly to the charging power supply. In either case, this path must have a very long time constant in order to insure that the two-regulating paths do not interact.

An alternative proposal which will provide a d.c. signal to be stored on the tape is to replace the write amplifier with an amplifier-modulator circuit, and the two read amplifiers with amplifier-demodulor circuits. A carrier frequency of about 10 kc would then be stored on the tape. Since commercial tape recorders operate to over 12 kc a correcting signal from d.c. to about 2 kc can be stored.

It is essential that the time between the write signal and the read head number 2 be always exactly one belt cycle. On the other channel of the stereo tape it is planned to write a time signal each time the belt makes one cycle. Such a signal can be derived by viewing a white spot on the belt with a photocell. The signal as read by channel two at the position of the #2 head can then be made to coincide with the arrival time of the next belt signal. The tape drive motor can then be servodriven so as to maintain these signals in coincidence.

An alternative method for maintaining proper timing is to utilize the 400 cycle 100 volt generator in the Van de Graaff terminal. A neon, or argon-filled, bulb connected to this generator will flash about 800 cps. This light signal can be viewed by a phototube placed at one of the windows in the base of the Van de Graaff. The resulting signal can be scaled down to 60 to 80 cps and used to drive the synchronous motor of the tape recorder. The positions of the read heads can be made adjustable to provide proper initial density adjustments.

We are planning to make a few more tests of the feasibility of a regulator of the type proposed here. If these tests are favorable, we will go ahead with construction of the device. (J. S. Heagney, T. J. Morgan, and F. H. Schmidt)

---

42. Beam Line and Auxiliary Equipment for Neutron and Photon Detection

The 45° right beam line of the tandem Van de Graaff has been placed in operation as a facility for experiments involving detection of neutrons and gamma radiation. The following criteria, provided by the intended users, guided the design of this beam line:

(1) Support structure and beam tube flexible enough in design to accommodate almost any small special-purpose scattering chamber.

(2) Ability to change scattering chambers quickly with easy realignment.

(3) No significant scattering mass within 6 feet of the target during neutron experiments.

(4) A low level of background from the beam stop.

(5) A support capable of holding the anticoincidence annulus gamma-ray spectrometer and its 1000 lb. shield.

A general plan view of cave 2 is shown in Figure 42-1.

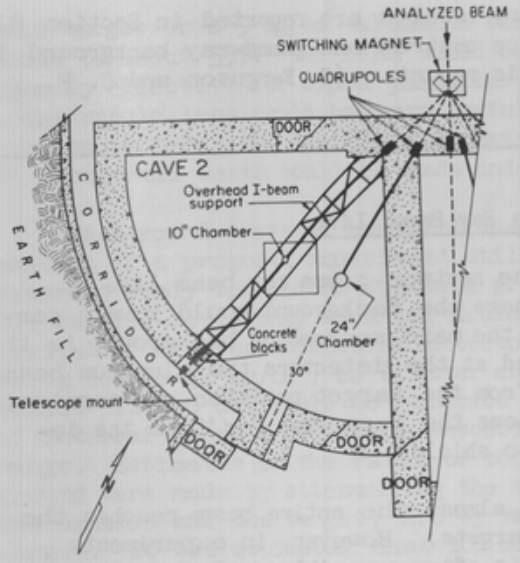

Fig. 42-1 Plan of Cave 2 showing the neutron-gamma ray beam line.

The beam tube consists of 4" i.d. aluminum tubing. The first 16-1/2 feet are permanently installed and contain the beam scanner, quartz beam viewer, defining slits, and the connection to the vacuum pumping system. The next 10 feet are available for the experimenter to fill as he wishes. The last section is 17 feet long and terminates in the shielding wall. This section is insulated and electrostatically shielded to form the Faraday beam cup.

In order to accommodate a variety of possible small scattering chambers, an overhead support bridge was built for the beam tube. This consists of two parallel 6" I-beams, with appropriate cross-bracing, running along a radius of the cave. The beam tube is suspended from this bridge by light-weight V-shaped hangers. The beam tube can be insulated from these hangers and is aligned by four adjusting bolts. The bridge is about 5 feet above the line of the beam so that no large scattering mass is near the target.

A permanent telescope mount has been installed in the corridor behind cave 2 to facilitate alignment of the scattering chamber. This mount has been accurately aligned on a fiducial mark on the exit of the switching magnet such that its axis lies along the desired beam direction.

Two special purpose scattering chambers have been constructed for use on this beam line. One chamber will be used to study neutrons associated with fission. The chamber is a 10" diameter, thin-walled aluminum sphere. It contains two small arms for fission fragment detectors and a two-frame target ladder. The neutron detectors will be placed at various angles outside the chamber. Another chamber is being used with the anticoincidence annulus. It is a 10" diameter, thin-walled aluminum sphere containing a 4-frame target ladder, and has a special port for the mounting of a solid state monitor detector.

A heavy platform with an arm pivoting about a vertical line through the center of the target serves as a support for the annulus or other massive detector. The annulus is held in such a manner that its distance from the target can be varied from 12" to 40" with a precision of 0.10", and its angle with respect to the beam can be varied in one degree steps from 20° to 160° with an angular precision of 0.1°. This platform can be retracted three feet below floor level into the pit underneath the light weight floor of the cave when neutron experiments are in progress. This places the platform eight feet from the target.

Experimental studies of radiative capture of protons and He^3 are now being

carried out using this facility. Preliminary results are reported in Section 21 of this report. The measures taken to reduce neutron and gamma-ray background in this cave are described in Section 43 of this report. (S. Ferguson and C. F. Williamson)

---

43. Background Studies on the Neutron-Gamma Ray Beam Line

The prime objective of the design of the neutron-gamma ray beam line of cave 2 (Section 42) was to provide a line where the background would remain particularly low in most bombardments. One of the main sources of background is the beam disposal system. To minimize background at the detectors the aluminum beam tube was extended about 22 feet downstream from the target position and terminated in the shielding wall of the cave. This places the beam stop far from the detectors and in a position where it is easy to shield.

This design should be very effective if almost the entire beam reaches the beam stop. This is the case for very thin targets. However, in experiments where neutrons and protons are observed, it is often possible, and sometimes necessary, to use thick targets. Under these circumstances there will be considerable multiple scattering in the target and some of the beam will hit the sides of the beam tube beyond the scattering chamber. To make sure that all of the beam is recorded, the entire post-chamber beam tube was electrically insulated and electromagnetically shielded to form a long Faraday cut. Graphite irises were placed at several positions inside this Faraday cup tube to stop any beam which would otherwise strike the walls. In addition to preventing multiply-scattered beam from stopping in aluminum (which generally produces more neutron background than graphite) the irises localize the sources of background in space, making them easier to shield.

Although graphite was found to be a particularly good beam stopping material as far as neutron production was concerned, it did give rise to considerable photon background (notably the C^{12} 4.4 MeV line). It was possible to eliminate this background by lead "shadow" shielding.

The effectiveness of the long Faraday cup would be greatly enhanced if the multiple scattering effects could be counteracted. Therefore, a study was made of the feasibility of refocusing the scattered beam with a quadrupole magnetic lens. Consider the target to be a point source of protons. Then a lens must be placed downstream a distance equal to its focal length to focus the protons into a parallel beam. The effectiveness of the lens can be judged in terms of the fraction of beam that will strike the wall of the tube before the beam can be focused.[1] This calculation is complicated by the fact that in one plane the quadrupole lens causes the beam to diverge more for a short distance before causing it to converge. The focal length of a quadrupole lens depends on the magnetic field gradient and on the dimensions of the poles.[2] As an example, consider a lens with pole pieces 4 inches long with a 2-inch space between the poles for a total length of 10 inches. Let the aperture be 2 inches and the field gradient be 5 kilogauss per inch. Such a lens could reduce the beam loss due to multiple scattering to 1% in the following cases: 5 MeV protons scattered by a 2 mg/cm^2 gold target or a 5 mg/cm^2 aluminum target; 15 MeV protons scattered by a 3.5 mg/cm^2

gold target or a 9 mg/cm^2 aluminum target. Without the lens the scattering loss would be about 35%. The lens would be less effective for deuterons and about equally effective for alpha particles. Thus there clearly exist situations where a quadrupole lens could be very useful in reducing background. It was, however, decided to delay the design and construction of a quadrupole lens until a number of background tests could be made under typical experimental conditions.

Background tests on the neutron-gamma ray beam line have been made in the context of a proposed experiment utilizing the anticoincidence annulus spectrometer to study the photon spectrum produced by proton bombardment of tin. Thus the results apply only to a particular detector, but this detector is probably typical of most scintillation detectors. The tin targets which were used were thick enough (2 mg/cm^2) to scatter about 25% of the beam into the Faraday cup walls. It was difficult to subtract the background spectrum from the spectrum of interest because both were essentially featureless and covered the same energy range. Estimates of the ratio of counting rates for target gamma-rays to background were made by attenuating the target gamma rays with lead placed between the annulus and the target, and by varying the distance of the annulus from the target. It was estimated that 10% of the total observed spectrum was due to background from the beam disposal system, mostly from multiply-scattered beam.

A survey of neutron flux was taken at different points in the cave. It appears that neutrons produce most of the background. Both the target and the beam stop are important sources of neutrons. Also, the beam profile monitor, if left running, is a significant source of neutrons.

Finally it was estimated that about 40% of the total observed gamma-ray spectrum from 15 MeV protons on tin is due to neutrons from the target. This implies that background cannot be reduced enough by additional refinements in the beam disposal system. The final elimination of background will be possible only when installation of the beam pulsing system on the Van de Graaff makes it possible to use time of flight to distinguish between pulses due to target photons and those due to target neutrons. (S. Ferguson, I. Halpern, D. L. Johnson, and C. F. Williamson)

---

1 J. B. Ball, Computation of Losses Due to Multiple Scattering of Charged Particles in Thin Foils, Oak Ridge National Laboratory Report No. ORNL-3311, 1962.

2 E. D. Courant, M. S. Livingston, H. S. Snyder, Phys. Rev. 88, 1190 (1952).

---

44. Beam Bunching System for the Tandem Van de Graaff

For most of the year progress was delayed on the bunching and chopping system for the University of Washington 2-stage FN tandem accelerator. Until a few months ago it was not known how much space would be available between the two-stage ion source and the tandem tank when the injector tank for the three-stage machine is installed. Final drawings showing the complete inter-tank beam transport layout were recently made available by High Voltage Engineering Corporation. The additional space needed to accommodate the bunching apparatus is included,

and an assurance was given that this will not be affected by the installation and operation of the neutral injector.

All the mechanical parts for the pulsing system excluding the high-energy wiper have been built and vacuum tested. These comprise:

(1) A set of deflecting plates (chopper) and slits (wiper) for chopping the low-energy negative ion beam into a series of short (20 to 60 nsec) bursts.

(2) A three-gap klystron buncher, which concentrates a given beam burst into a pulse of a few nsec duration at the target.

The purpose of the high-energy wiper is to clean up the edges of the bunched pulse so that its duration at the target may be accurately defined. This unit will be built only after some experience has been gained, using the low-energy bunching assembly.

The complete system is shown schematically in Figure 44-1, and the waveforms used by the chopper and buncher are shown in Figure 44-2. A sawtooth modulating waveform is applied to the klystron, which, in principle, can bunch up to 50% of

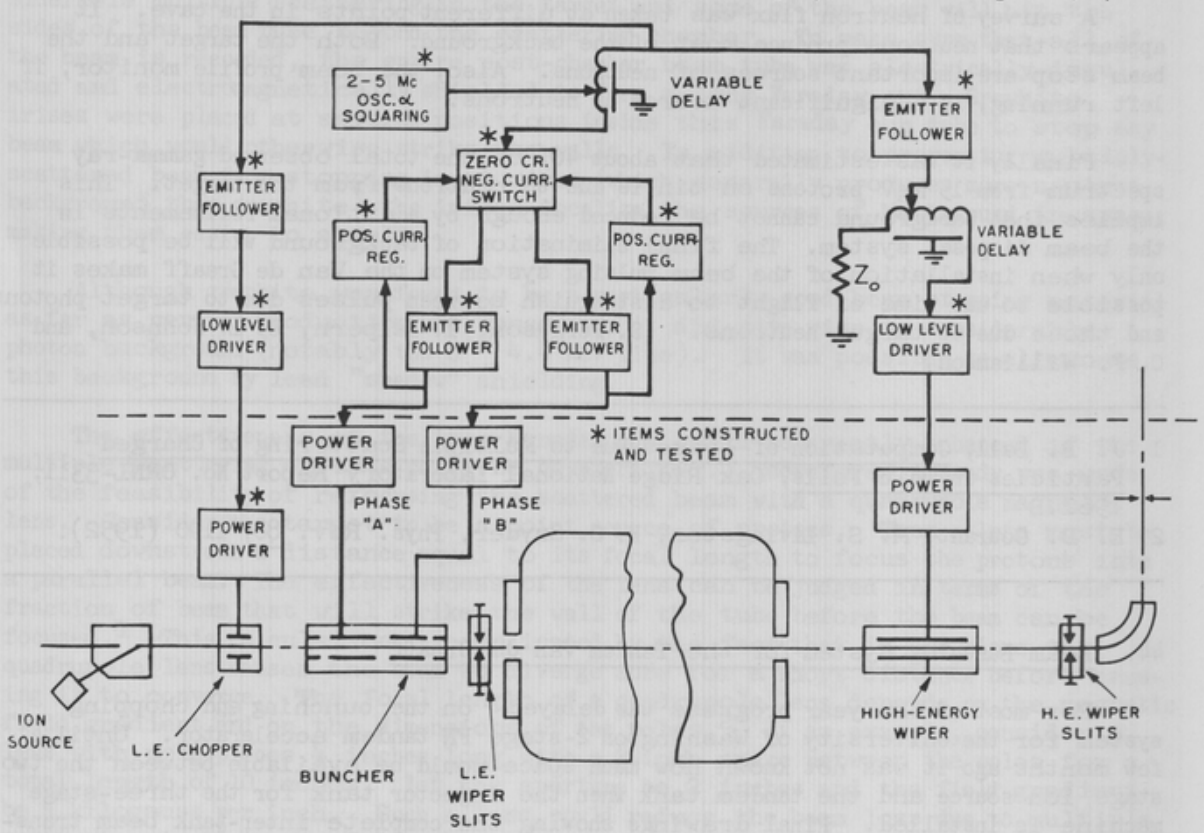

Fig. 44-1 Block diagram of FN pulsing system.

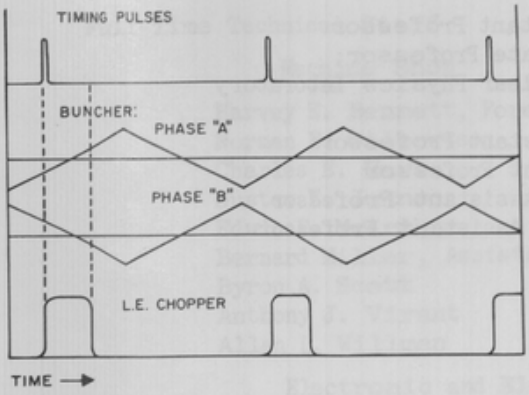

Fig. 44-2 Voltage waveforms applied to FN pulsing system.

the continuous beam. In practice it is difficult to generate this ideal waveform at high voltages. Furthermore, energy inhomogeneities in the low-energy beam and jitter in the beam position limit the ultimate pulse duration which is attainable. Initially, therefore, we will attempt to compress beam bursts no more than 50 to 60 nsec long.

These chopped beam bursts are generated by applying a rectangular pulse to the chopper plates at the correct phase relative to the buncher waveform (see Figure 44-2). The high-voltage driver for the low-energy chopper and the associated high voltage power supplies have been designed, constructed and are being installed. The control electronics (all solid state) are mounted in the accelerator control room. The final 1250 volt pulse applied to the deflector plates is developed by a ceramic 250-watt transmitting tube. The pulse shape is diode-clamped for flat-top response and approximately 30 nsec wide at the half-voltage points. The repetition rate is variable from 2 to 5 Mc/s. The final driver is mounted directly over the deflecting plates and is supported by the beam tube.

The chopper and wiper slits have been installed in the low-energy beam line, and tests are in progress. Installation of the buncher requires moving the whole ion source assembly. The decision when this is to be done will be made in the near future. (H. Fauska, I. Halpern, J. S. Lilley, and C. F. Williamson)

45. Nuclear Physics Laboratory Personnel

Faculty

John S. Blair, Professor
David Bodansky, Professor
John G. Cramer, Assistant Professor
Arthur W. Fairhall, Professor
George W. Farwell, Professor
James B. Gerhart, Professor
I. Halpern, Professor
Fred H. Schmidt, Professor
Robert Vandenbosch, Associate Professor

Nuclear Physics Laboratory Research Staff

Jonas Alster, Research Assistant Professor[1]
Charles D. Kavaloski, Research Assistant Professor

John S. Lilley, Research Assistant Professor
Ted J. Morgan, Research Associate Professor;
Supervisor, Nuclear Physics Laboratory
Jack C. Norman, Instructor
Patrick Richard, Research Assistant Professor
Nelson Stein, Research Assistant Professor
William G. Weitkamp, Research Assistant Professor
Claude F. Williamson, Research Assistant Professor

Predoctoral Research Associates

Chemistry

Walter Loveland[2]

Physics

Nelson Cue
Wojciech Kolasinski
Paul Mizera
Barry J. Shepherd[3]
David C. Shreve
Gurnam S. Sidhu[4]
Frederick W. Slee

Research Assistants

Chemistry

Charles J. Bishop
Dennis G. Perry
Clifford Rudy
Robert W. Shaw, Jr.
Kevin L. Wolf

Physics

Wilfred J. Braithwaite
David Chamberlin[5]
Gary M. Chenevert
Stephen M. Ferguson
Bernard Fernandez[6]
Thomas D. Hayward
Robert H. Heffner[5]
Roger A. Hinrichs
David L. Johnson
Patrick Landreth[7]
Ching C. Ling[5]
Donald M. Patterson
R. Jerome Peterson[8]
Ekkehard Preikschat[9]
David R. Rhiger[5]
Derek W. Storm
Joseph R. Tesmer[5]
Paul P. Urone[5]
Harry V. Winsor

Full-Time Technical Staff

Machine Shop

Harvey E. Bennett, Foreman
Norman E. Gilbertson
Charles E. Hart
Gustav E. Johnson
Edwin P. McArthur
Bernard Miller, Assistant Foreman
Byron A. Scott
Anthony J. Virant
Allen L. Willman

Electronic and Electrical

Laverne H. Dunning
Robert B. Elliott
Harold Fauska, Senior Physicist;
Research Electronics Supervisor
Joseph S. Heagney, Senior Physicist
George C. Monge
John W. Orth, Assistant Supervisor, Nuclear Physics Laboratory
Norman G. Ward

Technicians

Carl E. Linder
Georgia Jo Rohrbaugh
George E. Saling

Design and Drafting

Robert G. Clarke
Peggy Douglass
David W. Gough
Dolores Lenhart[10]
Peter Momcilovich, Engineer
Lewis E. Page

Accelerator Operators

Jacque M. Beechel
Bonnie C. Murray
Richard Clay[11]

Others

Tylaine C. Hansen, Office Assistant
Shirley Kellenbarger, Chemist
Kyum Ha Lee, Laboratory Technician
Joanne M. Sauer, Chemist[10]
Walter Ross Scott, Programmer
Helene Turner, Secretary

Part-Time Technical Staff
Student Helpers

John Beall[10]
Richard F. Berthelsdorf
Kurt M. Liewer
Kimball A. Milton
Charles J. Peterson
John T. Thaxton[10]
Richard J. Thomas[10]

Others

Mary A. Beard, Storekeeper

---

1 Now at Northeastern University, Boston, Massachusetts.
2 Now at Argonne National Laboratory, Argonne, Illinois.
3 Now at Brookhaven National Laboratory, Upton, L.I., N.Y.
4 Now at Lawrence Radiation Laboratory, University of California, Livermore, California.
5 Research Assistant without stipend.
6 Unpaid visitor from Saclay, France.
7 Now Teaching Assistant, Department of Physics.
8 Now at Princeton University, Princeton, N.J.
9 Now at The University, Birmingham, England.
10 Terminated.
11 Military leave.

---

46. Advanced Degrees Granted, Academic Year 1965-1966

W. D. Loveland: Ph.D. "Doubly Charged Particle Emission During Nuclear Fission at Moderate Excitation Energies."

R. J. Peterson: Ph.D. "A Study of the Inelastic Scattering of 42 MeV Alpha Particles from Nuclei with 20 Protons or 28 Neutrons.

B. J. Shepherd: Ph.D. "Angular and Energy Distributions of Gamma Rays Emitted following 42 MeV Alpha Particle Bombardment of Several Rare Earth Nuclei."

G. S. Sidhu: Ph.D. "An Experimental Study of the Spectrum Shape for the Gamow-Teller Transition $O^{14} \rightarrow N^{14}$."

F. W. Slee: Ph.D. "A Study of (d,Li^6) Reactions on Light and Intermediate Weight Nuclei."

W. J. Braithwaite, M.S., August 20, 1965.

47. List of Publications

"O^{16} $(\alpha, Be^{8})C^{12}$ Reactions," R. E. Brown, J. S. Blair, D. Bodansky, and C. D. Kavaloski, Phys. Rev. 138, B1394-1411 (1965).

"Comparison between Phase Shift and Complex Potential Descriptions of Elastic Scattering," J. Alster and H. E. Conzett, Phys. Rev. 139, B50-54 (1965).

"Level Structure of Ca^{48}," R. J. Peterson, Phys. Rev. 140, B1479-1482 (1965).

"Proton Gamma Competition in the $Cu^{63}(p,2p)$ Ni^{62} Reaction at 10.5 MeV," E. R. Parkinson and D. Bodansky, Rev. Modern Phys. 37, 372-374 (1965).

"A dE/dx-E-T Particle Identification System," E. R. Parkinson and D. Bodansky, Nuclear Inst. and Methods, 35, 347-349 (1965).

"Preparation of Sr, Ca, and Mg Accelerator Targets," J. Sauer, Rev. Sci. Instr. 36, 1374 (1965).

"Fission-Fragment Angular, Energy and Mass Division Correlations for the $U^{234}(d,pf)$ Reaction," R. Vandenbosch, J. P. Unik, and J. R. Huizenga, Physics and Chemistry of Fission Vol. I, p. 547 (International Atomic Energy Agency, Vienna, 1965).

"Alpha Particle Emission in Nuclear Fission," I. Halpern, ibid ., Vol. II p. 369.

"Proton Emission in 42 MeV Alpha-Particle Bombardments of Several Elements," R. W. West, Phys. Rev. 141, 1033-1052 (1966).

"Collective Excitations in Pb^{208}, and Bi^{209}," J. Alster, Phys. Rev. 141, 1138-1145 (1966).

"Nuclear-Structure Studies of Sr^{88} and Y^{89} by Inelastic Alpha-Particle Scattering," J. Alster, D. C. Shreve, and R. J. Peterson, Phys. Rev. 144, 999-1012 (1966).

"Decay of Isobaric Analogue States in the Lead Region," C. D. Kavaloski, J. S. Lilley, P. Richard, and N. Stein, Phys. Rev. Letters 16, 807-810 (1966).

Publications in Press:

"A Miniature Cooling System for Ge(Li) Solid-State Detectors," C. F. Williamson and J. Alster (Nuclear Instr. and Methods).

"Equilibrium Charge Distribution of 8 MeV Carbon Ions in Various Media," E. Preikschat and R. Vandenbosch (Nuclear Instr. and Methods).

"Polarization in p-α Scattering from 17 to 27 MeV," W. G. Weitkamp and W. Haeberli (Nuclear Phys.).

"Observation of the 4.12 MeV $O^{14} \rightarrow N^{14}$ Positron Spectrum Shape," G. S. Sidhu and J. B. Gerhart (Phys. Rev.)

Talks given at Meetings and Conferences:

"Isobaric Spin Conservation in the $C^{14}(\alpha,d)N^{14}$ Reaction at 42 MeV," C. D. Zafiratos, J. S. Lilley, and F. W. Slee, Bull. Am. Phys. Soc. (II) 10, 1195 (1965).

"Proton Spin Flip in the Reaction $C^{12}(p,p')C^{12*}(4.43)$ from 12 to 15 MeV," F. H. Schmidt, J. G. Cramer, and W. A. Kolasinski, Bull. Am. Phys. Soc. (II) 11, 99 (1966).

"Proton Spin Flip in the Reaction $Ni^{60}(p,p')Ni^{60*}(1,33)$ at 10.5 and 14.0 MeV," W. A. Kolasinski, J. G. Cramer, and F. H. Schmidt, Bull. Am. Phys. Soc. (II) 11, 100 (1966).

"(d,He^3) Studies on Y^{89} and Z^{90}," D. C. Shreve, C. D. Kavaloski, J. S. Lilley, and N. Stein, Bull. Am. Phys. Soc. (II) 11, 118 (1966).

"(α,Li^7) and (α,Li^6) Reactions at 42 MeV," P. F. Mizera, J. B. Gerhart, and F. W. Slee, Bull. Am. Phys. Soc. (II) 11, 316 (1966).

"Inelastic Alpha-Particle Scattering from Ca^{42}, Ca^{44}, Cr^{52}, and Fe^{54}," R. J. Peterson, Bull. Am. Phys. Soc. (II) 11, 349 (1966).

"Elastic Proton Scattering from Isobaric Analogue Resonances in the Lead Region," P. Richard, C. D. Kavaloski, J. S. Lilley, and N. Stein, Conference on Isobaric Spin in Nuclear Physics, Tallahassee, Florida (1966).

"Decay of Isobaric Analogue Resonances in the Lead Region," N. Stein, C. D. Kavaloski, J. S. Lilley, and P. Richard, ibid.

"Isomer Ratio Studies of Angular Momentum Effects in Nuclear Reactions," R. Vandenbosch, 150th National Meeting, Am. Chem. Soc., Atlantic City, N.J., September 1965.

"Doubly Charged Particle Emission During Nuclear Fission at Moderate Excitation Energies," W. D. Loveland, A. W. Fairhall, and I. Halpern, 151st National Meeting, Am. Chem. Soc., Pittsburgh, Pa., March 1966.